Quantum-Aided modeling and design techniques for advanced wireless network architectures

(Article begins on next page)

13 May 2024

Politecnico di Bari

LIBERATORIA PER L'ARCHIVIAZIONE DELLA TESI DI DOTTORATO

Al Magnifico Rettore
del Politecnico di Bari

Il sottoscritto Francesco Vista nato a Barletta (BT) il 09/01/1997 residente a Barletta in via Sant'Antonio, 67 e-mail vista.francesco97@gmail.com iscritto al 3° anno di Corso di Dottorato di Ricerca in Electrical and Information Engineering ciclo XXXVI ed essendo stato ammesso a sostenere l'esame finale con la prevista discussione della tesi dal titolo:

Quantum-Aided Modeling and Design Techniques for Advanced Wireless Network Architectures

DICHIARA

1) di essere consapevole che, ai sensi del D.P.R. n. 445 del 28.12.2000, le dichiarazioni mendaci, la falsità negli atti e l'uso di atti falsi sono puniti ai sensi del codice penale e delle Leggi speciali in materia, e che nel caso ricorressero dette ipotesi, decade fin dall'inizio e senza necessità di nessuna formalità dai benefici conseguenti al provvedimento emanato sulla base di tali dichiarazioni;

2) di essere iscritto al Corso di Dottorato di ricerca Electrical and Information Engineering ciclo XXXVI, corso attivato ai sensi del "Regolamento dei Corsi di Dottorato di ricerca del Politecnico di Bari", emanato con D.R. n.286 del 01.07.2013;

3) di essere pienamente a conoscenza delle disposizioni contenute nel predetto Regolamento in merito alla procedura di deposito, pubblicazione e autoarchiviazione della tesi di dottorato nell'Archivio Istituzionale ad accesso aperto alla letteratura scientifica;

4) di essere consapevole che attraverso l'autoarchiviazione delle tesi nell'Archivio Istituzionale ad accesso aperto alla letteratura scientifica del Politecnico di Bari (IRIS-POLIBA), l'Ateneo archivierà e renderà consultabile in rete (nel rispetto della Policy di Ateneo di cui al D.R. 642 del 13.11.2015) il testo completo della tesi di dottorato, fatta salva la possibilità di sottoscrizione di apposite licenze per le relative condizioni di utilizzo (di cui al sito http://www.creativecommons.it/Licenze), e fatte salve, altresì, le eventuali esigenze di "embargo", legate a strette considerazioni sulla tutelabilità e sfruttamento industriale/commerciale dei contenuti della tesi, da rappresentarsi mediante compilazione e sottoscrizione del modulo in calce (Richiesta di embargo);

5) che la tesi da depositare in IRIS-POLIBA, in formato digitale (PDF/A) sarà del tutto identica a quelle **consegnate**/inviate/da inviarsi ai componenti della commissione per l'esame finale e a qualsiasi altra copia depositata presso gli Uffici del Politecnico di Bari in forma cartacea o digitale, ovvero a quella da discutere in sede di esame finale, a quella da depositare, a cura dell'Ateneo, presso le Biblioteche Nazionali Centrali di Roma e Firenze e presso tutti gli Uffici competenti per legge al momento del deposito stesso, e che di conseguenza va esclusa qualsiasi responsabilità del Politecnico di Bari per quanto riguarda eventuali errori, imprecisioni o omissioni nei contenuti della tesi;

6) che il contenuto e l'organizzazione della tesi è opera originale realizzata dal sottoscritto e non compromette in alcun modo i diritti di terzi, ivi compresi quelli relativi alla sicurezza dei dati personali; che pertanto il Politecnico di Bari ed i suoi funzionari sono in ogni caso esenti da responsabilità di qualsivoglia natura: civile, amministrativa e penale e saranno dal sottoscritto tenuti indenni da qualsiasi richiesta o rivendicazione da parte di terzi;

7) che il contenuto della tesi non infrange in alcun modo il diritto d'Autore né gli obblighi connessi alla salvaguardia di diritti morali od economici di altri autori o di altri aventi diritto, sia per testi, immagini, foto, tabelle, o altre parti di cui la tesi è composta.

Bari, 26/09/2023   Firma ___Francesco Vista___

Il/La sottoscritto, con l'autoarchiviazione della propria tesi di dottorato nell'Archivio Istituzionale ad accesso aperto del Politecnico di Bari (POLIBA-IRIS), pur mantenendo su di essa tutti i diritti d'autore, morali ed economici, ai sensi della normativa vigente (Legge 633/1941 e ss.mm.ii.),

CONCEDE

- al Politecnico di Bari il permesso di trasferire l'opera su qualsiasi supporto e di convertirla in qualsiasi formato al fine di una corretta conservazione nel tempo. Il Politecnico di Bari garantisce che non verrà effettuata alcuna modifica al contenuto e alla struttura dell'opera.
- al Politecnico di Bari la possibilità di riprodurre l'opera in più di una copia per fini di sicurezza, back-up e conservazione.

Bari, 26/09/2023   Firma ___Francesco Vista___

Politecnico di Bari

Politecnico
di Bari

Department of Electrical and Information Engineering
Electrical and Information Engineering
Ph.D. Program
SSD: ING-INF/03 – Telecommunications

Final Dissertation

Quantum-Aided Modeling and Design Techniques for Advanced Wireless Network Architectures

by
Francesco Vista

Supervisors:

Prof. Luigi Alfredo Grieco

Coordinator of Ph.D. Program:
Prof. Mario Carpentieri

Course n°36, 01/11/2020-31/10/2023

Politecnico
di Bari

Department of Electrical and Information Engineering
Electrical and Information Engineering
Ph.D. Program
SSD: ING-INF/03 – Telecommunications

Final Dissertation

Quantum-Aided Modeling and Design Techniques for Advanced Wireless Network Architectures

by
Francesco Vista

Referees:

Prof. Riccardo Bassoli

Dr. Ing. Claudio Cicconetti

Supervisors:

Prof. Luigi Alfredo Grieco

Coordinator of Ph.D. Program:
Prof. Mario Carpentieri

Course n°36, 01/11/2020-31/10/2023

To my grandfather

Acknowledgements

This thesis represents the culmination of my experiences and growth over the past three years. Much of my academic and professional development, as well as my current identity, can be attributed to the invaluable guidance and mentorship of Professor Luigi Alfredo Grieco. His immense knowledge, constant support, and plentiful experience have encouraged me in all the time of my academic research and daily life.

I am also deeply indebted to my exceptional lab mates — Vittoria, Gianluca, Antonio, and Ingrid — for the cherished time we spent together in the lab and for being a constant source of motivation. It has been great fun working with you all!

To my family, including my parents, brother, and grandparents, I want to extend my thanks for their continued love and support. I am forever grateful for my caring, patient, and supportive family. Even though we may be separated by distance, I always feel your influence and encouragement on this path.

A special acknowledgements is reserved to my friends: Francesco, Mario, Valentina, Ivano, Giuseppina, Lorenzo and Davide. Your unwavering friendship has been my anchor, accompanying me through the highs and lows of this academic journey.

Lastly, I want to thank Alessandra. I am grateful to her for being my inspiration and motivation through what has been an arduous journey.

«Arrendersi per vincere
Un passo indietro e avanti tre»

La fine del giorno - Cosmetic

POLITECNICO DI BARI

Abstract

Department of Electrical and Information Engineering

Doctor of Philosophy

**Quantum-Aided Modeling and Design Techniques for Advanced Wireless
Network Architectures**

by Francesco VISTA

The next generation of wireless communication systems will be characterized by ever-
increasing computational demands and complex data processing requirements. Quan-
tum computing and quantum communications, underpinned by the principles of quan-
tum mechanics, promise to significantly enhance processing capabilities compared to
conventional classical approaches. This paradigm shift presents novel challenges that
demand sophisticated strategies to ensure a suitable integration. As a result, this the-
sis focuses on addressing these challenges from an architectural standpoint, proposing
and analyzing various strategies to incorporate quantum computing into future wire-
less communication systems. Moreover, this work delves into the entanglement dis-
tribution problem with the primary goal of optimizing the teleportation rate, a crucial
aspect of quantum communication efficiency.

Contents

List of Figures

List of Tables

List of Acronyms

5G 5-th Generation

6G 6-th Generation

AI Artificial Intelligence

AR Augmented Reality

B6G Beyond 6-th Generation

BCD Block Coordinate Descent

BQ Binary Quadratic

BS Base Station

BSM Bell State Measurement

CNOT Controlled NOT

DBN Deep Belief Network

DCNN Deep Convolutional Neural Network

DL Deep Learning

DQN Deep Q-Learning Network

DRL Deep Reinforcement Learning

DT Decision Tree

EGD Entanglement Generator and Distributor

EPR Einstein-Podolsky-Rosen

FL Federated Learning

HCS Human-Centric Services

IoT Internet of Things

IoNT Internet of Nano Things

IRS Intelligent Reflective Surface

KPI Key Performance Indicator

KNN K-Nearest Neighbors

KKT Karush-Kuhn-Tucker

LoS Line of Sight

ML Machine Learning

mURLLC massive Ultra Reliable Low Latency Communications

MC Mesh Client

MR Mesh Router

MINLP Mixed-Integer Non-Linear Programming

MBRLLC Mobile Broadband Reliable Low Latency Communications

MIMO Multiple-Input/Multiple-Output

NFV Network Function Virtualization

NFVO Network Function Virtualization Orchestrator

NLoS Non-Line of Sight

OFDM Orthogonal Frequency Division Multiple

OFDMA Orthogonal Frequency Division Multiple Access

PCA Principal Component Analysis

QA Quantum Annealing

qubit quantum bit

QC Quantum Computing

QI Quantum Interface

QML Quantum Machine Learning

QoS Quality of Service

QPU Quantum Processing Unit

QR Quantum Repeater

QUBO Quadratic Unconstrained Binary Optimization

RL Reinforcement Learning

RBM Restricted Boltzmann Machine

SA Simulated Annealing

SCA Successive Convex Approximation

SDN Software-Defined Networking

SN Sensor Node

SNR Signal to Noise Ratio

SPDC Spontaneus Parametric Down-Conversion

SVM Support Vector Machine

TS Tabu Search

THz Terahertz

TDMA Time Division Multiple Access

UAV Unmanned Aerial Vehicle

VLC Visible Light Communication

VR Virtual Reality

WMIS Weighted Maximum Independence Set

WMN Wireless Mesh Network

Scientific Contributions

All the scientific contributions produced during the doctoral course are listed below.

International Journals:

- G. Iacovelli, F. Vista, N. Cordeschi, and L. A. Grieco. A probability based optimization approach for entanglement distribution and source position in quantum networks. IEEE Journal on Selected Areas in Communications, 2024.

- F. Vista, G. Iacovelli, and L. A. Grieco. "Hybrid quantum-classical scheduling optimization in UAV-enabled IoT networks." Quantum Information Processing 22.1 (2023): 47.

International Conferences:

- F. Vista, V. Musa, G. Piro, L. A. Grieco, and G. Boggia. "Network intelligence with quantum computing in 6G and B6G: Design principles and future directions". In 2021 IEEE Globecom Workshops (GC Wkshps), pp. 1-6. IEEE.

- F. Vista, G. Iacovelli, and L.A. Grieco. "Quantum scheduling optimization for UAV-enabled IoT networks," In Proceedings of the CoNEXT Student Workshop (CoNEXT-SW '21), 2021.

- D. Sparapano, F. Vista, P. Benedetti, G. Piro, and L. A. Grieco. "A Novel Task Offloading Scheme for Robotics Applications in Information Centric Networks". In 2022 IEEE 11th IFIP International Conference on Performance Evaluation and Modeling in Wireless and Wired Networks (PEMWN), pp. 1-6.

Book Contribution:

- F. Vista, V. Musa, G. Piro, L. A. Grieco, and G. Boggia. "Boosting machine learning mechanisms in wireless mesh networks through quantum computing". In IET Wireless Mesh Networks for IoT and Smart Cities: Technologies and applications.

Introduction

In the last thirty years, quantum science and technology have witnessed a consistent rise in interest and investment [1]. In addition, this interest is further supported by massive public funds allocated to advance quantum research, with initiatives like the European Commission's launch of a flagship program worth €1 billion to develop a commercial quantum computer [2]. Furthermore, these significant efforts have been driven by the disruptive potential that promises to exceeds the capabilities of classical computers. In fact, leveraging the principles of quantum mechanics, Quantum Computing (QC) has paved the way for numerous innovative applications that are either impossible or highly challenging to achieve using classical approaches. Specifically, these applications ranges from the simulation of chemical reactions, financial modeling, and optimization within manufacturing and supply chain management. Recently, the telecommunications industry stands out among the different sectors expected to benefit from QC and quantum communications due to their potential in addressing complex computational problems, such as network optimization and resource management [3], [4]. Especially in future mobile communication systems, i.e., 6-th Generation (6G) and Beyond 6-th Generation (B6G), even though significant progress has been made in the fields of Artificial Intelligence (AI) and Machine Learning (ML), the predicted exponential growth of data generated by the users highlights the critical need for a significant boost in processing capability [5], [6].

To close this gap, the scientific community focuses its effort towards reformulating the information theory according to the quantum mechanics framework. This increasing interest is well-founded due to the wide range of applications across different fields, such as Quantum Machine Learning (QML), quantum optimization and quantum communications. In particular, QML and quantum optimization, for instance, can be exploited for boosting the training of ML model [7]–[10] or solving NP-hard optimization problem [11]–[13]. Quantum communications, a relatively emerging field, enables two parties to transmit quantum information by utilizing a pre-established quantum entanglement, offering advantages like anonymous data transmission [14] and the distribution of quantum computation [15].

Despite the advancement of quantum technologies offers immense potential benefits, their integration into existing computing and communication architectures presents several challenges, which are outlined below:

- The integration of quantum computers in future wireless communication networks is still requiring the definition of novel architectures and design principles to embed the deployment of pervasive network intelligence via quantum computing paradigm.

- The telecommunications industry faces a growing demand for solving complex optimization problem. Traditional computing approaches have limitations in handling these large-scale problems efficiently. Adiabatic quantum computing, such as Quantum Annealing (QA), can exploit quantum phenomena to solve real-world problem.

- To achieve a significant increase in computational capabilities, it is imperative to interconnect different quantum devices through quantum communications [16]. One of the primary bottlenecks in quantum communication is photon loss, as entangled photons are transmitted over fiber-optic cables or free-space, resulting in loss and error rates that worsen with increasing connection distance, posing challenges for long-distance quantum communication.

This thesis tackles the aforementioned technological issues in four Chapters. In particular, Chapter 1 presents the main difference between quantum systems and classical systems, deepen into the basic concepts of the quantum mechanics, the teleportation protocol and the adiabatic quantum computing. Chapter 2 provides the design principle and research challenge for integrating quantum computing capabilites into the future wireless communication systems. Chapter 3 outlines the preliminary evaluation and presents the results obtained by solving a binary optimization problem employing the QA technique. Chapter 4 presents a solution for the entanglement distribution problem by take into account the source position as well as any operation that can affect the successful transmission of quantum information. Finally, the last Chapter concludes the work and draws future research perspectives.

Chapter 1

Quantum Information

1.1 Quantum Mechanics Postulates

The underline mechanism governing the physical world remain a mistery. The scientific approach for explaining things around us is through modeling: a specific model or theory becomes a valuable instrument when the difference between what the theory predicts and the actual outcomes are constrained within a predetermined threshold. However, models show different perspective about the nature, offering various explanations on how the world works. Nevertheless, they are not able to explain why the world works in that way [17].

Every theory is built on assumptions that cannot be proven just theoretically, so they need experiments to show if these assumptions match how things really work in the world. In case of quantum mechanics, there are four fundamental assumptions known as postulates [18].

1.1.1 First Postulate

Every isolated physical system is associated with a complex vector space with inner product, i.e., a Hilbert space, referred to as the state space of the system. The state of the system is completely described by its state vector, which is a unit vector in the system's state space.

The simplest closed physical system is a two-dimensional Hilbert space. The first postulate states that the state of the system can represented by means of a two-dimensional vector as a linear combinantion of an orthonormal basis vectors of the Hilbert space. The coordinates of a quantum state vector are often referred as probability amplitudes because they play the role of amplitudes in Schrödinger wave functions describing the location of particles.

1.1.2   Second Postulate

The evolution of any closed physical system in time is described by means of unitary transformation, which depends only on the starting and finishing time of the evolution. Hence, the state $|\psi\rangle$ of the system at time t_1 is related to the state $|\psi'\rangle$ at time t_2 by a unitary operator U which depends on the time t_1 and t_2.

The second postulate describes the evolution of a closed system between discrete time instants, which is more suitable in the context of QC. A more refined version of this postulate describes the continuous-time evolution of a closed quantum system through the Schrödinger equation, which is [19]:

$$i\hbar\frac{\partial |\psi\rangle}{\partial t} = H |\psi\rangle , \tag{1.1}$$

where $\hbar$ denotes the Planck's constant and H represents the so-called Hamiltonian, a Hermitian operator characterizing the evolution of the system. If the Hamiltonian of a system and the Planck's constant are known, it becomes theoretically feasible to completely understand the dynamics of the system [18].

1.1.3   Third Postulate

Any quantum measurement can be described by means of a collection of measurement operators M_m. These operators act on the state space of the system involved in the measurement and the index m refers to the possible results.

If the state of the quantum system is $|\psi\rangle$ immediately before the measurement then the probability that result m occurs is expressed as follows [18]:

$$p(m) = \langle\psi| M_m^\dagger M_m |\psi\rangle \tag{1.2}$$

After the operation of measurement, the state of the system is:

$$\frac{M_m |\psi\rangle}{\sqrt{\langle\psi| M_m^\dagger M_m |\psi\rangle}}. \tag{1.3}$$

Considering that classical probability theory requires that:

$$\sum_m p(m) = \sum_m \langle\psi| M_m^\dagger M_m |\psi\rangle = 1, \tag{1.4}$$

the measurement operators have to satisfy the completeness relation:

$$\sum_m M_m^\dagger M_m = \mathcal{I} \tag{1.5}$$

Considering that measurements are not reversible, they represent the only exception under the unitarity constraint. This type of measurement is often known as complete projective measurement because the observable m is determined by any set of orthogonal projection operators M_m that fulfill the completeness relationship.

1.1.4 Fourth Postulate

The state space of a compound physical system is the product tensor of the state spaces of the component physical systems. If the system is composed of n subsystems and the $i-th$ component is in the state $|\psi_i\rangle$, then the state of the total system is $|\psi_1\rangle \otimes |\psi_2\rangle \otimes \cdots \otimes |\psi_n\rangle$.

This postulate describes how to construct the state space of a quantum system composed of two or more distinct physical systems from the state spaces of the component systems.

1.2 Quantum bit

In classical computation and classical information, the fundamental unit of measure is the bit, which is represented alternately by the digits 0 and 1. Conversely, in the realm of QC, the basic unit of information is the quantum bit (qubit), i.e., a two-dimensional quantum system. According to the first postulate, the state of a qubit can be described using the Hilbert space, denoted as $\mathbb{C}^N$, which encapsulates all the essential information needed to study its probabilistic characteristics. In this vector space, two possible states for a qubit are represented as $|0\rangle$ and $|1\rangle$. These states form an orthogonal basis, also kwnon as computational basis, and can be represented as a column vector using the Dirac notation:

$$|0\rangle = \begin{pmatrix} 1 \\ 0 \end{pmatrix}, \quad |1\rangle = \begin{pmatrix} 0 \\ 1 \end{pmatrix}. \tag{1.6}$$

The vectors $|0\rangle$ and $|1\rangle$ correspond to the two potential outcomes, 0 and 1, in which the state may be found following a measurement. Physically, for instance, a qubit can be described as the polarisation of a photon, where the two orthogonal basis states are the horizontal and the vertical polarisation of the photon. Hence, a qubit can be written as a linear combination of the computational basis states

$$|\psi\rangle = \alpha |0\rangle + \beta |1\rangle = \alpha \begin{pmatrix} 1 \\ 0 \end{pmatrix} + \beta \begin{pmatrix} 0 \\ 1 \end{pmatrix} = \begin{pmatrix} \alpha \\ \beta \end{pmatrix}. \tag{1.7}$$

This formulation, called superposition, better highlights the difference between a classical bit and a quantum bit. In fact, as the former can be in only one state, i.e., 0 or 1, the latter can be in both the states 0 and 1 simultaneously.

The values α and β, called amplitude probability, are complex numbers. The result of the quantum measurement depends directly on these values, which are associated with each state and any further measurement will give the same result. In fact, differently to the classical case, in quantum mechanics, direct observation of the quantum state of a qubit is prohibited. To gain insights into the quantum state, instead, it is allowed to observe the results of the measurements. Hence, when a qubit is measured, it can yield an outcome of 0 with a probability of $|\alpha|^2$ or an outcome of 1 with a probability of $|\beta|^2$. Importantly, these probabilities must satisfy the normalization condition, ensuring that $|\alpha|^2 + |\beta|^2 = 1$.

This normalization condition implies that the state of a qubit is a unit norm vector within a two-dimensional complex vector space. Thus, the (1.7) can be rewritten as
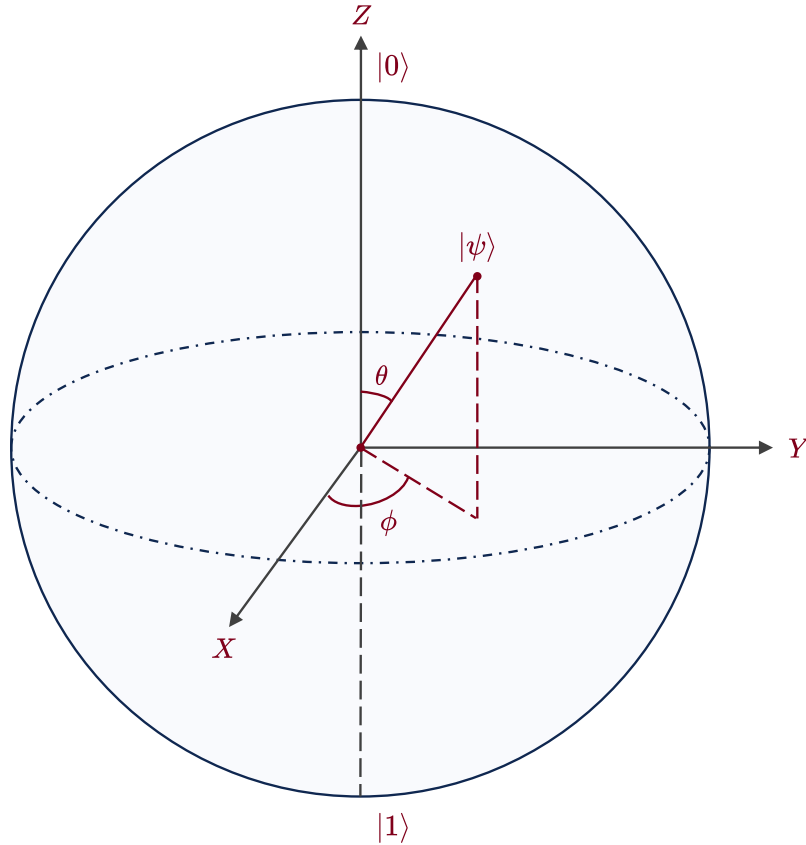
FIGURE 1.1: Geometrical representation of a qubit.

$$|\psi\rangle = e^{i\gamma}(\cos\frac{\theta}{2}|0\rangle + e^{i\phi}\sin\frac{\theta}{2}|1\rangle) = \tag{1.8}$$
$$= e^{i\gamma}(\cos\frac{\theta}{2}|0\rangle + (\cos\phi + i\sin\phi)\sin\frac{\theta}{2}|1\rangle),$$

where γ is a real number and $0 \leq \theta \leq 2\pi$, $0 \leq \phi \leq 2\pi$. The factor $e^{i\gamma}$, known as global phase, has no observable effects and this it can be ignored. Therefore, the wave function in (1.8) can be expressed as follows

$$|\psi\rangle = \cos\frac{\theta}{2}|0\rangle + e^{i\phi}\sin\frac{\theta}{2}|1\rangle, \tag{1.9}$$

and thus, $|\psi\rangle$ can be geometrically represented on a unit sphere in $\mathbb{R}^3$, called Bloch sphere, and is defined by the two angles θ and ϕ. This representation, shown in Fig. 1.1, holds for a single qubit. However, when dealing with more complex systems made up of multiple qubits, the dimension of the space increases, making it challenging to create a suitable visual representation.

When considering a quantum system composed of two qubits, the dimension of the Hilbert space increases. Consequently, a new basis needs to be identified. To achieve this, it is needed to introduce an important operator, which is used to combine vector spaces together to form a larger vector spaces. So, the tensor product of the two states $|\psi\rangle = \begin{pmatrix} \psi_1 \\ \psi_2 \end{pmatrix}$ and $|\phi\rangle = \begin{pmatrix} \phi_1 \\ \phi_2 \end{pmatrix}$ is:

$$|\psi\rangle \otimes |\phi\rangle = \begin{pmatrix} \psi_1\phi_1 \\ \psi_1\phi_2 \\ \psi_2\phi_1 \\ \psi_2\phi_2 \end{pmatrix},$$

or more commonly the resulting state is denoted as $|\psi\rangle \otimes |\phi\rangle = |\psi\phi\rangle$. With this in mind, the new computational basis are:

$$|00\rangle = \begin{pmatrix} 1 \\ 0 \\ 0 \\ 0 \end{pmatrix}, \quad |01\rangle = \begin{pmatrix} 0 \\ 1 \\ 0 \\ 0 \end{pmatrix}, \quad |10\rangle = \begin{pmatrix} 0 \\ 0 \\ 1 \\ 0 \end{pmatrix}, \quad |11\rangle = \begin{pmatrix} 0 \\ 0 \\ 0 \\ 1 \end{pmatrix}.$$

Then, a general state of the two qubit system can be written as follows:

$$|\psi\rangle = \alpha_1|00\rangle + \alpha_2|01\rangle + \alpha_3|10\rangle + \alpha_4|11\rangle,$$

where $\alpha = (\alpha_1, \alpha_2, \alpha_3, \alpha_4) \in \mathbb{C}^4$. Generalizing to N-dimensional quantum systems is a straightforward extension of the principles discussed for one and two qubits. In this context, the Hilbert space expands to $\mathbb{C}^N$, where N represents the dimensionality of the quantum system. The basis for this space consists of orthonormal vectors denoted as $|k_i\rangle_{i=1,...,N}$, where each index, from k_1 to k_N, belongs to the complex space $\mathbb{C}^N$.

In this framework, the state of the quantum system takes the form of a superposition, represented as $\sum_{i=1}^{N} \alpha_i \ket{k_i}$, where $\alpha_i \in \mathbb{C}$ and i ranges from 1 to N. This expression encapsulates the probabilistic amplitudes associated with each basis state, allowing for a versatile representation of quantum states in higher-dimensional spaces. Hence, according to the superposition principle, n qubits can encode all the 2^n possible states at once. As a consequence, the power of QC, as well as the information intrinsically kept, grows exponentially with the number of involved qubits [18].

1.2.1   Operations on qubits

In addition to kets, another fundamental concept in quantum mechanics is the use of bra. Mathematically, a bra is denoted as $\bra{\psi}$ and is formed by taking the conjugate transpose of the corresponding ket, represented as $\ket{\psi}^{\dagger}$. This notation serves as a valuable counterpart to kets and plays a crucial role in quantum mechanics enabling efficient mathematical manipulation and interpretation within the quantum framework. It is also useful to represent operations such as inner products, overlaps, and outer products.

The inner product of two quantum states, $\ket{\psi_1}$ and $\ket{\psi_2}$, is expressed as

$$\braket{\psi_1 | \psi_2}.$$

This operation quantifies the similarity or correlation between the two states and is fundamental in quantum calculations, including measurements and probability calculations.

Furthermore, the concept of overlap, represented as

$$| \braket{\psi_1 | \psi_2} |^2$$

provides a measure of the probability that two quantum states will yield the same measurement outcome. It plays a pivotal role in quantum interference phenomena and the understanding of quantum systems' behavior.

Lastly, the outer product, denoted as

$$\ket{\psi_1} \bra{\psi_2},$$

allows for the construction of quantum operators, which are essential for manipulating and evolving quantum states, making them a cornerstone in quantum algorithms and quantum information processing. The outer product also plays a pivotal role into the definition of density matrices, which are an alternative depiction of quantum states. Consider the state $\ket{\psi}$ of a system, the density matrix for that particular system is

formulated as follows

$$\rho = |\psi\rangle \langle\psi| ,$$

where $|\psi\rangle$ refers to a pure state. The derivation of this term stems from the concept that only having the information of $|\psi\rangle$ allows for the representation of a system in which all its particles assume an identical physical configuration. For example, the density matrix of a single-qubit pure state $|\psi\rangle = \alpha_1 |0\rangle + \alpha_2 |1\rangle$ is given by

$$|\psi\rangle \langle\psi| = \begin{bmatrix} |\alpha_1|^2 & \alpha_1\alpha_2^* \\ \alpha_1^*\alpha_2 & |\alpha_2|^2 \end{bmatrix}.$$

If $|\alpha_1|^2 > 0$ and $|\alpha_2|^2 > 0$, while satisfying the condition $|\alpha_1|^2 + |\alpha_2|^2 = 1$, then the system is in a superposition state of $|0\rangle$ and $|1\rangle$. Significant details are contained within the complex coefficients α_1 and α_2, revealing both the phase and amplitudes of the corresponding states $|0\rangle$ and $|1\rangle$. Conversely, mixed states only provide insights into the probabilities of encountering the system in one state or the other. The density matrix of a mixed state is defined as the sum of density matrices of pure states, weighted by probabilities:

$$\rho_{mixed} = \sum_{i=1}^{\#\text{ pure states}} p_i |\psi_i\rangle \langle\psi_i| .$$

This is the most general formula for a density matrix. It also allows to see that density matrices have unit trace, are positive semi-definite and Hermitian. Specifically, the eigenvalues are p_i and the eigenvectors, also called eigenstates, are $|\psi_i\rangle$ [18].

1.3 Quantum Gates

In order to control the state of a qubit, similar to classical computers, gates are essential. The operation that a gate performs on a qubit can be visualised as a rotation on the Bloch sphere of a vector $|\psi\rangle$ representing the qubit's state. The quantum gates X, Y, and Z are often denoted as σ_x, σ_y and σ_z and in their matrix representation are called Pauli matrices. Each Pauli matrix specifies a π radians rotation around a particular axis of the Bloch sphere up to a global phase [20], [21]. In the following equations are reported the common quantum gates and their representation as matrices.

$$\sigma_I = I = |0\rangle \langle 0| + |1\rangle \langle 1| = \begin{bmatrix} 1 & 0 \\ 0 & 1 \end{bmatrix} \tag{1.10}$$

$$\sigma_x = X = |0\rangle \langle 1| + |1\rangle \langle 0| = \begin{bmatrix} 0 & 1 \\ 1 & 0 \end{bmatrix} \tag{1.11}$$

$$\sigma_y = Y = i(|1\rangle \langle 0| - |0\rangle \langle 1|) = \begin{bmatrix} 0 & -i \\ i & 0 \end{bmatrix} \tag{1.12}$$

$$\sigma_z = Z = |0\rangle \langle 0| - |1\rangle \langle 1| = \begin{bmatrix} 1 & 0 \\ 0 & -1 \end{bmatrix} \tag{1.13}$$

$$H = \frac{1}{\sqrt{2}}[(|0\rangle + |1\rangle) \langle 0| + (|0\rangle - |1\rangle) \langle 1|] = \frac{1}{\sqrt{2}} \begin{bmatrix} 1 & 1 \\ 1 & -1 \end{bmatrix} \tag{1.14}$$

From a mathematical perspective, gates are depicted as matrices that operate on quantum states using vector notation. However, not all matrices can serve as gate representations, they must be unitary. Given a complex-valued matrix U, it is unitary when it satisfies the following condition

$$U^\dagger U = I. \tag{1.15}$$

These matrices preserve the inherent reversibility of quantum mechanics, implying that performing two gates on a quantum state will lead back to the initial state. In QC, state manipulation involves applying a unitary operation since remains a reversible process. One key characteristic of unitary matrices is their ability to preserve the norm. In fact, since qubit states live within the Hilbert space $\mathbb{C}^N$, the inner product correspond to the conventional euclidean norm. This can be exploited to demonstrate that unitary operators maintain norm integrity:

$$\|U |\psi\rangle\|^2 = \langle \psi| U^\dagger U |\psi\rangle = \langle \psi|\psi\rangle = \|\langle \psi|\|^2 ,$$

where $|\psi\rangle \in \mathbb{C}^N$. As a consequence of this property, the application of gates to qubits does not alter probability amplitudes. This is a fundamental aspect because most quantum algorithms are constructed using sequences of gates. With this assurance, it is possible to proceed with quantum computations without concern that the application of gates will affect the probabilities of our desired outcomes.

1.3.1 X Gate

The Pauli-X gate, known also as bit-flip gate, is the quantum equivalent of the NOT gate for classical computers with respect to the standard basis $|0\rangle$, $|1\rangle$. In particular, its action is the following

$$|0\rangle \to |1\rangle, \quad |1\rangle \to |0\rangle$$
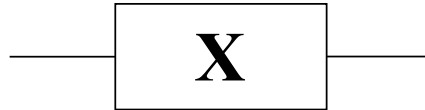
FIGURE 1.2: Graphical representation of an X gate.

1.3.2 Y Gate

The Pauli-Y gate is a single-qubit rotation through π radians around the y-axis.

$$|0\rangle \to i\,|1\rangle, \quad |1\rangle \to -i\,|0\rangle$$

FIGURE 1.3: Graphical representation of an Y gate.

1.3.3 Z Gate

The Pauli Z, sometimes called phase-flip, leaves the basis state $|0\rangle$ unchanged and maps $|1\rangle$ to $-|1\rangle$.

$$|0\rangle \to |0\rangle, \quad |1\rangle \to -|1\rangle$$
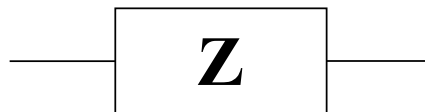
FIGURE 1.4: Graphical representation of a Z gate.

1.3.4 Hadamard Gate

The Hadamard gate performs a rotation of π about the axis $\frac{(\hat{x}+\hat{z})}{\sqrt{2}}$ at the Bloch sphere.

FIGURE 1.5: Graphical representation of an H gate.

It creates an equal superposition state if given a computational basis state:

$$|0\rangle \rightarrow \frac{|0\rangle + |1\rangle}{\sqrt{2}} = |+\rangle , \quad |1\rangle \rightarrow \frac{|0\rangle - |1\rangle}{\sqrt{2}} = |-\rangle .$$

1.3.5 CNOT Gate

A multi-qubit quantum logic gate, known as the Controlled NOT (CNOT) gate, involves two input qubits: the control qubit and the target qubit. The circuit is represented in Fig. 1.6, where the top line represents the control qubit, while the bottom line represents the target qubit. The action of the gate can be described as: when the control qubit is set to 0, the target qubit remains unchanged. However, if the control qubit is set to 1, the target qubit undergoes a flip [22].
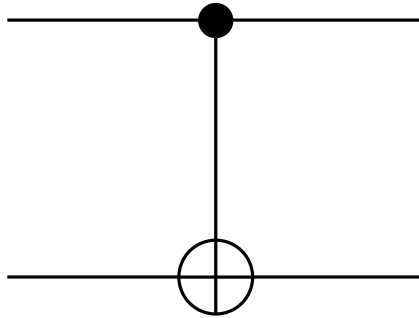
FIGURE 1.6: Graphical representation of a CNOT gate.

1.4 Entanglement

Quantum entanglement is a strange phenomena that does not have a counterpart in classical world, in fact, it describes a multi-particle systems of two or more particles that can no longer be described as a combination of independent one-particle states, but only as a common state, which in principle must be described within a single wave function [23], [24]. This strange quantum correlations still remain valid

also even if the particles are delivered onto two distant locations. In fact, even if the entangled particles are separated by billions of miles, a variation in one particle induces a change in the other. Actually, even though quantum entanglement appears to transmit information instantaneously, it does not violate the classical speed of light [17].

The Bell states, also defined as Bell pairs, Einstein-Podolsky-Rosen (EPR) states or EPR pairs, are maximally entangled pure two-qubit states [25]. Maximal entanglement means that Bell pairs have the strongest non-classical correlations of all possible two qubit states.

$$|\Phi^+\rangle = \frac{|00\rangle + |11\rangle}{\sqrt{2}} \tag{1.16}$$

$$|\Phi^-\rangle = \frac{|00\rangle - |11\rangle}{\sqrt{2}} \tag{1.17}$$

$$|\Psi^+\rangle = \frac{|01\rangle + |10\rangle}{\sqrt{2}} \tag{1.18}$$

$$|\Psi^-\rangle = \frac{|01\rangle - |10\rangle}{\sqrt{2}} \tag{1.19}$$

These four pure states, which are maximally entangled, form an orthonormal basis of the Hilbert space of the two qubits. The Bell pairs, thus quantum entanglement, are a key resources to enable teleportation in quantum networks. Accordingly, two remote quantum computers which want to communicate must share entangled particles. In this context, three different methods can be employed to generate and distribute entanglements [26].

The first method, referred to as Spontaneus Parametric Down-Conversion (SPDC) [27], generates an entangled photon pair by manipulating their polarization. A nonlinear crystal is illuminated by a laser beam, creating two photons with vertical and horizontal polarizations. These photons, known as flying qubits, traverse the quantum channel to reach the designated nodes. Subsequently, at each node, the flying qubits are converted into computational qubits using transducer devices to execute quantum operations.

The second method employs optical fibers to link optical cavities between nodes [28], [29]. Specifically, entanglement is initiated at the sender's side by exciting an atom with a laser beam, which causes the emission of a photon entangled with the atom. This photon travels through the optical fiber to the receiving node and is absorbed by an optical cavity. This process effectively transfers the entanglement from the atom-photon pair to an atom-atom entanglement.

The third method also utilizes optical cavities and generates entanglement between remote quantum computers [30]. In this approach, both atoms are simultaneously excited to create entanglement. The emitted photons then interact with a specialized device capable of performing a Bell State Measurement (BSM). This measurement converts the atom-photon entanglement on both sides into an atom-atom entanglement, thus linking the remote quantum computers.

1.5   Quantum Teleportation

Quantum teleportation is a protocol that allows to send quantum information by linking the quantum state of the sender to the receiver's one [31]. It was theoretically proposed in 1993 [32] and then it was experimentally realized in 1997 by two research groups, led by Sandu Popescu and Anton Zeilinger, respectively [33], [34]. Subsequently, experiments validating quantum teleportation have encompassed diverse carriers of information, such as photons, atoms, electrons, and superconducting circuits. These investigations have also explored teleportation over different distances. Notably, a groundbreaking milestone was successfully achieved in 2017 over a distance of 1,400 km using the Micius satellite for space-based quantum teleportation [35].

Since teleportation allow to send quantum information without the transmission of physical particles that stores the quantum state, i.e., data qubits, which would be irremediably lost due to attenuation or environment interaction. For this reason, in order to perform teleportation, an entangled pair, i.e., flying qubit, needs to be distributed between the source and destination. As shown in Fig. 1.7, to teleport an unknown quantum state $|\varphi\rangle$ from a sender to a receiver, the former applies a set of operations on the data qubit and the flying qubit $|\Phi^+\rangle$. This sequence of steps, referred to as BSM, involves specific operations. This entails initiating a CNOT gate between the received flying qubit and the data qubit, followed by an H gate and two quantum measurements. The CNOT gate triggers a flip in the target qubit $|\Phi^+\rangle$ if the control qubit, like $|\varphi\rangle$, is in the state one; otherwise, the target qubit remains unaltered. Subsequently, an H gate is employed on the initial qubit, inducing a superposition state. Quantum measurements are then performed, yielding results denoted as c_1 and c_2, which are conveyed to the receiver through a classical channel. To retrieve the original state, the receiver applies X or Z gates (or both) based on the provided correction bits. Notably, due to the nature of BSM, both the data qubit and the flying qubit held by the sender are destroyed during teleportation. Furthermore, the recovered quantum state must be transferred to a data qubit using the SWAP instruction [36] in order to be used. Considering that the measurement at the source destroys the entangled pair,
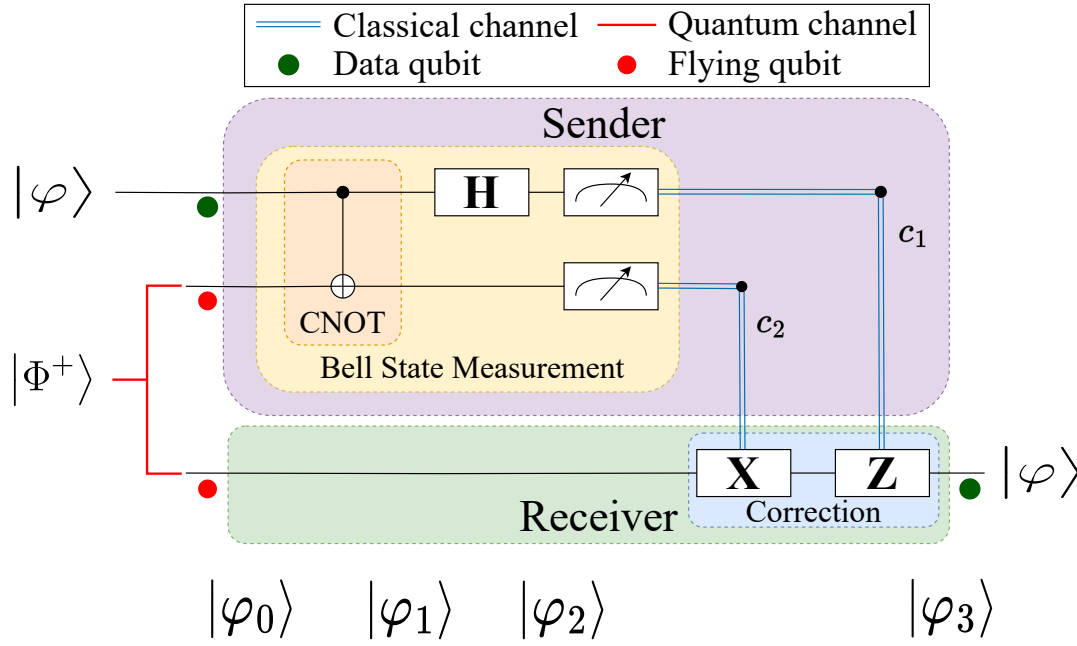
FIGURE 1.7: Quantum teleportation circuit.

if another qubit needs to be teleported, it is necessary to distribute a new Bell pair between the source and the destination. The following part analyses the phases of the teleportation process in more detail considering the circuit depicted in Fig. 1.7.

Suppose there are two distant parties, Alice and Bob. Alice has a qubit $|\psi_C\rangle = \alpha |0_C\rangle + \beta |1_C\rangle$, where α and β are unknown amplitudes, that she wants to send to Bob via a classical channel. Without further resources this would be impossible, because the amplitudes may require an infinite number of bits of precision to write them down exactly [17]. Suppose Alice also shares with Bob an EPR-pair, i.e., Alice holds the first qubit and Bob the second, their joint state is

$$|\psi_0\rangle = |\psi_C\rangle |\Psi_{AB}^+\rangle =$$
$$= \frac{1}{\sqrt{2}}[\alpha |0_C\rangle (|0_A0_B\rangle + |1_A1_B\rangle) + \beta |1_C\rangle (|0_A0_B\rangle + |1_A1_B\rangle)] \qquad (1.20)$$

Henceforth, for notational simplicity, the subscripts on the ket will be suppressed. This convention by keeping will consider the first two qubits belong to Alice, while the third one to Bob. The desired state transfer is achieved through the following steps.

1. Alice sends her qubits through the CNOT port obtaining

$$|\psi_1\rangle = \frac{1}{\sqrt{2}}[\alpha |0\rangle (|00\rangle + |11\rangle) + \beta |1\rangle (|10\rangle + |01\rangle)] \qquad (1.21)$$

2. She then sends her first qubit through the Hadamard gate, which maps the basis
   state $|0\rangle$ to $(|0\rangle + |1\rangle)/2$, and the state $|1\rangle$ to $(|0\rangle - |1\rangle)/2$ obtaining

$$|\psi_2\rangle = \frac{1}{2}[\alpha(|0\rangle + |1\rangle)(|00\rangle + |11\rangle) + +\beta(|0\rangle - |1\rangle)(|10\rangle + |01\rangle)] \quad (1.22)$$

The equation can be rewritten as follows:

$$\begin{aligned}|\psi_2\rangle = &\frac{1}{2}[|00\rangle\,(\alpha\,|0\rangle + \beta\,|1\rangle) + |01\rangle\,(\alpha\,|1\rangle + \beta\,|0\rangle) + \\ &+ |10\rangle\,(\alpha\,|0\rangle - \beta\,|1\rangle) + |11\rangle\,(\alpha\,|1\rangle - \beta\,|0\rangle)]\end{aligned} \qquad (1.23)$$

3. Alice then measures her qubits relative to the computational basis to obtain a
   2-bit string 00, 01, 10 or 11.

Note that the the unitary operations in (i) and (ii) simply serve to rotate the Bell basis
into the computational basis of the two qubits and Bob's qubit now is disentagled from
the qubits of Alice, i.e., it is in a fixed transformation of $|\psi\rangle$ [37]. In fact, depending
on the outcomes of the measurement and not on the α and β values, Bob's qubit state
is in one of the following possible state:

$$|\psi_3\rangle = \alpha\,|0\rangle + \beta\,|1\rangle \tag{1.24}$$

$$|\psi_3\rangle = \alpha\,|1\rangle + \beta\,|0\rangle \tag{1.25}$$

$$|\psi_3\rangle = \alpha\,|0\rangle - \beta\,|1\rangle \tag{1.26}$$

$$|\psi_3\rangle = \alpha\,|1\rangle - \beta\,|0\rangle \tag{1.27}$$

The measurement outcomes, i.e., c1 and c2, are sent through the classical channel to
Bob, which applies the appropriate quantum gates on his qubit in order to recover the
state $|\psi\rangle$, as shown in Table 1.1. Note that no remnant of any information about $|\psi\rangle$
remains with Alice: after step (iii) she is left with only a 2-bit string, chosen uniformly
and randomly, while the original state is always totally destroyed. Consequently, the
teleportation process is fully consistent with the no-cloning theorem, as indeed it must
be. Furthermore, it is important to highlight that Bob's ability to restore the original
state depends entirely on the classically shared bit pair from Alice. Thus, this method
does not enable faster-than-light communication, which is in full accordance with the
special relativity theory.

Outcome	Corrections
00	I
01	X
10	Z
11	XZ

TABLE 1.1: Correction gates to recover the original state.

1.6 Adiabatic Quantum Computing

In the realm of QC, there exist two distinct approaches for operating on qubits: universal gate-model and analog quantum computers. The former are the most common and widely discussed quantum computers [38]. They operate using qubits and quantum gates, similar to classical bits and logic gates in classical computers. The key advantage of universal gate-model quantum computers is their ability to implement any unitary transformation on qubits through a sequence of quantum gates. This property is known as quantum universality, and it means that such a quantum computer can theoretically simulate any quantum system and execute any quantum algorithm given enough qubits and resources [39]. The latter, instead, which includes adiabatic quantum computers, takes a different approach. Instead of manipulating qubits through quantum gates, these computers are designed to evolve a quantum system from an initial state to a final state that encodes the solution to a problem. Adiabatic quantum computing is based on the adiabatic theorem from quantum mechanics and it involves setting up a Hamiltonian, which carries information about the energy of the system, and gradually changing it over time to let the system evolve into its ground state, which contains the solution to the problem [40].

Both approaches have their strengths and limitations, and the choice of which one to use depends on the specific problem being solved and the technological advancements in building and controlling qubits. Universal gate-model quantum computers are more flexible and can potentially solve a wider range of problems, while analog approaches like adiabatic quantum computing might outperform at certain optimization and sampling problems [41].

The study of Hamiltonians and their associated eigenvalues and eigenvectors, often referred to as eigenstates, assumes a pivotal role. The smallest eigenvalue is called ground state energy and the corresponding eigenstate is the state in which the system reaches the lowest value of energy. Any other state for which the corresponding eigenvalue is greater is called excited state. In adiabatic quantum computing, the idea is to transform the initial Hamiltonian into a final Hamiltonian that represents the solution to a problem. If this transformation is carried out slowly enough, according to the adiabatic theorem, the system will remain in its ground state throughout the evolution,

and measuring the qubits at the end of this process will provide the desired solution
[42].
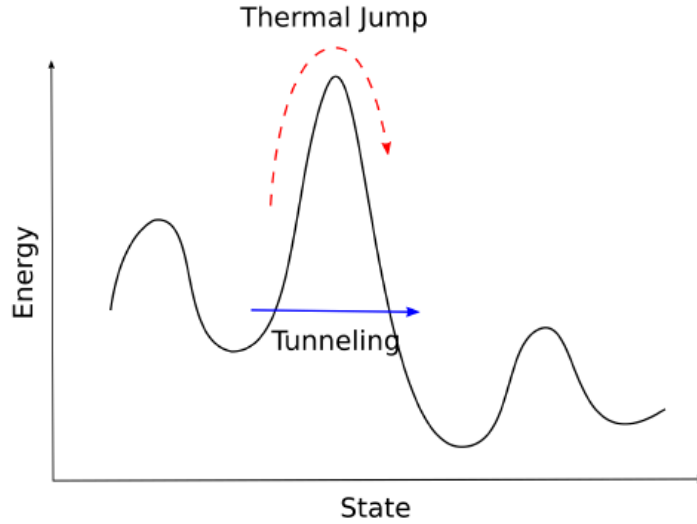
FIGURE 1.8: Sketch of an energy landscape described by a Halmitonian. While optimizing
the cost function of a problem, classical simulated annealing try to escape local minima via
thermarl jump (red). Quantum annealing, instead, relies on quantum-mechanical fluctuations
to enable quantum tunneling through energy barriers (blue). When the energy barrier is high,
classical thermal jump becomes very difficult. However, if the barrier is narrow enough,
quantum tunneling can facilitate the traversal of barriers [41].

In order to use adiabatic quantum computers, also called quantum annealears, the
objective function of an optimization problem is indeed mapped to a Hamiltonian,
where the ground state, i.e., the lowest energy state, of the Hamiltonian corresponds to
the optimal solution of the problem. This mapping is crucial for solving optimization
problems on quantum annealers like those built by D-Wave Systems [43].

In Fig. 1.8 is shown a sketch of an energy landscape drawn as a function of the
configuration of the system. To minimizes the energy of the system, qubit undergo
a process called quantum annealing and it works in a very similar way to its classi-
cal counterpart, i.e., Simulated Annealing (SA). Specifically, qubits start in an initial
configuration, each associated with a specific energy value (related to the optimiza-
tion problem's objective function). This initial configuration serves as a starting point
for the optimization process. Then, the quantum system evolves over time and it tends
to transition into lower-energy states, thereby working towards the objective of min-
imizing the system's energy (and, by extension, optimizing the objective function).
This evolution occurs under the influence of a time-dependent Hamiltonian. Similar
to classical simulated annealing, where the search for a solution depends on a tem-
perature parameter, the goodness of the system's configuration in quantum annealing
is determined by its energy. Lower energy configurations are preferred because they

correspond to better solutions. As the annealing process continues, the quantum system gradually reaches a state that minimizes its energy. This state may represent a local minimum or even the global minimum of the energy landscape, depending on the specific problem and annealing parameters.

The main difference between these two approaches lies in a unique property of quantum systems known as quantum tunneling. Quantum system, in fact, can transition between different energy levels without the need to climb uphills in the Hamiltonian, as depicted by the blue line in Fig. 1.8. On the other hand, simulated annealing is forced to occasionally accept solutions that are worse with respect to the current one based on a probability that depends on temperature. This may lead to suboptimal solution, but is necessary for simulated annealing to escape local minima and is reffered to as a thermal jump, as illustrated by the red dotted line in Fig. 1.8. In summary, quantum annealing and simulated annealing share the idea of gradually improving a system's configuration to minimize energy or optimize an objective function. However, quantum annealing leverages quantum effects, such as tunneling, to explore energy landscapes more efficiently and potentially find solutions that are challenging for classical methods to reach.

Since quantum annealing is a process that strongly relies on properties of physical systems that naturally try to reach the ground state configuration, leds to the construction of quantum hardware with significantly more qubits compared to gate-based quantum computers. However, this advantage comes with a trade-off: quantum annealers are not universal computers, unlike gate-model quantum computers, which means they have limitations in terms of the operations they can perform. In mathematical terms, this limitation means that quantum annealers are specialized for a single type of Hamiltonian, specifically the Ising model. Let σ_i denote the spin of i-th qubit in an n-qubit system, then the Ising Hamiltonian takes the form:

$$H_{Ising} = \sum_{i=1}^{n} h_i \sigma_i + \sum_{i=1}^{n} \sum_{j=i+1}^{n} J_{i,j} \sigma_i \sigma_j, \tag{1.28}$$

where $\sigma_i \in \{-1, 1\} \quad \forall i = 1, \ldots, n$ and h_i and $J_{i,j}$ are coefficients called biases and couplers.

The inherent limitations of state-of-the-art quantum annealers, such as their ability to solve only a specific subset of optimization problems and the lack of constant control over qubit states, have strongly debates regarding whether they are advantageous over classical computing [38]. Nevertheless, ongoing advancements in their development have resulted in notable improvements in their performance. Consequently, researchers and technology companies are increasingly utilizing quantum annealers to explore their potential in addressing a wide range of large-scale tasks [44]–[46].

Chapter 2

Boosting Network Intelligence Through Quantum Computing

In this Chapter, two innovative architectures are introduced to integrate the usage of quantum computers into the future wireless communication systems. This concept is built upon a set of fundamental principles that pave the way for enhancing computational capabilities addressing the increasingly stringent performance requirement of emerging networks. The highlighted design principles and the corresponding research challenges are crucial to revolution the nowadays computing capabilities, leading to a new research area.

2.1   Introduction

In the last decade, the demanding of new services with ultra-reliability, low latency, high data rate, and increasing user density was met through the development of 5-th Generation (5G) mobile communication networks. While further studies are done for the realization of the 3GPP Release 16, concluding the 5G standardization, the scientific community is already investigating the next frontier of mobile communication networks, such as 6G and beyond, and Wireless Mesh Networks (WMNs) [47]–[49]. The growing stringent of Key Performance Indicators (KPIs) will be accomplished by innovative enabling communication, network management, and computing technologies. From the communication perspective Terahertz (THz) band communications, Visible Light Communications (VLCs), Intelligent Reflective Surfaces (IRSs), and cell-free massive Multiple-Input/Multiple-Output (MIMO) will be deployed for achieving high communication data rates [50]. The network management, instead, will still be supported by softwarization and virtualization techniques already used, like Software-Defined Networking (SDN), Network Function Virtualization (NFV), and network slicing.

Furthermore, the pervasive adoption of ML algorithms as computing technology will provide intelligence features, supporting the growing heterogeneity and complexity [51]. Despite ML is gaining momentum in the scientific community, arising as a key approach for several novel applications, the expected voluminous amount of data to be processed in future wireless communication systems will require excessive computing power and computational time [52].

In this direction, the emerging of QC could be a turning point, allowing to speed-up the training phase and making ML techniques suitable also for computationally complex and real-time applications. While most of the scientific contributions on QML focus on the design and implementation of specific algorithms (see for example [53]–[56]), very few works introduce QML as an essential building block for future wireless communication systems [52], [57], [58]. Unfortunately, the integration of quantum computers in 6G and B6G systems, as well as in WMNs, the investigation of the resulting network architectures, and the analysis of design implications derived from the deployment of pervasive network intelligence schemes still represent an unexplored research topic.

To provide initial answers in this direction, this work presents design principles for a QC-aided network intelligence and illustrates the related emerging research challenges. The study considers both centralized and distributed network architectures, properly extending the architectures with specific nodes to support QC functionalities. The former is supposed to sustain QML by means of quantum computers developed by Tech Giants in their clouds. Considering that IBM, Google, and Microsoft already have quantum computers with up to a hundred qubits [59] (and further improvements are expected in the next years), the centralized architecture could be an initial reasonable approach. At the same time, the growing scientific interest and the technological advancements in quantum computing systems is expected to enable, in a very far future, the interconnection among geographically distributed quantum devices by means of quantum Internet (as explicitly stated in [60]). This approach may lead towards the design of a distributed architecture where simpler quantum computers are deployed at the edge of the network. The pros and cons of both architectures are deeply investigated by considering communication latency, network congestion, load balancing, security, and implementation facets.

2.2 6G and Beyond: KPIs and Communication Technologies

The challenging KPIs characterizing the emerging services and applications will require the strengthening of some methodologies already born with the 5G, as well as the introduction of novel enabling technologies [47], [61], [62]. For instance, SDN and NFV paradigms will still sustain network management tasks. The pervasive monitoring of network equipment and users' behaviour is fundamental for dynamically configuring virtualized network functionalities and isolating resources and services within specific portions of the network, namely network slices [47]. Differently, new communication schemes, like THz, VLCs, IRSs and cell-free massive MIMO, are gaining momentum for providing very high data rates in scenarios with reduced or controllable noise and propagation phenomena [61], [62]. Nevertheless, excepting these valuable network management and communication technologies, network intelligence will significantly boost the evolution of 6G and B6G.

2.2.1 Key Performance Indicators

The continuous evolution of the societal needs demands the enhancement of performance requirements with respect to 5G [50]. The main differences, illustrated in Fig. 2.1, are [63]:

- *Data rate.* In 6G services, the peak and experienced data rate will reach at least 1 Tbps and 1 Gbps, which are approximately 100 and 10 times that of 5G, respectively.

- *Latency.* Given that most of 6G use cases are real-time, the expected latency is lower than 1 ms and the required jitter will be 1 μs.

- *Mobility.* While 5G networks aim at providing high Quality of Service (QoS) also in cases with 500 km/h mobility, 6G is expected to serve users in much higher mobility scenarios (i.e., $\geq$ 1000 km/h).

- *Connectivity density and traffic capacity.* 6G networks will support 10 times the connectivity density of 5G, reaching up to 10^7 devices/km^2 and an area traffic capacity up to 1 Gb/s/m^2.

- *Spectrum and energy efficiency.* In 6G, the peak and experienced spectrum efficiency will be 2-10 times those of 5G, respectively. The expected energy efficiency, instead, is 10–100 times that of 5G networks.
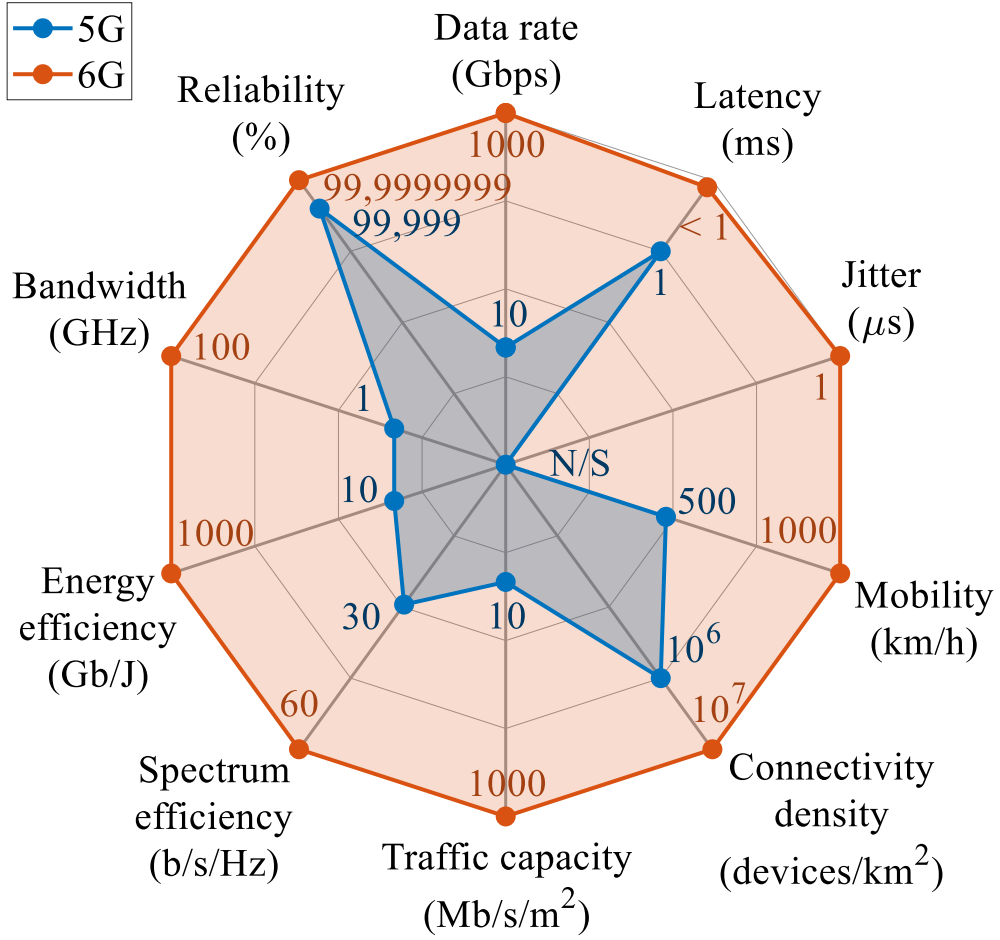
FIGURE 2.1: Comparison between 5G and 6G KPIs.

- *Bandwidth and reliability.* 6G use cases will demand also 100 times the bandwidth of 5G and higher reliability (i.e., 99.9999999%).

To satisfy these KPI, it is required the development of new enabling technologies for 6G and beyond [47]. Fig. 2.2 depicts the timeline of the main communication, network management, and computing technologies from 5G to B6G.

2.2.2   Communication Technologies

The growing demand of higher data rate can be achieved with the adoption of THz band communications and VLC, exploiting frequency bands never considered before. Communications in the THz band (i.e., 0.1 - 10 THz) is enabled by the usage of novel materials for transceiver and antenna design. This frequency band supports very high data rate communications, paving the way to novel 6G applications, such as local and personal area networks, data center networks, wireless network on chip, nano-networks, and inter-satellite communications [47]. Nevertheless, the high adopted frequencies lead to side effects (e.g., propagation loss, molecular absorption, and
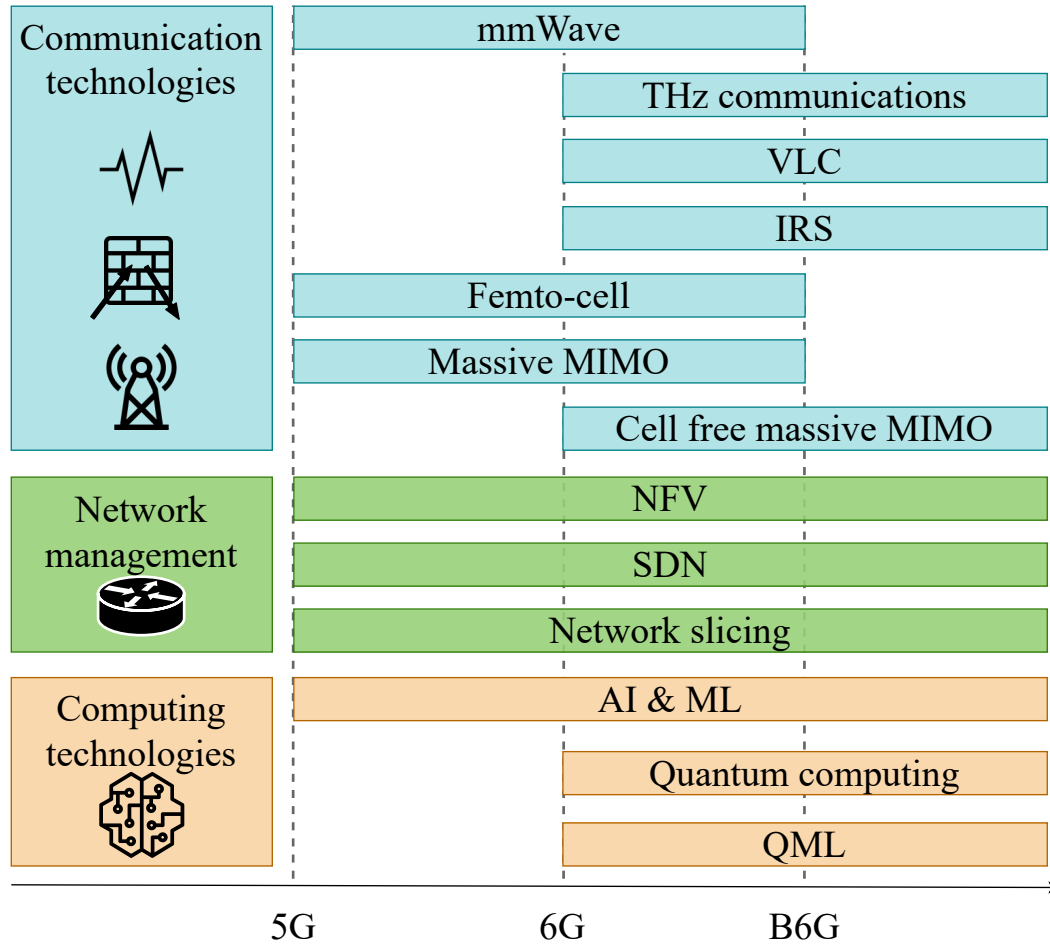
FIGURE 2.2: Enabling technologies from 5G to B6G.

high penetration loss), drastically reducing the communication distance. On the other hand, VLC exploits higher frequency (i.e., 400 - 800 THz), using a source of light (e.g., light emitting diode) able to modulate signals with different light intensities. Its introduction can extend the cellular coverage and guarantee high-speed data rate in indoor and outdoor scenarios, such as vehicle-to-vehicle and vehicle-to-infrastructure. However, VLC suffers from noise given by other source of light and has a limited coverage range [62].

To provide higher communication distances and not only line-of-sight communications, the environment can be exploited as a controllable signal reflector introducing new type of passive reflectarrays, called IRSs. Control algorithms and IRSs, deployed on surfaces like building facades, ceilings, or walls, can be used to dynamically control the reflection angle of the impinging electromagnetic signals, thus allowing non line-of-sight communications, enhancing the strength of the received signal, and reducing interference given by multiple user in a restricted area [47]. Moreover, IRSs enable the usage of emerging holographic radio, thus improving spectrum efficiency and network capacity [61].

The growing connectivity density and area traffic capacity will cause an increasing of inter-cell interference due to users located at the cell boundaries. To avoid these kinds of interference, 6G networks will be deployed as a cell-free architecture, where each user is associated with all Base Station (BS), or with a subset of BS collaborating with each other [47]. This architecture, called cell-free massive MIMO, will strongly reduce the overhead due to handovers, also guaranteeing the expected QoS [62].

The usage of these technologies will be supported by ML techniques providing intelligence to the whole network.

2.2.3 Use cases

The proposed network architectures aim at supporting the wide and heterogeneous range of 6G use cases, depicted in Fig. 2.3. They can be grouped in the following application areas: 1) Mobile Broadband Reliable Low Latency Communications (MBRLLC) combining data rate, latency and reliability requirements; 2) massive Ultra Reliable Low Latency Communications (mURLLC) including massive communications with low latency and high reliability; 3) Human-Centric Services (HCS) supporting novel applications in medical field [61].

Virtual and Augmented Reality

Augmented Reality (AR) and Virtual Reality (VR) allow users to add artificial 3D models to the environment (e.g., text and/or multimedia information) and to dive in a digitally reproduced reality, respectively. The human interaction with the virtual environment must be real-time, leading to limited communication latency requirements. Moreover, the huge amount of data to be transmitted demands high data rate and spectrum efficiency, thus requiring THz band communications, and large area traffic capacity, enabled by cell-free architectures [63].

Unmanned Vehicles

Unmanned vehicles are mobile devices that can be remote controlled or can autonomously move by sensing their environment, supporting many applications. For instance, drones can be used for search and rescue operations, agriculture, and infrastructure inspection, while autonomous cars can be useful in transportation public systems, offering safe travel and improving traffic management. Here, key issues are the increasing number of equipped sensors and the need of high level of safety for humans also in mobility scenarios, thus requiring growing data rate, high reliability, and low latency. THz communications and VLC can be exploited to enable high data

rates, IRS deployed on building facades can reduce the attenuation of THz spectrum and cell-free massive MIMO can guarantee safety requirements in mobility cases [63].
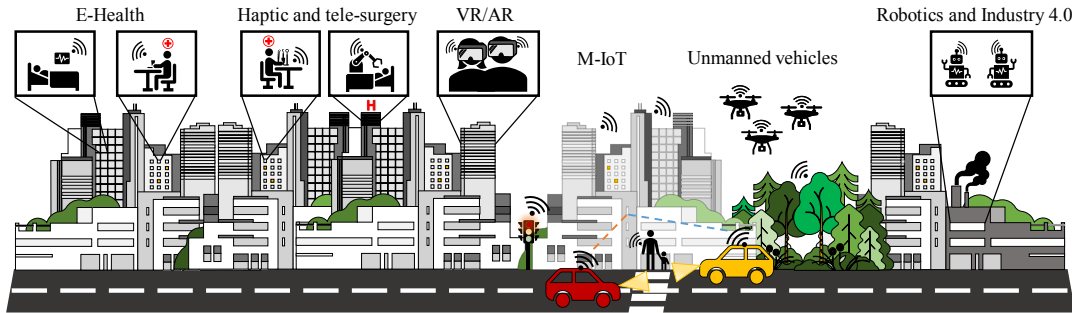
FIGURE 2.3: 6G application scenarios.

Massive Internet of Things

The main characteristic of 6G networks will be the interconnection of a massive number of Internet of Things (IoT) devices able to efficiently transmit small amount of data. This kind of fully connected devices enables a wide area of indoor and outdoor applications, like smart factories or fully integrated smart cities. The expected growing number of involved devices causes the increment of generated data and the inter-cell interference, demanding for new enabling technologies, like THz communications, VLC, and cell-free massive MIMO [64].

Robotics and Industry 4.0

Robotics and Industry 4.0 is emerged as a new paradigm to revolutionize the manufacturing environment. In future 6G networks, robots will be equipped with ML capabilities to improve their sensing ability and decision-making operations, thus supporting real-time processes (i.e., low latency and jitter) and transmitting huge amount of data. High data rates and spectrum efficiency requirements can be fulfilled by using THz communications, where attenuation is reduced by IRS deployed of the walls inside the factories [64].

E-Health

In healthcare domain, intelligent devices (e.g., e-Health sensors) can early detect medical information and send them to a remote doctor, exploiting 6G communication technologies [62]. In this context, Internet of Nano Things (IoNT) is emerging as a new paradigm where nano-devices can be implanted, ingested, or worn by humans to collect information directly from inside the body. The high number of involved devices must communicate huge amount of data in real-time guaranteeing high QoS

and energy efficiency, also in mobility scenarios. THz communications and VLC can support the required data rate, while cell-free massive MIMO guarantees the QoS avoiding handover issues.

Haptic and Tele-Surgery

Haptic communications allows the remote interaction between humans and robots, thus enabling new applications especially in healthcare domain. For instance, a doctor can perform a clinical examination or a surgery operation without the physical presence of the patients, exploiting robots and receiving visual information feedback through flat screens (i.e., display and tablet) or immersive 3D models (i.e., AR and VR) [62]. In this context, the main requirements are: latency and reliability due to the critical application scenarios; spectrum efficiency, area traffic capacity, and data rate due to the complex and voluminous data to be exchanged. These KPIs can be accomplished with communication technologies like THz communications, VLC, and cell-free massive MIMO.

2.3   Wireless Mesh Networks

The ever-increasing demand of data rate and node density, along with low latency and reliability features, makes the introduction of WMNs a key solution for future wireless communication networks [48], [49]. WMNs, in fact, are self-organised and self-configured networks, where every node is able to autonomously establish and manage its connection to the network in real-time. In detail, a WMN consists of two different types of nodes, named Mesh Routers (MRs) and Mesh Clients (MCs). MRs, as in traditional wireless communication systems, are usually equipped with multiple interfaces to integrate the WMN with internet and various existing wireless networks (e.g., wireless sensor networks, wireless-fidelity (Wi-Fi), and mobile networks). MCs, instead, correspond to typical wireless devices which, differently from MRs, can be mobile and cannot be used as gateways (e.g., laptops, mobile phones, and tablets) [65]. Based on node functionalities, WMNs can be deployed by following three different network architectures. In backbone WMNs, only MRs build the mesh network by creating an infrastructure for clients and providing access to the backbone by leveraging existing wireless interfaces. In client WMNs, instead, also end-users act as relay nodes forwarding incoming packets through the network. To reduce the overall network cost and complexity of the previous architectures, the hybrid WMN considers that each MC can directly communicate with neighbouring MCs or access the mesh network exploiting MRs.

Despite the manifold advantages introduced by the adoption of WMNs in terms of reliability, network installation costs, long-range communications, and large-coverage connectivity, several critical factors negatively affect WMN performance, including network capacity and management issues, scalability, and mobility [65], [66]. Some of these drawbacks can be partially solved through the introduction of novel enabling technologies already investigated by the scientific community. For instance, the network flexibility and capacity can be strongly enhanced by the introduction of single-user or multi-user MIMO systems [67], [68]. Moreover, several works exploit unique capabilities of SDN paradigm, such as global visibility, real-time programming, and agility, to guarantee optimal network management and further improve the system performance [69], [70]. The QoS of the communication system can be also enhanced by the adoption of IRSs which improve the Signal to Noise Ratio (SNR) both in Line of Sight (LoS) or Non-Line of Sight (NLoS) scenarios by exploiting the environment as a controllable signal reflector [71]. A further improvement in terms of capacity and QoS, while guaranteeing secure and fault-tolerant communications, is provided by the application of ML algorithms to solve design and management tasks in WMNs [72]. In the last years, in fact, the scientific community is promoting the adoption of ML techniques to strongly enhance the network adaptability according to real-time conditions also in highly variable scenarios.

2.4 Machine Learning Overview

ML algorithms are a subset of AI tecnhiniques that are used to learn the characteristics of a system when specific conditions are met, including the absence of an exact mathematical model and the availability of a huge volume of training data. These models account for a wide range of tasks, such as classification, regression, and enabling intelligent agents to interact with their environments. A general overview of some of ML methods is provided in the following.

Supervised Learning. It is a fundamental paradigm in machine learning. In this approach, the model learns from a labeled training dataset, which consists of input-output pairs. Hence, the training dataset is crucial, as it serves as the foundation for the model to learn and generalize from. The goal is to develop a model that can predict the correct output for new, unseen input data. To this end, supervided learning algorithms aim to minimize a loss function, which quantifies the difference between the model's predictions and the actual target values in the training datasets. This is done in an iterative manner by modifying the hyperparameters of the model, such as learning rate and network architecture, in order to optimize the model performance on the training data. Supervised learning is widely used in various applications, including

image classification, speech recognition, natural language processing, and medical diagnosis [73].

Unsupervised Learning. As opposed to supervised learning, it is a machine learning paradigm where the algorithm works with unlabeled data to discover patterns or structures within it. In unsupervised learning, the model is not provided with explicit output labels. Instead, it must explore the data and find hidden relationships or groupings. One common application is clustering, where the algorithm groups similar data points together based on their intrinsic characteristics. It is also used for dimensionality reduction or detecting data points that deviate significantly from the norm [74].

Reinforcement Learning (RL). It operates by utilizing a feedback mechanism, often referred to as a reward, which is generated by the environment in response to specific actions or decisions made by an agent. The objective is to iteratively refine the agent's behavior by maximizing the cumulative reward received. This learning approach can be viewed as a middle ground between supervised and unsupervised learning. In particular, it is commonly employed for solving problems related to control, decision-making, and classification.

Deep Learning (DL). It is a sub-field of ML which involves multiple layers for the processing of input raw data in order to progressively extract higher-level features. It commonly uses an artificial neural network composed of many perceptrons organised in multiple dense hidden layers. To properly train a model, it also needs an initial step useful to tune the hyperparameters starting from a huge amount of data. Specifically, DL algorithms train the model by minimising the loss function over the training dataset and extracting the weights of the final model [75].

Deep Reinforcement Learning (DRL). It combines two sub-fields of ML: RL and DL. To efficiently use RL, in fact, agents must infer a good representation of the environment, thus choosing the action which maximises the reward by following a trial and error strategy. However, if the state spaces or action spaces are too large, this decision can be a complex task that requires more computational time. In this context, DL can help agents to make decisions by learning policies directly from high-dimensional and unstructured input data [76].

Federated Learning (FL). This techniques, in the last years, is arising as a new distributed learning approach. Since traditional centralized ML algorithms require users to transmit their collected data to a central server for training purpose, this can lead to privacy issues. Furthermore, in some cases, may be impractical and uncovenient

transmit local data for training a ML models. In this context, FL enables to collaboratively learn a shared ML model without the data transmission by sending to the central server only the parameter of the model trained with local data. Then, the server generate a global FL model and sent it back to the users.

2.5 How to Achieve Network Intelligence

Thanks to their ability to extract fine-grained analytics from available data, ML and QML are key instruments to achieve network intelligence.

2.5.1 The Role of ML in 6G and B6G systems

According to the scientific literature, in the context of 6G and B6G systems, ML algorithms can be used at different network levels to retrieve technical details through data mining, investigate and predict the system behaviour, and optimally configure communication protocols, resources, and services, also at large scale [47]. Few valuable examples are reported below.

- At the physical layer, deep and convolutional neural networks are used for optimizing Orthogonal Frequency Division Multiple (OFDM) receivers, signal classification, channel decoding, and signal detection [77]. ML is also employed for channel estimation to optimally choose the communication frequency and control the IRSs reflection angle, thus reducing attenuation effects of high-frequency communications [47].

- At the data-link layer, ML algorithms optimize the packet retransmissions process and the dynamic allocation of network resources, while reducing network overhead and latency also in heterogeneous scenarios [57].

- At the network layer, ML techniques predict data contents to be cached in specific places of the network, choose serving and target cells during handover, and efficiently balance the network load with traffic classification [77]. The prediction of users' mobility sustains NFV/SDN paradigms to optimally configure the network and allocate communication and computing resources.

- At the application layer, ML studies packet features (e.g., packet sizes and inter-arrival times) and classifies the application type of data stream in order to optimize the resource allocation [77].

Pervasive network intelligence is a cornerstone enabling factor also for many 6G and B6G use cases. Table 2.1 summarizes the main KPIs and the involved communication technologies for these use cases, and highlights the main role covered by ML techniques.

TABLE 2.1: Communication features and network intelligence usage in main 6G and B6G use cases.

Application Area	Use cases	Main KPI	Communication Technologies				How is ML used?
			THz	VLC	IRS	Cell-free	
MBRLLC	**VR/AR**	Peak data rate: > 1 Tbps Traffic capacity: 1 Gbps/m^2 Spectrum efficiency: $2 - 10$x Latency: < 1 ms	✓			✓	- predict users' mobility; - estimate channel conditions; - allocate network resources; - reduce network traffic by reproducing the interested image portion.
	Unmanned vehicles	Peak data rate: > 1 Tbps Connectivity density: 10^7 d/km^2 Mobility: 1000 km/h Reliability: 99.9999999% Latency: < 1 ms	✓	✓	✓	✓	- optimize the vehicles path; - predict vehicles mobility; - recognize obstacles; - optimize the resource allocation.
mURLLC	**M-IoT**	Connectivity density: 10^7 d/km^2 Energy efficiency: $10 - 100$x	✓	✓		✓	- identify patterns; - classify the collected data; - adapt communication features based on environment conditions; - predict users' mobility.
	Robotics and Industry 4.0	Peak data rate: > 1 Tbps Jitter: 1 μs Spectrum efficiency: $2 - 10$x Latency: < 1 ms	✓		✓		- optimize data processing; - robot localization; - improve the human-robot interaction.
HCS	**E-Health**	Peak data rate: > 1 Tbps Connectivity density: 10^7 d/km^2 Energy efficiency: $10 - 100$x Reliability: 99.9999999% Mobility: 1000 km/h	✓	✓		✓	- detect medical diseases; - drive real-time decisions of devices; - support the doctor in treatments prescription.

	Haptic and telesurgery	Peak data rate: > 1 Tbps
		 Traffic capacity: 1 Gbps/m^2
		 Spectrum efficiency: $2 - 10$x
		 Reliability: 99.9999999%
		 Latency: < 1 ms
			✓	✓		✓	- predict and reproduce doctor's movements
							  in case of packets loss;
							 - network traffic reduction by reproducing
							  the interested image portion.

2.5.2   The Role of ML in WMNs

Unlike optimisation schemes, ML algorithms are strongly adaptable to environmental conditions, resulting particularly suitable for time-variable use cases, such as WMN-based applications. Given that, they can also be used in WMNs to solve different design and management tasks [77]. Fig. 2.4 summarises the main ML algorithms exploited in WMN scenarios, which are explained in details as follow:

- **Supervised learning.** In this context, the most commonly used algorithms for WMNs are Decision Tree (DT), Support Vector Machines (SVMs), and K-Nearest Neighbors (KNN), typically performing classification or regression tasks. Specifically, DT algorithms exploit a tree-like structure to solve both classification and regression problems. The attributes of the input data are compared with features labelling internal nodes of the tree. Starting from the root node and performing these comparisons, the algorithm traverses the tree until it reaches the leaf nodes which represent the class or the relationship between dependent and independent variables. SVM, instead, is a ML technique commonly used for classification tasks. In this case, the algorithm constructs
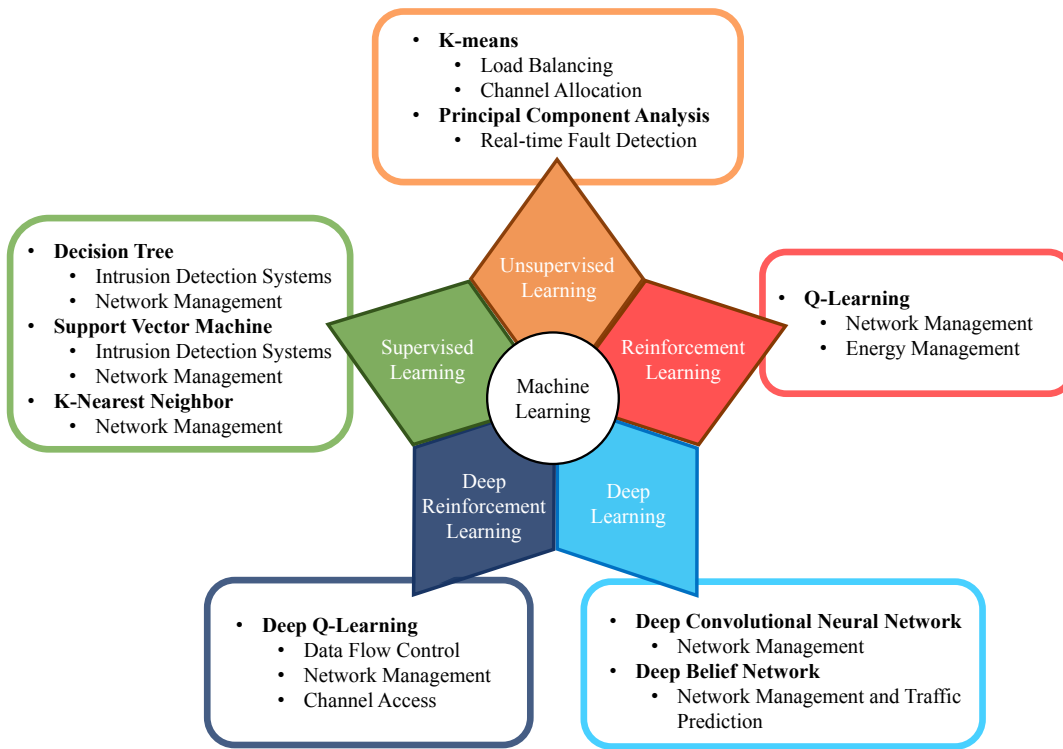
FIGURE 2.4: Summary of ML techniques and corresponding role in WMNs.

hyperplanes aiming at maximising the width of the gap between points belonging to different classes in order to increase the classification precision of successive input data. SVM and DT algorithms are employed in WMNs to build efficient cross-layer-based [78] and network-layer-based [79] intrusion detection systems. In this case, the model is trained starting from packet delivery ratio, packet arrival interval, and end-to-end delay statistics in order to easily detect anomalous behaviour and remove malicious nodes. These algorithms are also integrated with a threshold that avoids false decisions. An easier algorithm used to perform both classification and regression tasks is the KNN. Here, the input data is classified by considering a similarity concept (i.e., every data point falling near others belongs to the same class). Considering an IoT network supported by a software-defined WMN, the presented supervised learning approaches (i.e., DT, SVM, and KNN) are used for optimising the management of the network and perform time granular analysis of the network traffic. The comparison among these learning strategies demonstrated that the KNN algorithm provide the best performance in terms of accuracy [69].

- **Unsupervised learning.** The main unsupervised algorithms used in WMNs are

K-means and Principal Component Analysis (PCA). K-means is a clustering algorithm that groups the input unlabelled data in k clusters with an iterative procedure. Specifically, at each iteration, the n observations are grouped in order to minimise the variance intra-cluster and maximise the distance inter-cluster. Here, the distance, usually measured through a Euclidean metric, is computed considering the cluster centres, named centroids. The iterative procedure ends when the algorithm converges. In WMNs, K-means can be used for the load balancing of the network [80] or the channel allocation [72]. In detail, load balancing is performed in order to optimise the resource allocation, increase the overall load of the network, and reduce the congestion at the gateways [80]. Moreover, the K-means clustering can be used to group the MRs efficiently, choosing the cluster head according to the computed centroid [72]. The PCA algorithms, instead, aim at reducing the data dimensionality by describing each data point only with several uncorrelated principal components, while maintaining the highest training-data variance in the first component. Given that the PCA algorithm allows handling high-dimensionality application scenarios, it is particularly suitable for real-time fault detection in high-interference environments, such as WMNs [81].

- **Reinforcement Learning.** The most known RL algorithm is the Q-learning. Its main feature is the capability to train a model without the knowledge of the environment. Q-learning algorithms, in fact, are based on a Q-value that is updated at each iteration: the optimal action corresponds to the largest cumulative Q-value. In WMNs, RL strategies can be exploited for routing purposes in order to decide the optimal route, among many possible paths, to take from source to destination node. RL fits very well with this kind of problem: the next MR could be chosen, at each iteration, from a set of possible actions in that state. Moreover, Q-learning can be used to avoid critical problems, such as the congestion at the gateway, by dynamically learning an optimal routing scheme that considers several metrics (e.g., loss-ratio, interference, and load at the gateways) [82]. Since classical routing protocols may suffer from excessive energy consumption and do not consider past experience, Q-learning can also optimally enhance the energy balance of the network [83].

- **Deep Learning.** The main DL architectures used for WMNs are Deep Convolutional Neural Network (DCNN) and Deep Belief Network (DBN). DCNN is an example of DL architectures, mostly used in computer vision. In this case, the classification task is performed by filtering the input data using convolution layers in order to extract low-level information. Then, the size of the

extracted features is reduced by pooling layers, thus obtaining the output of the fully connected layer (i.e., a vector which contains the result of the classification process). In WMNs, gateways receive traffic information from both MRs and MCs, leading to a higher probability that several nodes become congested. To overcome this issue, DCNN can be used to periodically train a model in order to make optimal routing decisions based on past events [84]. On the other hand, DBN is a class of deep neural network defined as a stack of Restricted Boltzmann Machines (RBMs), which is a two-layer undirected graphical model. Each RBM layer is connected with both the previous and next layers and the nodes alongside any layer are not connected with each other. Since RBMs training process is unsupervised, a DBN ending with a Softmax layer can be used both for classification and clustering of unlabelled data. This makes the DBNs algorithms particularly suitable in WMNs to improve the network management operations in terms of network traffic prediction [85].

- **Deep Reinforcement Learning.** The most promising example of DRL for WMNs is the Deep Q-Learning Network (DQN). DQN combines deep neural networks and Q-learning in order to estimate and maximise the Q-values by considering both states and rewards. It can be employed in WMNs to control the data flow and enhance the throughput. In fact, classical control flow methods suffer from the continuous growth of the number of mesh nodes and the complexity of data applications which make these kinds of scenarios strongly dynamic. DQN, instead, intrinsically has the capability to manage and optimise complex traffic communication flows [86]. DRL algorithms can also be used for optimally planning the network in real-time, thus optimally deploying gateways in the WMN and choosing the network topology [87]. Moreover, DRL can manage the channel access in dynamic spectrum scenarios, where multiple discrete channels are shared by different types of nodes without any a priori knowledge [88].

2.5.3   Open Issues in the Application of ML

When considering the application of ML in the context of 6G/B6G and WMNs, several unique challenges and open issues emerge. ML algorithms often demand extensive computation times and high computing power.

Regarding the 6G/B6G applications where low-latency communication and real-time analysis are essential. Meeting QoS constraints while handling resource-intensive ML computations can pose a significant challenge. Moreover, as this system expand, the number and types of devices involved grow exponentially. This results in larger

and more heterogeneous datasets. Since the time to train traditional ML methods is heavily influenced by the dimensionality for the data, this would lead to a longer training times that can potentially causing delays incompatible with real-time requirements.

The aforementioned issues for 6G/B6G are still valid for WMNs. However, here, another problem is related to the dynamic and ever-changing nature of this network systems. For this reason, the ML models applied in WMNs need costant updates to accurately reflect the network behavior. Thus, a periodical re-training of ML models becomes necessary, introducing management overhead.

In summary, the application of ML in 6G/B6G and WMNs faces challenges related to computation efficiency, resource allocation, data management, and the dynamic nature of network environments. Addressing these issues will be crucial to harness the full potential of ML in these advanced wireless communication systems. To do this, the development of novel strategies to enable intelligent decision-making without excessive delays are needed.

2.5.4   Quantum Machine Learning

Thanks to quantum mechanics principles (i.e., quantum superposition, quantum decoherence, no-cloning theorem, and quantum entanglement), QC is gaining momentum as a new technology able to solve complex problems that would otherwise be impossible with classical computers [60].

The combination of QC and ML is emerging as a new powerful technique to improve learning algorithms [53]. Specifically, depending on whether the input data and the information processing system are quantum or classical, there are four different approaches to merge QC and ML [54], [89]:

- *Classical-classical approach*. It implements quantum-inspired classical algorithms on classical computers. Here, classical data are processed by classical computers, by employing traditional ML algorithms based on quantum principles theory.

- *Quantum-classical approach*. It consists in employing ML techniques in a QC system. In particular, ML can help quantum computers to learn from data. For instance, ML can be used to analyse measurement data, thus reducing the number of measurements of a quantum state.

- *Classical-quantum approach*. It is commonly known as QML. This approach aims at translating classical ML algorithms into a quantum-compliant language to take advantage of quantum mechanics by running it on quantum computers.

The adoption of this approach requires a pre-processing step to convert the classical input data into suitable data for quantum computers. Nowadays, the research community proposes several encoding methods, such as basis encoding and amplitude encoding [54], [56].

- *Quantum-quantum approach*. It aims to develop quantum algorithms to manipulate quantum data. In this approach, it is not required to encode data, as the input is directly the quantum state of the system.

In particular, this work considers the third approach, as in the real world scenario most of the input data are classical. Moreover, since quantum-inspired algorithms are executed on classical computers, the achievable speed-up is not comparable with running it on quantum computers [53].

In this context, due to the continuous growth of the number of devices involved, consequently, the amount of exchanged information, QML can help to speed up algorithms used in future wireless communication systems. In fact, it can improve the computational time, thus getting results faster and also in real-time, as well as increasing the learning capacity and efficiency by discovering more intricate patterns from the input data [57], [90]. In detail, preliminary studies on the performance comparison between QML and ML algorithms demonstrated that the QML is convenient in the case of high-dimensionality input data [91]. Hence, future wireless networks must take into account the possibility to jointly use traditional ML and QML capabilities by supporting the integration of quantum computers.

Nevertheless, QC and its application in QML have to face significant hardware challenges. Quantum states, which form the basis of QC, are highly fragile, susceptible to the decoherence principle, and can be perturbed by gate operations, ultimately restricting the capabilities of quantum computers. To mitigate these issues, the scientific community has proposed two primary strategies. Firstly, the embedding of quantum circuits into specialized large-scale infrastructures equipped with cooling systems capable of maintaining temperatures near absolute zero is suggested [59]. Secondly, the preservation of qubit states can be achieved through the implementation of quantum error correction schemes, which distribute the information originally associated with a single logical qubit across several physical qubits [92].

Expanding the number of operational qubits can enhance the computational power. In fact, the search space of QC exponentially increases with the number of qubits. This can be accomplished by distributing machine learning algorithms across multiple interconnected quantum computers, with a centralized control system managing the distributed computing resources [93]. However, unlike classical data, quantum information cannot be copied due to the no-cloning theorem, which prohibits traditional

error correction mechanisms and imposes limitations on communication distances. Nonetheless, quantum states can be transferred using quantum communication methods like entanglement and teleportation. This capability opens the door to leveraging quantum communication to improve QC capabilities, creating a network of interconnected quantum computers that share a higher number of qubits, recently denoted as the quantum Internet [60].

2.6 Design Principles for QC-aided Network Intelligence

The application of QML methodologies in future wireless communication systems, such those introduced before, can be achieved only with the definition of novel network architectures. In fact, the integration of quantum and traditional computers performing QML and ML algorithms, respectively, requires new logical entities embedded with new functionalities. To this end, this Section presents design principles for the realisation of two innovative network architectures, denoted by centralized and distributed approaches, able to combine the benefits provided by traditional and quantum computers deployed either in the cloud or at the edge of the network.

2.6.1 Centralized Architecture Overview

The integration of QML functionalities requires the introduction of quantum computers in their architectures. Nowadays, some Tech Giants, such as IBM, Google, and Microsoft, have already developed quantum computers with up to a hundred qubits, also envisioning strong improvements in this direction for the next years [59]. Accordingly, a first suitable approach for integrating quantum computers can be achieved using the Tech Giants' quantum computer by accessing their cloud to perform QML algorithms.

Centralized Architecture for 6G and B6G

The centralized architecture for 6G and B6G systems, depicted in Fig. 2.5, is described across four general tiers:

- The access network hosts heterogeneous network attachment points, which offer mobile connectivity through different wireless communication technologies (i.e., mmWaves, THz communications, VLC, IRS, and so on).
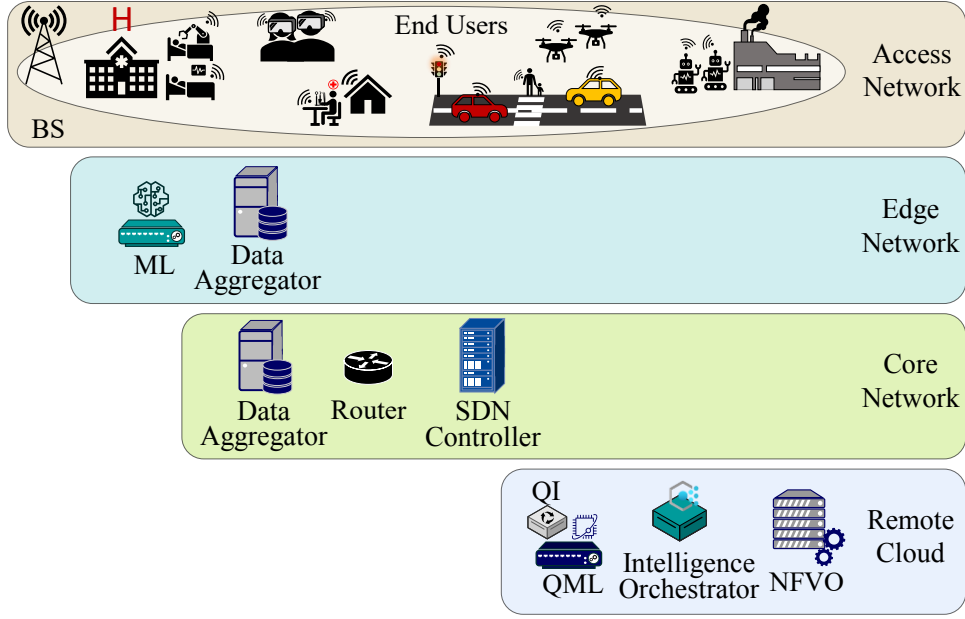
FIGURE 2.5: 6G and B6G centralized deployment.

- The edge network provides a flexible interface between access and core networks, while managing virtualized network functionalities and implementing advanced services and applications very close to the end-users.

- The core network forwards traffic flows across geographically distributed nodes. Its features are dynamically monitored and configured by SDN controllers.

- The remote cloud provides network and service management functionalities through the Network Function Virtualization Orchestrator (NFVO) and computing resources to the entire network.

All the resources that an infrastructure provider deploys across the four tiers can be exploited by various service providers for offering vertical services. Without loss of generality, the discussion below assumes that a single service provider has data available in its network. But, the whole protocol architecture can be easily extended by considering the possibility to perform data mining and big data analytics on information shared across organizations and boundaries.

As for the current 5G deployments, a service provider can still use nodes at the network edge with their local computing capabilities for executing very simple ML tasks. At the same time, the centralized architecture takes advantage of quantum computers in the cloud for carrying out QML techniques. In this context, service providers can leverage the computing capabilities of third-party tech giants such as IBM, Google, and Microsoft for QML tasks, subject to subscription fees. The allocation of computing resources among ML and QML tasks is done by a centralized Intelligence Orchestrator, deployed in the remote cloud.
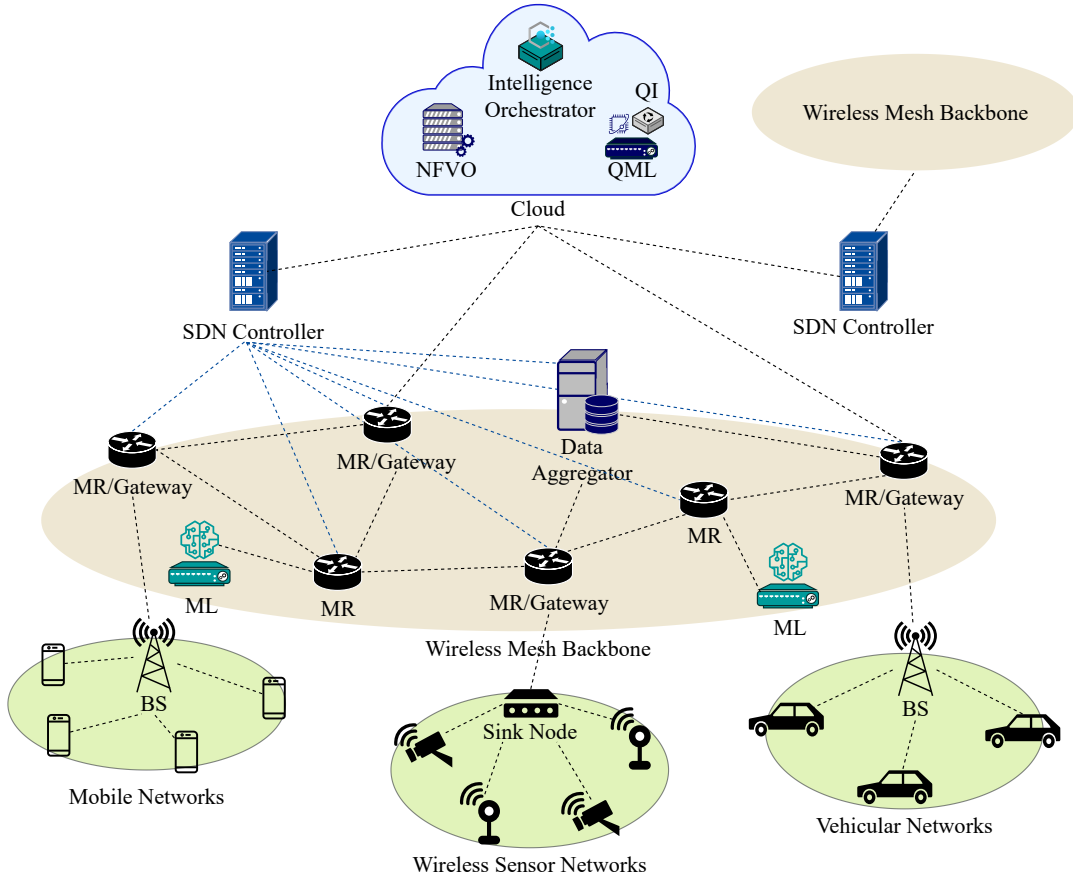
FIGURE 2.6: WMNs centralized deployment.

Centralized Architecture for WMNs

The proposed architecture for WMNs is composed of three main components:

- The access network includes all the application scenarios sustained by the WMN (e.g., mobile networks, wireless sensor networks, and vehicular networks) and the related network attachment points which provide the connection to the mesh network (e.g., BS and sink node).

- The wireless mesh backbone hosts MRs (with or without gateway capabilities), a Data Aggregator node which stores and transmits dataset for intelligence operations, and traditional computers designed for solving simple and low-dimensionality ML problems. Furthermore, given the heterogeneity and complexity of the wireless mesh backbone, the traffic flow is managed by an SDN controller, thus avoiding network congestion issues.

- The remote cloud provides orchestration and high-dimensionality computational capabilities to the overall network. In detail, the Intelligence Orchestrator performs the allocation of computing resources among ML and QML

tasks according to their data-dimensionality, while the NFVO provides service management functionalities.

Both architectures emphasize the use of centralized intelligence for allocating computing resources, with an Intelligence Orchestrator playing a key role. Quantum computers in the cloud are leveraged for QML tasks, and SDN controllers manage traffic flow for optimized network performance.

The Information Exchange in the Centralized Architecture

As illustrated in Fig. 2.7, the information exchange in the centralized architecture can be summarised as in what follows.

- *Phase 1: Dataset Creation.* Each node belonging to the network generates information data to be processed by traditional or quantum computers for the purposes listed in Sections 2.5.1 and 2.5.2. The collected data strongly depends on the considered node. While end-users (e.g., mobile phones, sensors, and vehicles) acquire data from the surrounding environment, such as channel quality indicators and performance levels of high-level applications, network equipment (e.g., MRs, BSs, sink nodes, SDN controllers, and NFVO) provide information related to the network functionalities, such as bandwidth and energy consumption. All the collected data are transmitted to Data Aggregators by means of REST or RESTful communication protocols in order to increase the performance, scalability, simplicity, and reliability of the network. Then, Data Aggregators pre-process incoming data and compare them with existing network information in order to create and/or update datasets useful for intelligence operations.

- *Phase 2: Tasks Assignment.* The Intelligence Orchestrator must assign the generated datasets to computing resources (e.g., traditional or quantum computers). To this end, given the huge amount of data to be exchanged, the Data Aggregators periodically create and transmit to the Intelligence Orchestrator a data descriptor message containing high-level information about the available datasets, such as data format, data size, and statistical variability with respect to previous updates. Starting from this information and considering the status of computing resources, the Intelligence Orchestrator performs the task allocation and sends a task assignment message to the Data Aggregators in order to efficiently transmit the datasets to designed traditional or quantum computers.
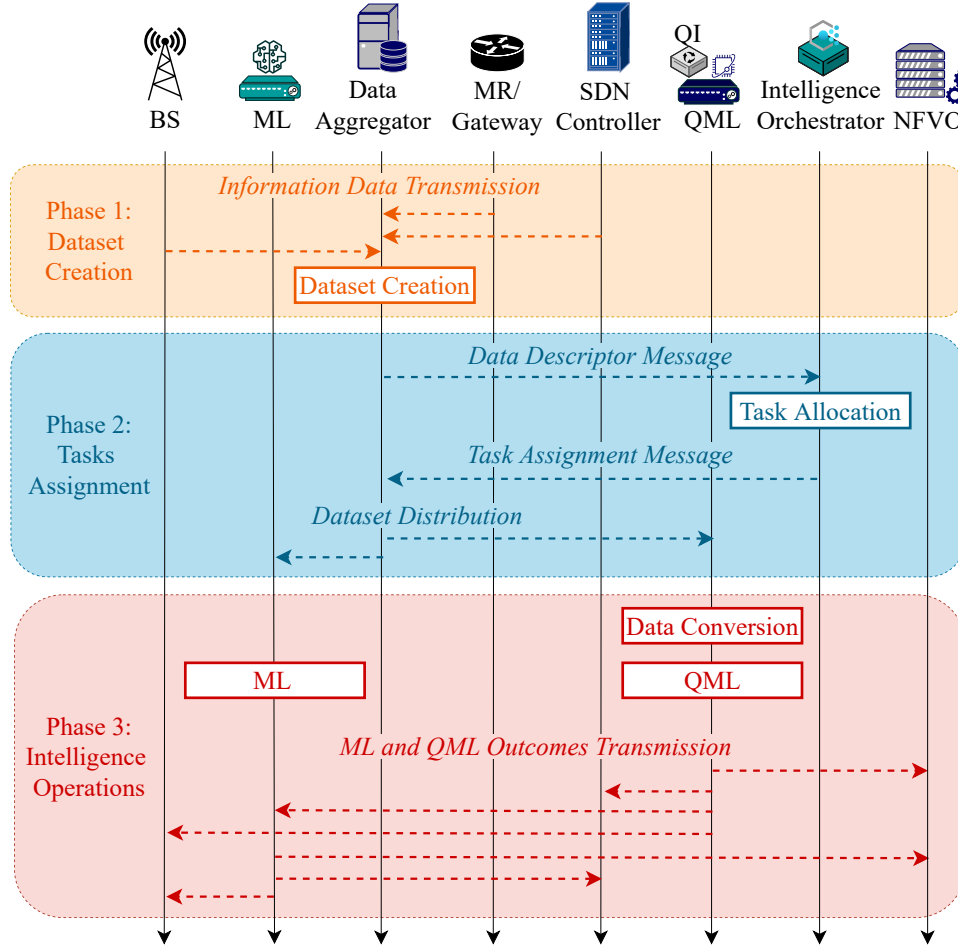
FIGURE 2.7: Message sequence diagram of the centralized architecture.

- *Phase 3: Intelligence Operations.* Quantum computers in the cloud offer a suitable environment where implementing QML techniques. However, classical data cannot be directly used as input of quantum computers. Accordingly, when QML capabilities are required, a Quantum Interface (QI) logical entity is first used for converting classical data into quantum data, and vice-versa. Without loss of generality, this work considers that these logical entities are directly equipped in the quantum computer. After the data pre-processing, ML and QML operations are performed by traditional and quantum computers, respectively, thus obtaining the corresponding outcomes (e.g., the hyperparameters of the model in case of learning procedures; classification, prediction, or specific actions in other cases). These results are, finally, transmitted to different network equipment for specific purposes, ranging from service management to network optimisation. For instance, the NFVO can exploit these outcomes for optimally managing upper layer services and allocating virtual resources among active applications. SDN controllers, instead, dynamically configure network functionalities (e.g., flow forwarding and load balancing) and solve

complex routing problems based on users' mobility and traffic dynamics. Finally, edge nodes and BSs use ML and QML outcomes to update ML models or perform resource scheduling and allocation.

2.6.2 Distributed Architecture Overview

Today, the availability of quantum computers and qubits is severely restricted due to physical and economic constraints. Consequently, the centralized approach appears as the most practical strategy for implementing QC-aided network intelligence. Nevertheless, in a long-term vision, the scientific community envisions a future where geographically distributed quantum computers are interconnected through the quantum Internet [60]. In such a scenario, a distributed architecture becomes feasible, allowing for the direct execution of complex QML algorithms at the network's edge. In this distributed model, service providers could strategically deploy their quantum computers, each equipped with a limited number of qubits, to manage deployment costs effectively.

Distributed Architecture for 6G/B6G and WMNs

The distributed quantum computing architecture, depicted in Fig. 2.8 for 6G/B6G and in Fig. 2.9 for WMNs, introduces a framework that can be applied to both scenarios while addressing the constraints of limited quantum computing resources.
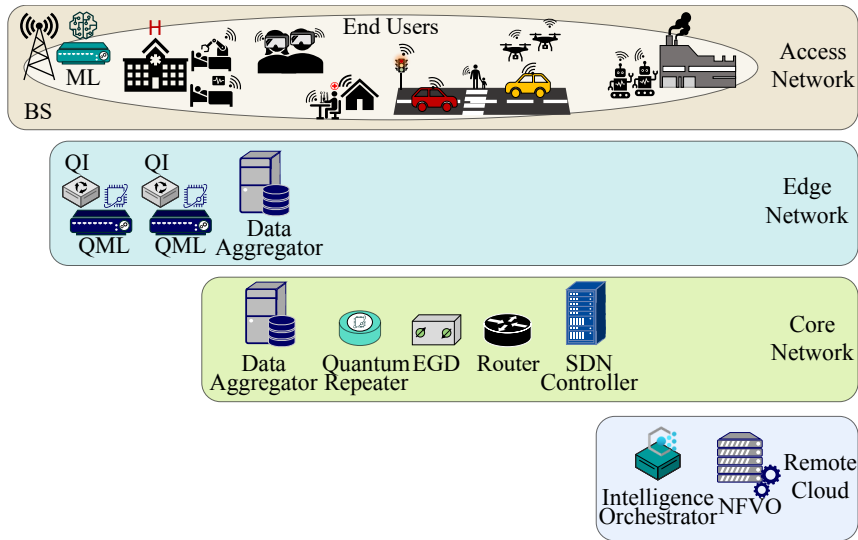
FIGURE 2.8: 6G and B6G distributed deployment.
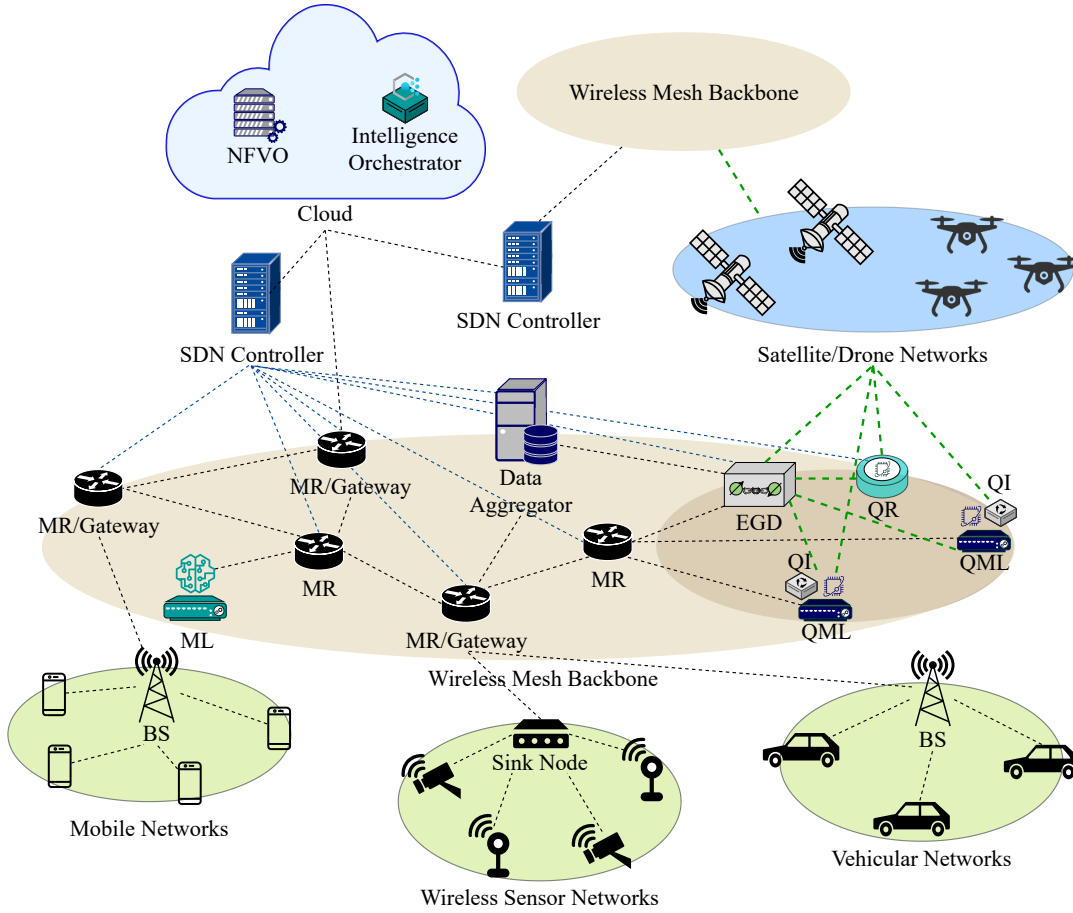
FIGURE 2.9: WMNs Distributed deployment.

In this context, this architecture requires the introduction of both novel logical and physical nodes, in addition to those previously discussed for the centralized architecture. These additions are essential to effectively support the deployment and operation of distributed quantum computers. More specifically, these nodes are:

- Quantum Nodes: The distributed architecture leverages quantum nodes deployed at the network edge for data mining tasks and big data analytics. Quantum nodes are in charge of implementing complex Machine Learning (ML) and Quantum Machine Learning (QML) algorithms.

- Quantum Clusters: To scale up computational capabilities and address complex ML and QML tasks, the Intelligence Orchestrator creates networks of quantum nodes, denoted as quantum clusters, based on the required computational complexity.

- Entanglement Distribution: Quantum nodes within the same cluster share entangled particles, which are crucial for transmitting quantum information. These

entangled particles are distributed by a third node, defined as the Entanglement Generator and Distributor (EGD) node.

- Quantum Repeater (QR): To overcome limitations related to the distance between quantum computers and since the no-cloning theorem does not allow to simply read and copy qubits, quantum repeaters are introduced. They perform entanglement swapping to establish longer-distance end-to-end entanglements [94]. For example, as depicted in Fig. 2.10, considering two distant quantum computers and a quantum repeater, the entanglement swapping procedure mainly consists of four phases: (i) the EGD transmits a pair of entangled particles to the first quantum computer and the quantum repeater, (ii) the quantum repeater performs a Bell-state measurement on entangled particles shared with the two quantum computers causing the collapse of the corresponding particles, (iii) the obtained results are sent to quantum computers through classical channels, and (iv) quantum computers execute local operations to retrieve the entanglement state. Without loss of generality, this procedure can be extended for multiple quantum repeaters scenarios.

  The entangled particle distribution can be also supported by a satellite or a drone network. Satellites and drones, in fact, can act as QRs for the entanglement distribution of two distant quantum remote computers, completely substituting ground QRs or simply supporting them. On the one hand, the main benefit of using satellite is that photons loss takes place at low levels of the troposphere and the transmission path has no photon absorption [95]. On the other hand, since low-orbital satellites serve specific ground quantum computers only for a limited time, drones can be used as QR, receiving a photon and retransmitting it to the involved quantum remote computer, the next drones, or the next ground QR [96].

By merging these elements, we establish a unified framework for distributed quantum computing architecture applicable to both 6G/B6G and WMNs. It is important to note that the EGD can be either a separated physical node of the network or simply a logical entity equipped by involved QRs (e.g., ground QRs, satellites, or drones).

The Information Exchange in the Distributed Architecture

The distributed architecture, shown in Fig. 2.11, works as in what follows.

- *Phase 1: Dataset Creation.* As for the centralized architecture, in the first phase of the information exchange procedure, end nodes belonging to different use cases and network equipment deployed in the access network for 6G/B6G systems or in the wireless mesh backbone for WMNs and in the cloud generate a
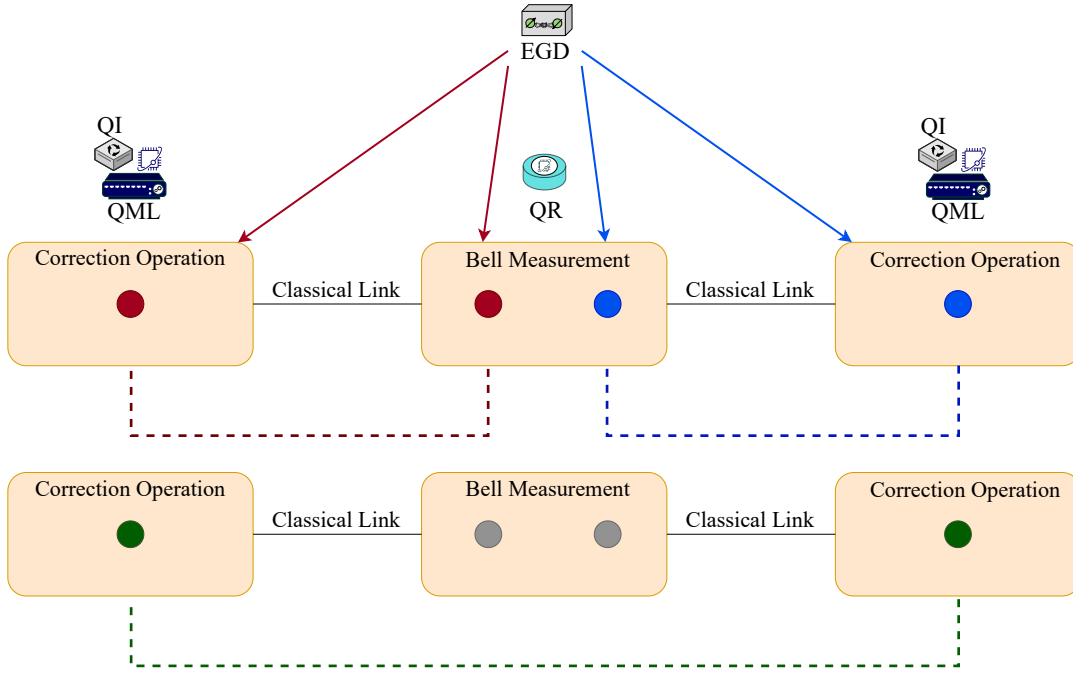
FIGURE 2.10: Representation of the entanglement swapping procedure.

huge amount of data. This information is, then, transmitted to the Data Aggregator which creates new datasets or updates existing ones.

- *Phase 2: Task Assignment.* Also the second phase, aiming at allocating tasks among computing resources (i.e., traditional and quantum computers), is equivalent to the corresponding phase in the centralized architecture. Here, Data Aggregators transmit metadata of the generated datasets (such as the format or size of data) to the Intelligence Orchestrator, thus avoiding the exchange of an excessive amount of information and, in turn, the congestion of the network. The Intelligence Orchestrator, starting from the aforementioned metadata and from the status of the intelligence network, assigns specific tasks to computing resources and sends a task assignment message to the Data Aggregator. Involved datasets are, finally, delivered to traditional or quantum computers.

- *Phase 3: Network Setup.* Differently from the centralized architecture, in the distributed approach quantum nodes are deployed at the network edge and dynamically grouped in clusters in order to scale up the number of qubits and efficiently solve more complex QML problems. In this case, the Intelligence Orchestrator creates quantum computer networks aiming at grouping computing resources based on the number of available qubits and the distance between them in order to reduce attenuation effects. Since quantum computers belonging to the same cluster share quantum states through the aforementioned teleportation protocol, the third phase of the information exchange envisages setting

up the QML network by generating and transmitting entangled particles among involved quantum nodes. They are, then, able to establish a long-distance end-to-end entanglement through the entanglement swapping procedure.
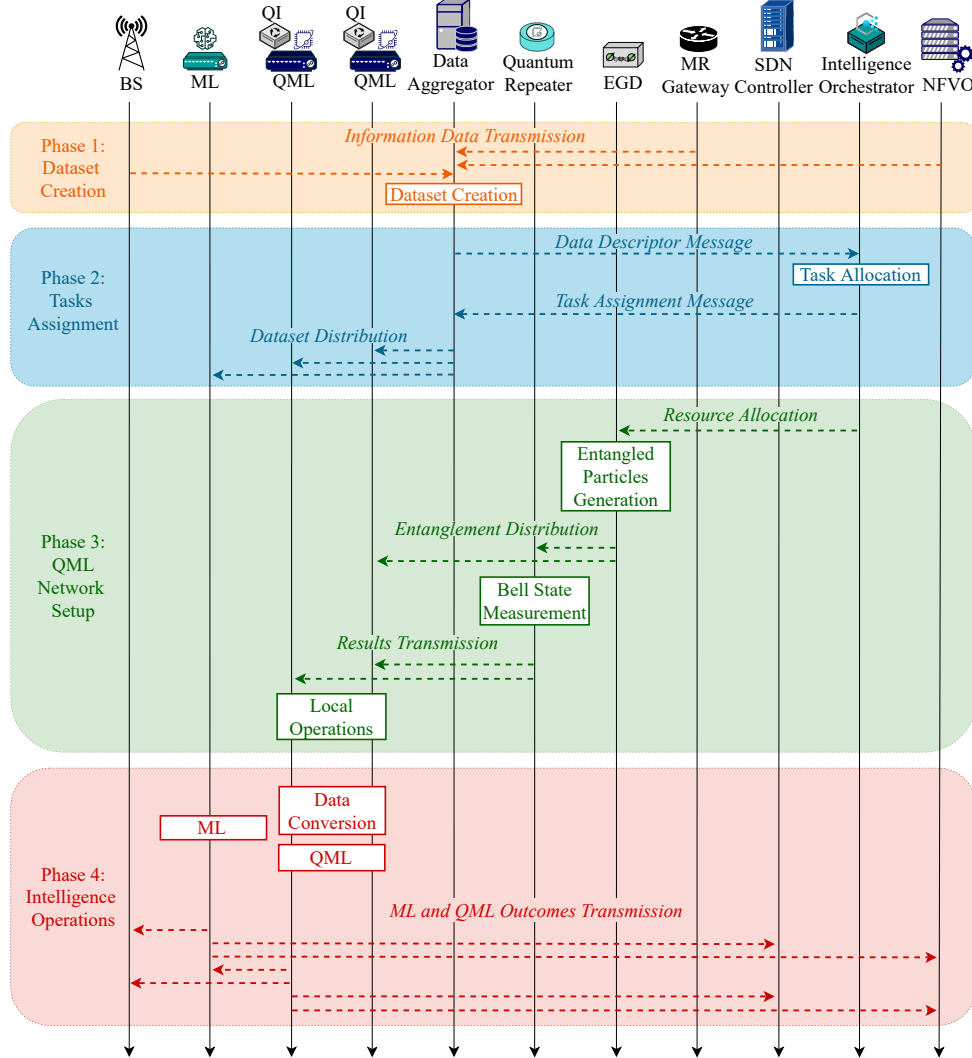
FIGURE 2.11: Message sequence diagram of the distributed architecture.

- *Phase 4: Intelligence Operations.* Again, when quantum computers are involved in the computing operation, the received dataset is converted by the Quantum Interface (QI) devices before executing QML algorithms. The outcomes of ML and QML operations are, finally, transmitted to the nodes of the network for different purposes (e.g., the SDN controllers for optimal routing procedures, the NFVO for allocating virtual resources, BSs for optimal resource scheduling).

Chapter 3

Quantum Scheduling Optimization for UAV-Enabled IoT Networks

This Chapter explores a scenario where a group of Unmanned Aerial Vehicles (UAVs) serves a set of Sensor Nodes (SNs) using a Time Division Multiple Access (TDMA) scheme. The goal is to achieve fair resource allocation and create an optimal scheduling plan of network resources, which is formulated as a combinatorial problem with binary constraints. QA is employed to solve this optimization problem, leveraging its inherent capabilities. The problem is transformed into a Quadratic Unconstrained Binary Optimization (QUBO) form to be processed by a Quantum Processing Unit (QPU). Due to the limited qubits and inter-qubit connectivity in state-of-the-art quantum annealers, a hybrid quantum-classical approach is used to obtain the scheduling plan. The study then compares the results obtained from this approach with those from two classical solvers in terms of data, objective function values, and execution time.

3.1   Introduction

Quantum computing has found a significant application in optimization problems, where a huge number of heuristics and meta-heuristics algorithm exist. However, as problem complexity grows, no single algorithm consistently outperforms the rest. The choice of an optimization strategy heavily depends on the specific problem and its associated parameters. In most cases, exact methods, capable of finding the global optimum, are not feasible due to the computational demands. Instead, we often rely on algorithms that provide suboptimal solutions. This trade-off arises because as problems become larger and more complex, exploring the entire solution space or running exact algorithms becomes impractical, leading to an excessive number of operations.

Quantum computing, instead, offers an alternative heuristics that can sometimes yield solutions of comparable sub-optimality as classical counterparts but with the

promise of significantly faster computation. This advantage stems from the novel approaches enabled by quantum-mechanical properties, providing solutions to intricate problems that would be challenging to implement efficiently on classical computers. However, due to the decoherence principle, the number of qubits is limited. In fact, maintaining the state of a qubit is very challenging, since it requires specialized infrastructure equipped with a cooling system able to maintain a near absolute zero temperature.

Despite the challenges introduced by this powerful technology, it is employed in several application domains [97] such as (i) chemistry, (ii) machine learning, (iii) finance, and (iv) telecommunications [98]. Recently, the pros and cons brought by quantum optimization have been investigated in the telecommunications field, mainly focusing on scheduling in wireless networks.

In particular, [99] investigates a scenario in which a set of sensors are organized in a tree network topology as a part of a wireless network. Several parent sink nodes are in charge of collecting and aggregating sensing data generated by their child nodes. With the aim of minimizing the overall collecting time, an optimization problem is formulated to obtain the optimal scheduling plan, while considering constraints related to interference among nodes and TDMA adopted scheme. Quantum annealing together with other methods are used to find the solution and obtained results are compared in terms of quality and computational time. With the same aim, [100] investigates a similar scenario in which a K-hop interference model is adopted. A Weighted Maximum Independence Set (WMIS) problem is formulated based on a conflict graph corresponding to possible collisions due to the activation of network nodes. The scheduling solution obtained through QA is then compared with the SA's one, where the effect of extra penalty weight adjustment is discussed. Lately, the same authors studied the same scenario in [101] but with particular focus on the adoption of Dirichlet protocol in wireless networking, showing significant improvements in the D-Wave 2X solution compared with that of its predecessor, the D-Wave II.

Although interesting, these works do not consider the channel model and the optimization of network resources. To fill the gap, in this Chapter are presented two works aiming to (i) give a preliminary evaluation of QA algorithm applied to resource scheduling, emphasizing its benefits and drawbacks and (ii) further investigate these aspect in a UAV-enabled IoT networks.

3.2 Motivations

Various techniques have been developed to leverage quantum computing for optimization problems. Gate-based quantum computers typically require finding problem-specific formulations. While they offer the advantage of universal computation, meaning they can theoretically solve any type of task, they require complex investigations to adapt them to specific problems. Additionally, they have a limited number of qubits, making them unsuitable for solving large-scale problems.

Quantum annealers, on the other hand, offer a significantly higher number of qubits compared to gate-based quantum computers. However, they lack the fine-grained control of individual qubits. This limitation actually makes annealers particularly well-suited for optimization tasks. In the case of an optimization problem, it needs to be formulated through a time-dependent Hamiltonian $H(t)$ defined as

$$H(t) = s(t)H_0 + (1 - s(t))H_1, \tag{3.1}$$

where H_0 is an initial Hamiltonian whose ground state, i.e., minimal energy configuration, is easy to find and prepare. H_1 represents the given problem and, as a consequence, its lowest energy level corresponds to the optimal solution. The adiabatic theorem of quantum mechanics states that if $s(t)$, which mathematically represents the transition function, is decreased slowly enough from 1 to 0, the system converges to a state close to the ground one of H_1 [42]. Concretely, at the beginning of the process $H(0) = H_0$, while at the end of the computation, after τ seconds, $H(\tau) = H_1$.

3.3 Workflow of Solving Optimization Problems with QPUs

The above process inspired the construction of D-wave's QPUs and addressing an optimization problem using this hardware requires following a specific workflow. It is worth emphasizing that the procedure itself offers a limited flexibility and making practical adjustments primarily entails fine-tuning the parameters that users can access within this system. Hence, the QPU, which is a physical representation of an undirected graph with a limited number of qubits and connections among them, can be viewed as a specialized black-box optimization algorithm with highly defined parameters and restrictions. The specific workflow is as follow [38]:

- **Mapping the classical formulation into Binary Quadratic (BQ) form**. Once the problem has been classical formulated, since the standard input format for quantum annealers is either the Ising or QUBO formulation, it needs to be

mapped into the interest form. The former is commonly used in statistical mechanics and considers the solution variables as spins $s_i \in \{+1, -1\}$, which can assume two states, i.e., spin up ($\uparrow$) and spin down ($\downarrow$). Relationships between the spins, represented by couplings, are correlations or anti-correlations. The objective function defined through the Ising Model is

$$\sum_{i=1}^{N} h_i s_i + \sum_{i=1}^{N} \sum_{j=i+1}^{N} J_{i,j} s_i s_j, \qquad (3.2)$$

where N denotes the number of qubits, h_i describes the linear coefficients, i.e., qubit biases, and $J_{i,j}$ are the coupling strengths of the quadratic spin terms.

The latter is traditionally employed in computer science, since it uses binary variables, i.e., x_i, which remind classical bits. The QUBO objective function can be expressed as follows:

$$\sum_{i}^{N} Q_{i,i} x_i + \sum_{i<j}^{N} Q_{i,j} x_i x_j, \qquad (3.3)$$

where $Q \in \mathbb{R}^{N \times N}$ is an upper triangular matrix, whose diagonal elements correspond to linear coefficients while off-diagonal ones are the coupled coefficients. An equivalent concise matricial form is

$$x^T Q x. \qquad (3.4)$$

The above formulation, which is used in this work, does not inherently account for the presence of constraints that have to be included by adopting specific strategies, such as penalty methods. It is worth noting that (3.2) and (3.3) are exchangeable by means of a linear transformation, i.e., $x_i = (s_i + 1)/2$.

Then, depending on the chosen formulation, the problem statement is presented as the search for the optimal assignment of either {-1, 1} or {0, 1}, respectively.

- **Embedding procedure.** Subsequently, it is necessary to translate it onto the constrained topology of the QPU. This operation, known as embedding, is practically done by selecting a set of physical qubits to represent optimization variables, called logical variables, and identifying the couplings or connections between the physical qubits in order to establish the appropriate interactions among the logical variables. Furthermore, whereas the problem structure can not be directly embedded into the QPU topology, e.g., due to the limited connection between qubits, a logical variable is represented by a chain of physical

qubits. Note that a solution is consistent if all qubits in a chain have the same value. The embedding can be performed manually or by heuristic algorithms, such as MinorMiner [102].

- **Configuration.** Configuring the quantum annealer involves the assignment of parameters that characterize the embedded problem. This task includes establishing the weights for individual qubit biases, which control the magnetic field influencing each qubit, as well as determining the strengths of the couplers, which affect the interactions between qubits.

- **Annealing process.** This phase is the core of the workflow in which the embedded problem is solved as the system progresses from the initial to the final Hamiltonian using predefined annealing functions.

- **Readout and resampling.** At the end of the annealing process, each qubit is in a classical state that represents the minimum energy state of the problem, or one very close to it. So, the qubits are read-out and their configuration represents a candidate solution of the problem. Furthemore, since the quantum annealing is a heuristic and the annealing time is finite, there is a chance that the system ends up in an excited state. This can be mitigated by repeating the anneal-readout cycle for a specific problem in order to acquire multiple candidate solutions and build a distribution of these possible solutions.

3.4 System Model

The mission duration T is discretized into $k = 1, \ldots, K$ intervals, each one lasting δ_t seconds. A swarm of $m = 1, \ldots, M$ drones, located at $\mathbf{q}_m \in \mathbb{R}^3$, hover over a set of $n = 1, \ldots, N$ SNs, placed in $\mathbf{u}_n \in \mathbb{R}^3$. Moreover, it is assumed that each drone and each node are equipped with one wireless communication unit. To avoid interference among UAVs and SNs, the communications towards different drones take place on different sub-bands, by adopting the Orthogonal Frequency Division Multiple Access (OFDMA) scheme, and different timeslots, by employing the TDMA scheme. Therefore, the scheduling plan is described by means of a 2D binary matrix $\mathbf{x} \in \{0,1\}^{M \times N}$, containing column vectors denoted as $\mathbf{x}_n[k] \in \{0,1\}^{M \times 1}$ and its components defined as $x_{m,n}[k]$. Specifically, only when $x_{m,n}[k] = 1$ the m-th UAV serves the n-th SN. It is further assumed that all nodes are equipped with a wake-up receiver which allows to (i) recover from a sleep state to save energy and (ii) identify the associated UAV and its corresponding sub-band. Besides, the transmission power of each SN is constant and hence it is defined as $P_n \forall n$. The channel gain [103] between a UAV m and a node n, for each k, is equal to $h_{m,n} = \sqrt{\beta_0 d_{m,n}^{-\alpha}}$, where β_0 is the

reference channel power gain, α is the pathloss coefficient, and $d_{m,n} = \|\mathbf{q}_m - \mathbf{u}_n\|$ is the UAV-SN distance. Therefore, the channel capacity of a UAV-SN link can be expressed as $r_{m,n} = B \log_2 \left(1 + \frac{P_n |h_{m,n}|^2}{\sigma^2} \right)$, where σ^2 denotes the noise power and B is the bandwidth. Given the m-th UAV, $\mathbf{r}_n = [r_{1,n}, \ldots, r_{m,n}, \ldots, r_{M,N}]^\mathsf{T}$ is the column vectors containing the achievable data rates of all SNs.

3.5   Problem Definition

To reduce the computational complexity, the proposed formulation accounts for a fixed timeslot j, which corresponds to lower the dimensionality from $K \times M \times N$ to $M \times N$.

3.5.1   Classical Formulation

To derive the whole scheduling plan, it is necessary to solve the following problem for each timeslot:

$$(P1) : \min_{\mathbf{x}[j]} \sum_{\substack{\{n,n'\}=0, \\ n \neq n'}}^{N} \left(\sum_{k=1}^{j} \mathbf{x}_n[k]^\mathsf{T} \mathbf{r}_n - \sum_{k=1}^{j} \mathbf{x}_{n'}[k]^\mathsf{T} \mathbf{r}_{n'} \right)^2 \quad \textbf{s.t.}$$

$$\sum_{n=1}^{N} x_{m,n}[j] = 1, \quad \forall m : 1...M, \tag{3.5}$$

$$\sum_{m=1}^{M} x_{m,n}[j] = 1, \quad \forall n : 1...N, \tag{3.6}$$

$$x_{m,n}[j] \in \{0, 1\}, \quad \forall m : 1...M, n : 1...N. \tag{3.7}$$

Problem $(P1)$ aims to optimally allocate timeslot j to SNs, thus fairly distributing resources throughout the mission. This can be mathematically modeled as minimizing the difference between data rates for each sensor couple. It is worth noting that the objective function takes into consideration the information exchanged in previous instants. In fact, given $\{n, n'\}$

$$\Delta_{j,n,n'} \triangleq \sum_{k=1}^{j-1} \mathbf{x}_n[k]^\mathsf{T} \mathbf{r}_n - \sum_{k=1}^{j-1} \mathbf{x}_{n'}[k]^\mathsf{T} \mathbf{r}_{n'}, \tag{3.8}$$

is a known quantity, derived from past iterations (when $j = 1$ also $\Delta_{j,n,n'} = 0$). Therefore, an equivalent formulation of $(P1)$ is

$$(P2): \min_{\mathbf{x}[j]} \sum_{\substack{\{n,n'\}=0, \\ n \neq n'}}^{N} \left(\mathbf{x}_n[j]^\mathsf{T} \mathbf{r}_n - \mathbf{x}_{n'}[j]^\mathsf{T} \mathbf{r}_{n'} + \Delta_{j,n,n'} \right)^2 \ \textbf{s.t.}$$

$$(3.5), (3.6), (3.7).$$

Constraint (3.5) imposes that, in timeslot j, no more than one sensor can communicate with the same UAV. Similarly, (3.6) states that a drone has to serve a single SN, in instant j. The constraint (3.7) guarantees that the scheduling plan is composed of binary values.

Algorithm 1 Proposed scheduling optimization algorithm

1: Initialize the sensors and drones position as $\mathbf{q}_m$ and $\mathbf{u}_n$, respectively;
2: Compute channel capacity $r_{m,n}$ for each drone-sensor couple;
3: Let $\Delta_{1,n,n'} = 0$;
4: **for** $k = 1$ to K **do**
5:     Solve (P3) to obtain the optimal solution $\{\mathbf{x}[k]^*\}$;
6:     Compute $\Delta_{k+1,n,n'}$ as described in (3.8);
7: **end for**

3.5.2 QUBO Formulation

To solve the problem by employing a QPU, the original problem $(P2)$ is mapped to QUBO form [104]. Therefore, the final objective function is defined as the Hamiltonian $H = H_A + H_B + H_C$ where

$$H_A = \sum_{\substack{\{n,n'\}=0, \\ n \neq n'}}^{N} \left(\mathbf{x}_n[j]^\mathsf{T} \mathbf{r}_n - \mathbf{x}_{n'}[j]^\mathsf{T} \mathbf{r}_{n'} + \Delta_{j,n,n'} \right)^2,$$

$$H_B = \lambda \left(1 - \sum_{n=1}^{N} x_{m,n}[j] \right)^2,$$

$$H_C = \eta \left(1 - \sum_{m=1}^{M} x_{m,n}[j] \right)^2,$$

and $\{\lambda, \eta\} > 0$ as penalty factors. Note that the objective function of $(P2)$ is already in quadratic form and, hence, does not require any manipulation. On the contrary, constraints (3.5) and (3.6) have been reformulated involving the quadratic penalty method [104]. Besides, (3.7) is inherently addressed since quantum optimization is

employed. The final unconstrained formulation of the QUBO problem is

$$(P3) : \min_{\mathbf{x}[j]} \sum_{\substack{\{n,n'\}=0, \\ n \neq n'}}^{N} \left(\mathbf{x}_n[j]^{\mathsf{T}} \mathbf{r}_n - \mathbf{x}_{n'}[j]^{\mathsf{T}} \mathbf{r}_{n'} + \Delta_{j,n,n'} \right)^2$$
$$+ \lambda \left(1 - \sum_{n=1}^{N} x_{m,n}[j] \right)^2 + \eta \left(1 - \sum_{m=1}^{M} x_{m,n}[j] \right)^2 ,$$

that can be implemented on a quantum system to be solved, as described in Algorithm 1.

3.6   Preliminary Evaluation

Section based on the article: "Quantum scheduling optimization for UAV-enabled IoT networks"

Considering the promising potential of quantum computing, the following research questions arise:

- *What are the advantages of solving the reference NP-hard problem with quantum computing?*

- *Are there major trade-offs that would hinder the applicability of this technology to the aforementioned problem?*

- *What are the differences in terms of computational time and found solutions over classical approaches?*

To prove the advantages brought by quantum computing, a preliminary comparison with different classical algorithms, e.g., SA and Tabu Search (TS), has been carried out considered a simplified version of the reference problem. All the algorithms found a comparable solution in terms of throughput but, as depicted in Fig. 3.1, QA outperforms the competitors in terms of computational time [105]. Nevertheless, certain aspects must be taken into account. In fact, to mitigate the communication and queue delay, a possible solution in a long-term vision, is to place QPUs at the edge of the network. Another issue is related to the embedding process that, in case of large problems, can hinder the convergence in a proper time. The next steps consist of solving the original problem by tuning hyperparameters and by investigating also hybrid quantum-classical approaches.
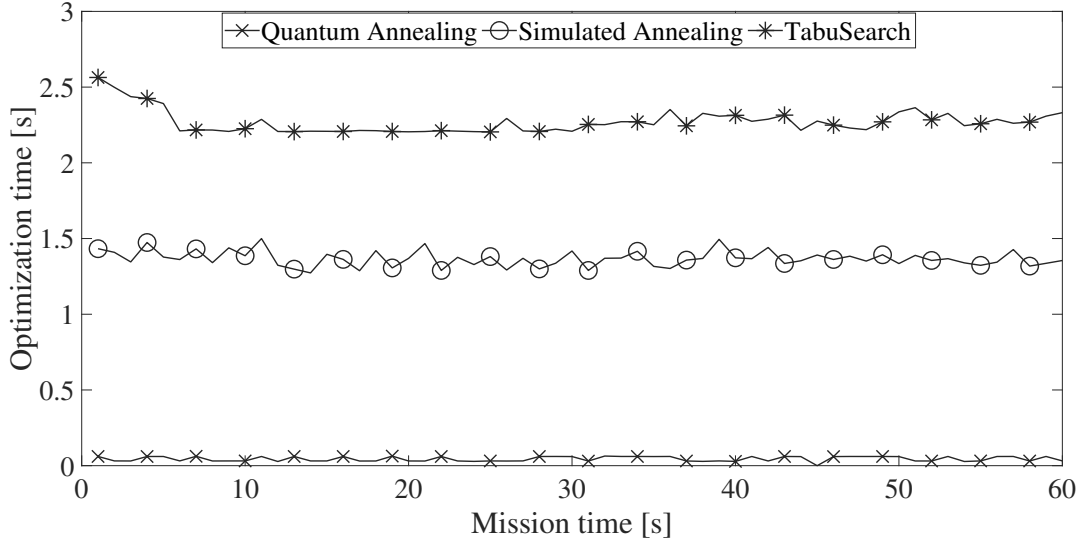
FIGURE 3.1: Preliminary comparison among different optimization algorithms.

3.7 Numerical Results and Discussion

In this Section, a simulation campaign has been conducted to evaluate the effectiveness of the proposed formulation by employing the D-wave Leap Hybrid solver, which uses a hybrid quantum-classical approach. This solver is suitable for problems with a large number of variables that cannot be mapped directly into QPU's topology. In particular, a classical process divides the original problem into sub-problems that are dispatched to the QPU and to the cloud's classical computing capabilities. The obtained results are compared with two classical optimization algorithms, i.e., SA and TS, implemented in the D-Wave Python library, running on a computer with an Intel i5 6200U @ 2.8 GHz and 4 GB of RAM.

For the D-wave Leap Hybrid solver, default parameters have been adopted, e.g., number of reads set to 100. Besides, the minimum penalty factors have been chosen such that no improvement of the solution is obtained, i.e., $\lambda = 10^{17}$, $\eta = 10^2$. The mission time T has been split into $K = 60$ timeslot of $\delta_t = 1$ second each. Furthermore, $M = 4$ drones are deployed in $[15\ 15\ 80]^T$, $[20\ 70\ 100]^T$, $[75\ 20\ 110]^T$, and $[80\ 80\ 90]^T$, serving $N = \{25, 50, 75, 100\}$ SNs uniformly distributed over a 100x100 m area. As for the transmission, $B = 1$ MHz, $P_n = 10$ mW $\forall n$, $\alpha = 2$, $\sigma^2 = N_0 B$, and $N_0 = -174$ dBm/Hz [106].

Given the scheduling plan **x**, obtained as the solution of problem $(P3)$, it is possible to compute the sum-rates of each sensor at the end of the mission.

Thanks to the proposed formulation, as can be seen from mean and standard deviation reported in Tab. 3.1, UAVs are able to fairly serve nodes regardless the number of SNs and algorithm used, without showing any sensible difference. As a matter of

TABLE 3.1: Sum-rate means and standard deviations of the algorithms.

		Algorithms					
		H		SA		TS	
		Mean	Std	Mean	Std	Mean	Std
	25	263.09	12.074	264.41	12.783	262.55	11.697
	50	132.38	10.556	132.53	10.748	132.31	10.417
SNs	75	87.72	13.084	87.86	10.769	87.23	10.41
	100	65.69	13.084	65.88	13.129	65.45	12.961

fact, when the number of SNs approaches the number of drones, the amount of gathered data increases since a drone serves less sensors during the whole mission, vice versa when $M \ll N$ the sum-rate decreases. Indeed, in the first configuration, the swarm is able to collect ~ 260 Mbits, while in the last one just ~ 65 Mbits.

To provide further insights, for each sensor, the sum-rates in case of $N = 25$ and $N = 50$ are shown in Figs. 3.2 and 3.3, respectively. Although different amounts for each SN are exhibited, the transmission fairness is clearly achieved, regardless the employed algorithm.
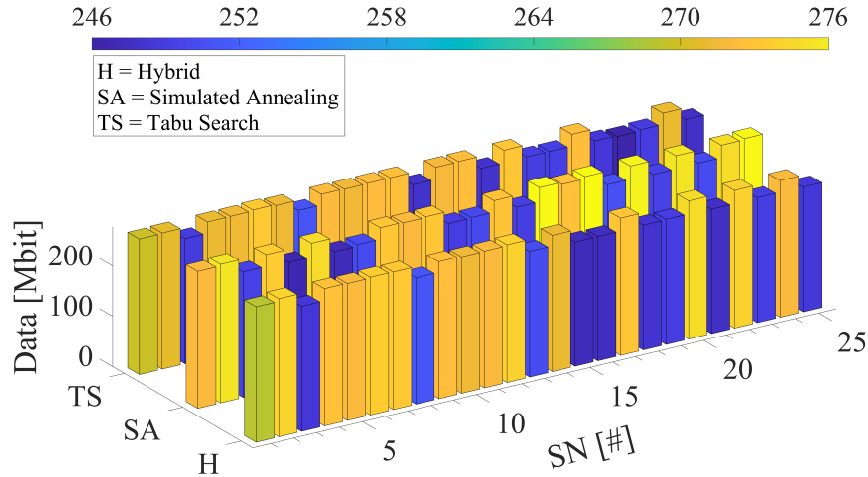
FIGURE 3.2: Acquired data at the end of the mission, with $N = 25$.

A comparison among the different objective function curves for different algorithms is presented in Fig. 3.4. When 25 SNs are considered, the classical SA algorithm performs worse than the hybrid approach and TS algorithm, which instead provide comparable results. As the number of SNs increases, i.e. $M \ll N$, a difference is still present although irrelevant.

Finally, a thorough comparison of the algorithms' execution time, to solve the formulated optimization problem, is hereby analyzed. For what concerns the hybrid
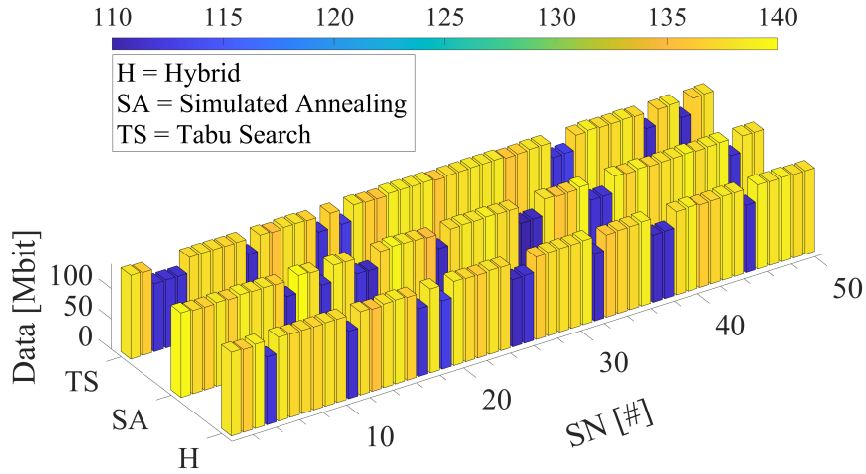
FIGURE 3.3: Acquired data at the end of the mission, with $N = 50$.

solver, the total time and the QPU access time are reported separately [107] [108]. The latter is a portion of overall hybrid solver time and consists of (i) a one-time setup procedure to prepare the QPU and (ii) the sampling time. It should be noted that the embedding procedure period, the network latency and the queuing time, which all take approximately 4 seconds, are not included in this analysis [109].

As depicted in Fig. 3.5, regardless the number of SN, the hybrid solver takes about 3 seconds to complete the process. Instead, for $N = 25$ and $N = 50$, classical algorithms perform slightly better in terms of execution time, which confirms the results obtained in [107], [108], and [109]. As the number of sensors increases, the execution time of SA and TS increases as well. In particular, for $N = 75$, classical algorithms and hybrid solver give comparable results. This trend remains for $N = 100$, except for SA which performs worse, i.e., ~ 5 seconds.

(A) $N = 25$

(B) $N = 50$

(C) $N = 75$

(D) $N = 100$
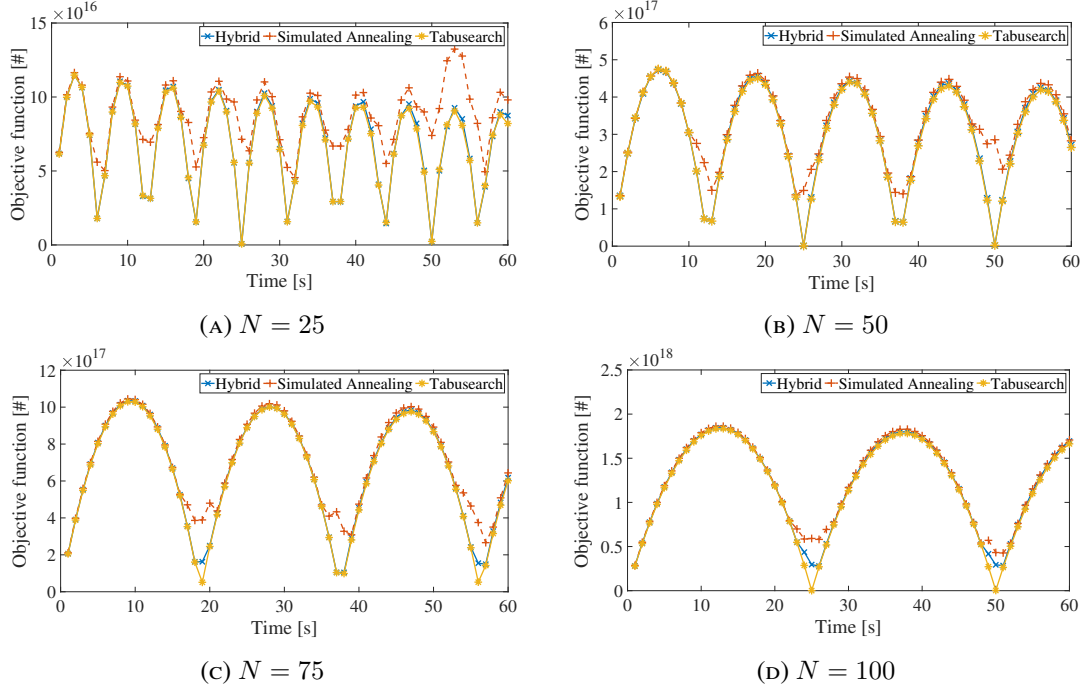
FIGURE 3.4: Comparison of objective function curves with different number of SNs
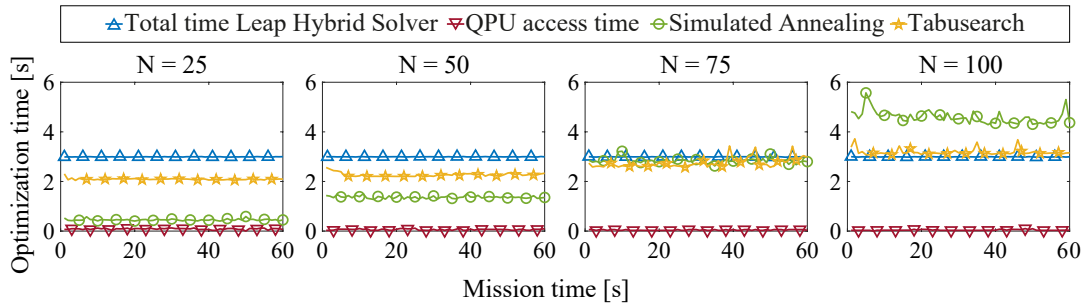
FIGURE 3.5: Comparison of execution time for each solver.

Chapter 4

A Probability-Based Optimization Approach for Entanglement Distribution and Source Position in Quantum Networks

Quantum Internet is a network of interconnected quantum computers designed to exchange information using qubit. While, Quantum Internet offer significant advantages, they can be susceptible to various factors that may disrupt communication. To assess network performance, this study develops a comprehensive probability expression to estimate the successful reception of qubits by nodes. Building on this analysis, in this Chapter is formulated a Mixed-Integer Non-Linear Programming (MINLP) problem, which aims to optimize the fair exchange of qubits between pairs of nodes while jointly optimizing the positioning of the quantum source and the distribution of entanglement.

4.1 Introduction

Quantum Internet has been introduced [97], [110], [111] as a cutting-edge technology and communication paradigm. Among the vast plethora of possible applications, quantum networks can be employed to overcome the current computational power limitations. For instance, the scientific community envisions the integration of quantum computing devices at the edge of 6G networks as a mean to enhance service provisioning [112]. Indeed, thanks to Quantum Internet, in the near future multiple qubit-limited devices will be interconnected to share quantum states among each other [16] through a quantum channel, i.e., fiber or free space optical links. However, even if the state of a qubit can be directly encoded by using the polarization of a photon, it may be lost due to attenuation or noise. In such cases, the quantum information

is irretrievably destroyed, and it cannot be recovered through measurement or copying, as stated by the postulate of quantum measurement and the no-cloning theorem. Thus, a common employed approach is to generate and distribute a particular two-qubit state to remote nodes, leveraging the entanglement phenomenon [24]. Indeed, when two particles are entangled, the quantum state of one particle becomes correlated with the state of the other, regardless of the distance between them. This unique property, along with the transmission of classical information, is at the basis of the quantum teleportation protocol [32]. Nevertheless, due to attenuation in the medium, the entanglement distribution exponentially decreases over distance. Additionally, the presence of noise during the generation process or entanglement decoherence can produce an imperfect entangled state or cause the transition to an undesired one, making it unusable for a reliable teleportation operation [94].

For these reasons, the scientific community has investigated the maximization of the entanglement distribution while considering different aspects. One of them is the adoption of purification techniques [113]–[117], which enhance the goodness of an entangled state and hence of the communication as a whole. Another important considered facet is quantum memory [118]–[122], which represents one of the most constrained resources and plays a crucial role in preserving and retrieving on-demand entangled states to improve the robustness and reliability of entanglement distribution. However, these works assume that a dedicated quantum source is placed in the middle between each node. In practice, this assumption overlooks the fact that such hardware is expensive and often limited, thus potentially constraining the number of nodes in the network [123]. Moreover, the rate at which entangled particles can be generated also impacts the number of entanglement links that can be established.

To the best of the authors' knowledge, the existing scientific literature has not investigated the optimization of the quantum source position by taking into account the non-negligible failure probability associated with the photon transmission and teleport operations. These facets are of pivotal importance to ultimately improve the efficiency of the whole communication system. In this regard, this Chapter provides several significant contributions, which are outlined below.

- A comprehensive probability expression is derived to determine how many qubits are expected to successfully arrive at the receiver. The proposed model takes into account the attenuation of the fiber, as well as the depolarazing and dephasing noise introduced during the execution of the operations related to the teleportation protocol.

- Based on the above derivation, a MINLP problem is formulated to fairly maximize the number of qubits exchanged among the nodes and jointly optimize

(i) the position of the quantum source, assuming to have a priori knowledge of the quantum node location, and (ii) the scheduling plan, describing how many entangled pairs should be allocated at each node couple.

- To cope with the non-convexity of the original formulation, a dedicated optimization strategy is designed. First, the Block Coordinate Descent (BCD) technique is employed to split the problem into two sub-problems. The first is initially relaxed and then exactly solved leveraging the Karush-Kuhn-Tucker (KKT) conditions. Capitalizing on the first solution, the second one is addressed by adopting the Successive Convex Approximation (SCA) method.

- A simulation campaign is carried out to assess the effectiveness of this work. In particular, the derived probability expression and the proposed optimization algorithm are evaluated under different parameters, such as node topology, depolarizing and dephasing rate, fiber attenuation, and generation chance. Moreover, the algorithm is compared with a baseline approach which adopts the centroid of the nodes as the source location, while exploiting the already derived optimal scheduling plan.

The theoretical findings indicate that in case of quantum networks deployed in relatively small areas, i.e., a few square kilometers, the proposal and the baseline approach have similar performance. However, when wider areas are considered, the derived optimal solution provides a significant advantage in terms of number of qubits successfully received by the nodes. This demonstrates that the proposed algorithm is able to capture the non-linearity of the derived probability and can be employed as tool for optimal design and assessment of large-scale quantum networks.

Notation: Boldface lower case letters refer to vectors; $\mathbf{x}^\mathsf{T}$ is the transpose of a generic vector $\mathbf{x}$; $|\mathbf{x}\rangle$ is the column vector of a generic quantum state $\mathbf{x}$; $\mathcal{O}(x)$ denotes the time-complexity of an algorithm of input size x, i.e, big O notation; $\mathcal{U}(\cdot, \cdot)$, $\mathrm{Beta}(\cdot, \cdot)$, and $\mathcal{T}(\cdot, \cdot, \cdot)$ define the uniform, beta, and triangular distributions. The main adopted symbols of this paper are summarized in Table 4.1.

4.2 Related Works

In the literature there is a growing interest regarding several aspects of quantum communications, with the goal of maximizing the entanglement photon distribution, and hence the throughput, by considering factors such as fidelity and quantum memory.

In particular, fidelity represents the probability that a pair of entangled qubits are in the desired state, i.e., maximally entangled, which in turn affects the communication efficiency. In this context, authors in [113] investigate entanglement link fidelity

by shortening the amount of time links are maintained, before swapping operations are performed. In [114], to maximize the rates in a quantum network while ensuring a minimum end-to-end fidelity requirement, the entanglement distribution problem is presented as a linear programming problem. An upper bound on the path's length is imposed to fulfill the fidelity, which lowers with each entanglement swapping operation along the path. Purification methods can be considered in cases where an entanglement link is characterized by low fidelity. Specifically, purification techniques consist in entangling multiple pairs of qubits with low fidelity and then merging them into a single one with high fidelity [124]. In this regard, [115] proposes an adaptive routing scheme to manage multiple communication requests. The approach involves a preliminary step of purifying the links, so that only the links whose fidelity is above a given threshold are used in the routing process. Similarly, authors in [116] design an algorithm to select a path which satisfies a end-to-end fidelity constraint. [117] presents an algorithm to maximize network throughput by preparing multiple candidate entanglement paths and determining optimal purification schemes. Then, the final set of entanglement paths that maximize network throughput under the given quantum resource constraints are selected.

The other major aspect considered in the literature is quantum memory, which can store the quantum state of a photon to be used when needed. Quantum memory is a key component of quantum routers, also known as quantum repeaters, that are essential for the distribution of entangled states over long distances in large-scale quantum networks. However, the performance of quantum repeaters is far from ideal, owing to the limited quantum memory in quantum repeaters, which impairs the rate and efficiency of entanglement distribution. To overcome this challenge, in [118] it is proposed a quantum queuing model, based on dynamic programming, in order to track the delay. In particular, a policy is developed to exponentially reduce the average queuing delay with respect to memory size. The same authors, in [119], present a first entanglement distribution protocol that can achieve a high distribution rate by considering imperfect entanglement swapping operations at quantum repeaters. However, it is assumed that the quantum repeater node has unbounded memory, and the stored qubit are not affected by the decoherence phenomena, resulting in ideal fidelity. In [120], an entanglement rate optimization problem is investigated considering a system able to process a set of requests at the same time. In particular, the quantum routing problem is decoupled in i) scheduling, in which an end-to-end entanglement path is assigned to a pair of quantum nodes, and ii) path selection, where the best path is found. A novel approach for maximizing entanglement distribution rate while considering quantum repeaters with a limited memory is proposed in [121], which is subsequently decomposed into entanglement generation and swapping sub-problems.

Symbol	Description
N	Number of quantum nodes.
M	Number of quantum node pairs.
$\mathbf{q}$	Location of the quantum source.
$\mathbf{u}_n$	Location of the quantum node n.
$\boldsymbol{\gamma}$	Photon distribution plan.
$\overline{\gamma}$	Maximum photon pairs generated by the source.
c	Propagation speed in the fiber.
d_n^{S}	Distance between a node n and the quantum source.
d_m^{N}	Distance between the nodes of couple m.
P_n^{QL}	Probability of successfully receiving a photon.
P^{G}	Probability of losing a photon after generation.
P_m^{CL}	Probability of successfully sending classical information.
P^{DL}	Probability that qubit depolarization does not occur.
$\hat{P}^{\mathrm{DH}}, \check{P}_m^{\mathrm{DH}}$	Probability that qubit dephasing does not occur at TX/RX.
P_m^{Δ}	Dephasing contribution due to different distances from the source.
P_m	Overall probability of successfully receive a qubit.
R^{DL}	Depolarizing rate.
R^{DH}	Dephasing rate.
η	Attenuation factor of the fiber.
τ	Operation time per quantum instruction.
ρ	Number of qubits successfully received by the node pairs.
ℓ	Sides' length of the square-shaped reference area.
t_n^{Q}	Propagation delay of the quantum channel.
t_m^{C}	Propagation delay of the classical channel.
Δ_m^{Q}	Propagation delay of the classical channel.

TABLE 4.1: Main notation adopted in this work.

A greedy algorithm for short-distance entanglement generation is proposed, such that the quantum memories can be employed in an efficient manner. The swapping sub-problem, modelled through an entanglement graph, is solved with a heuristic technique which divides the original problem into several sub-problems, each of which can be solved in polynomial time using dynamic programming. Instead, [122] introduces a framework for optimizing the entanglement generation and distribution among quantum users having different resources and application requirements. This approach aims to optimally distribute entangled pairs among quantum users while satisfying a minimum entanglement rate requirement for each user.

Although interesting, these works consider the quantum source placed in a fixed position, e.g., the middle point among quantum nodes. Moreover, most of them, neglect the limited rate at which Bell pairs can be generated. Further, no investigations have taken into account the failure probability associated with photon transmission and teleport operations.

4.3   System Model

This work envisions a quantum network composed of a quantum source, located at $\mathbf{q} \in \mathbb{R}^2$, and a group of N quantum nodes, each one placed in $\mathbf{u}_n \in \mathbb{R}^2$ with $n = 1, \ldots, N$. All nodes are connected, via optical fiber, to the quantum source and among themselves [125]. For the sake of notation, each couple of nodes (n, n'), with $n \neq n'$, is denoted by $m = 1, \ldots, M$, where $M = \frac{N(N-1)}{2}$. Each node is equipped with the necessary devices to perform quantum measurements, thus allowing the exchange of quantum states by means of teleportation protocol, whose sequence diagram is depicted in Fig. 4.1. In this work, it is assumed that the quantum memory is large enough to store the received qubits, for all nodes, and (ii) the quantum source runs for a fixed time window large enough to successfully generate a maximum number of entangled pairs $\overline{\gamma}$. For the sake of generality, $\overline{\gamma}$ is left as a free parameter which however must take into account the success probability related to the generation process, which in turn depends on the specific hardware implementation. Moreover, for each couple of nodes m, the quantum source allocates $\gamma_m \in \mathbb{N}$ entangled photon pairs, with $\boldsymbol{\gamma} = \{\gamma_m\}$. Due to hardware limitations, the total number of entangled photon pairs cannot exceed the upper bound $\overline{\gamma}$.

4.3.1   Overall teleportation probability

A wide range of factors may affect the probability of successfully retrieving the quantum state of a transmitted qubit when the teleportation protocol is adopted.

In particular, the distance between the source and the receiver introduces a propagation delay $t_n^{\mathrm{Q}} = \frac{d_n^{\mathrm{S}}}{c}$, where $d_n^{\mathrm{S}} = \|\mathbf{q} - \mathbf{u}_n\|$ is the length of the source-node link and c is the propagation speed in optical fiber.

In addition to the delay, the fiber introduces also attenuation, which can cause the loss of the travelling photon along each path. As a result, the probability of successfully receiving it [120], for each node n, is:

$$P_n^{\mathrm{QL}} = (1 - P^{\mathrm{G}})10^{-\frac{\eta d_n^{\mathrm{S}}}{10}}, \tag{4.1}$$

where P^{G} is the probability of losing the flying qubit immediately after generation due to hardware imperfections, and η is the attenuation factor. Similarly, on the sender side, once the BSM is performed, the information employed for reconstruction is delivered through the classical channel, which introduces a propagation delay $t_m^{\mathrm{C}} = \frac{d_m^{\mathrm{N}}}{c}$, where $d_m^{\mathrm{N}} = \|\mathbf{u}_n - \mathbf{u}_{n'}\|$ is the distance associated to node pair m. The probability of successfully sending classical information [126], for each couples of nodes m, can
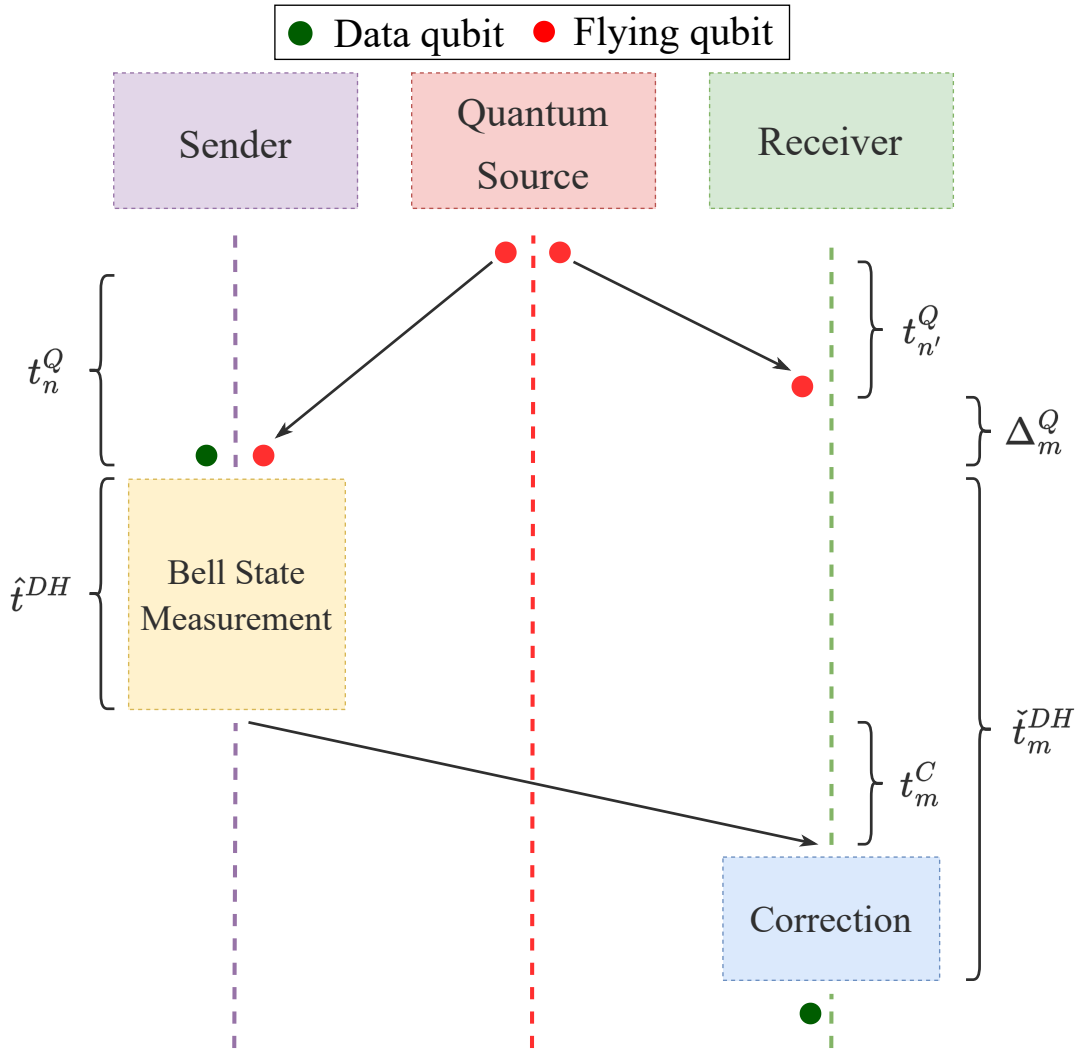
FIGURE 4.1: Sequence diagram of quantum teleportation.

be modelled as:

$$P_m^{\text{CL}} = 10^{-\frac{\eta d_m^{\text{N}}}{10}}. \tag{4.2}$$

Qubits stored in quantum memory are subject to different sources of noise, each one depending on different aspects, such as hardware imperfections and the system-environment interaction. Specifically, errors in the gate operations can lead to bit-flip, phase-flip, or both errors with equal probabilities. All of these have the same probability to occur and can be simulated by the Pauli X, Z, or Y operation, respectively. As a result, gate infidelities can be modelled according to the depolarizing noise and, thus, the probability that qubit depolarization does not occur can be written as follow [120]:

$$P^{\text{DL}} = e^{-\tau R^{\text{DL}}}, \tag{4.3}$$

where τ is the time spent for the execution of a single operation and R^{DL} is the depolarizing rate.

Another type of noise is the dephasing one, which arises from the interaction between qubits and their environment, leading to qubit decoherence. The probability of dephasing depends on the amount of time that the qubit stays in memory and can be simulated by stochastically applying the Pauli Z gate. Assuming that the data qubit is generated at the same time as both entangled photons arrive, the probability that data or flying qubit dephasing does not occur [120] is given by:

$$\hat{P}^{\text{DH}} = e^{-\hat{t}^{\text{DH}} R^{\text{DH}}}, \tag{4.4}$$

where R^{DH} is the dephasing rate and $\hat{t}^{\text{DH}}$ depends only on the amount of time that the sender requires to perform the Bell state measurement, i.e. $\hat{t}^{\text{DH}} = 4\tau$. From a receiver side, instead, the probability can be written as:

$$\check{P}_m^{\text{DH}} = e^{-\check{t}_m^{\text{DH}} R^{\text{DH}}}, \tag{4.5}$$

where $\check{t}_m^{\text{DH}}$ denotes the amount of time needed to receive the measurement outcome and perform the correction operations, i.e. $\check{t}_m^{\text{DH}} = t_m^{\text{C}} + 6\tau$. Besides, since the two communicating nodes can be located at different distances from the source, it is necessary to consider a further time contribution related to the qubit dephasing probability:

$$P_m^{\Delta} = e^{-\Delta_m^{\text{Q}} R^{\text{DH}}}, \tag{4.6}$$

where $\Delta_m^{\text{Q}} = |t_n^{\text{Q}} - t_{n'}^{\text{Q}}|$. Note that the above term affects only the node closer to the source. Indeed, when the source is equidistant from both nodes, (4.6) is zero.

It is important to specify that the time spent for execution of local operations at the sender and the receiver might affect gate infidelity due to depolarizing noise, resulting in higher infidelities. It is also worth mentioning that the depolarizing and dephasing rates can vary depending on the specific quantum hardware used for quantum nodes. Nonetheless, the above modeling can account for these phenomena by considering a larger operation time per instruction τ.

Finally, considering (4.1)-(4.5), the overall probability of correctly receiving a qubit in the worst case scenario, i.e., in which both X and Z gates are applied at the receiver, is:

$$P_m = P_n^{\text{QL}} P_{n'}^{\text{QL}} \left(\hat{P}^{\text{DH}}\right)^2 \check{P}_m^{\text{DH}} \left(P^{\text{DL}}\right)^5 P_m^{\text{CL}} \left(P^{\text{DL}}\right)^2 P_m^{\Delta}, \tag{4.7}$$

where $\left(\hat{P}^{\text{DH}}\right)^2$ is the dephasing probability of the data qubit and the corresponding absorbed photon at the sender, $\left(P^{\text{DL}}\right)^5$ and $\left(P^{\text{DL}}\right)^2$ are the probabilities that the

depolarization does not occur at both sender and receiver*. The exponents of these probabilities correspond to the number of operations performed, as discussed in Section 3.2.

Therefore, after some algebric manipulation, Eq. (4.7) can be written as:

$$P_m = a10^{-\frac{\eta}{10}(d_n^{\mathrm{S}}+d_{n'}^{\mathrm{S}}+d_m^{\mathrm{N}})}e^{-(15\tau+t_m^{\mathrm{C}}+\Delta_m^{\mathrm{Q}})R^{\mathrm{DH}}-6\tau R^{\mathrm{DL}}}. \tag{4.8}$$

where $a = (1 - P^{\mathrm{G}})^2$. The above expression, which accounts for all the discussed phenomena, can be used to design and assess a quantum network architecture.

4.4 Problem Formulation

To enable fair teleportation among quantum nodes, a dedicated strategy for the distribution of entanglement has to be employed. To this aim, it is necessary to optimally derive (i) a photon distribution plan $\boldsymbol{\gamma}$ and (ii) the position of the quantum source $\mathbf{q}$, defined at the beginning of Section 4.3. Therefore, to derive the optimal entanglement distribution, the following optimization problem is formulated:

$$\max_{\rho,\boldsymbol{\gamma},\mathbf{q}} \rho \quad \textbf{s.t.} \tag{4.9}$$

$$\rho \leq P_m\gamma_m, \quad \forall m = 1,\ldots,M, \tag{4.10}$$

$$\sum_{m=1}^{M} \gamma_m \leq \overline{\gamma}, \tag{4.11}$$

$$\boldsymbol{\gamma} \in \mathbb{N}^M \tag{4.12}$$

Problem (4.9) aims to fairly maximize the minimum number of qubits ρ successfully received by each couple of quantum nodes m through the joint optimization of the scheduling distribution plan $\boldsymbol{\gamma}$ and the position of the source $\mathbf{q}$. In particular, constraint (4.10) states that ρ cannot be higher than the average number of photons received by each couple. Equivalently, ρ guarantees to have minimum common number of successfully teleported qubits in the quantum network. Moreover, constraint (4.11) limits the number of entangled photon pairs generated by a maximum value $\overline{\gamma}$. Finally, (4.12) imposes that the number of assigned photon couples is always a positive integer.

---

*In this work, it is assumed the probability of depolarization for one qubit does not depend on the state of others [18]. Therefore, the depolarization related to the CNOT gate must be counted twice, as it affects both control and target qubit.

70

Chapter 4. A Probability-Based Optimization Approach for Entanglement Distribution and Source Position in Quantum Networks

4.5 Proposed Solution

As immediate results from its formulation, (4.9) is a non-convex programming problem, which is challenging to solve. Specifically, constraint (4.10) couples the scheduling plan $\boldsymbol{\gamma}$ with the source position $\mathbf{q}$, which is encompassed in the distance d_n^{S} within probability P_m. To cope with these issues, problem (4.9) is split into two sub-problems which are separately solved to derive an optimal solution.

4.5.1 Sub-problem 1: Photon pair distribution

Given the optimal quantum source location, ρ is employed to fairly maximize the photon distribution with respect to the scheduling plan. Therefore, the first sub-problem reads

$$\max_{\rho, \boldsymbol{\gamma}} \rho \quad \textbf{s.t.} \quad (4.10), (4.11), (4.12). \tag{4.13}$$

which is non-convex, due to constraint (4.12). Nonetheless, (4.13) can be relaxed by neglecting such a constraint, thus becoming a convex optimization problem whose solution can be then rounded with a floor operation. Hence, a generic solver can be employed at the cost of computational complexity in the order of $\mathcal{O}\left((M+1)^{3.5}\right)$ [127]. To reduce such complexity, the KKT conditions can be applied to derive a closed-form solution [128].

Theorem 1. *The optimal photon distribution plan, for each couple of nodes m, and the maximum number of qubits per node are*

$$\gamma_m = \overline{\gamma} \left(P_m \sum_{m'=1}^{M} \frac{1}{P_{m'}} \right)^{-1}, \quad \rho = \overline{\gamma} \left(\sum_{m=1}^{M} \frac{1}{P_m} \right)^{-1}, \tag{4.14}$$

which only depend on the position of the quantum source embedded in the probabilities P_m.

Proof. The Langrangian function corresponding to the relaxed problem (4.13) is

$$\mathcal{L} = \rho - \sum_{m=1}^{M} \lambda_m \left(\rho - P_m \gamma_m \right) - \mu \left(\sum_{m=1}^{M} \gamma_m - \overline{\gamma} \right),$$

where $\lambda_m \geq 0$ and $\mu \geq 0$ are the multipliers related to the constraints (4.10) and (4.11), respectively. Therefore, the KKT conditions read

$$\frac{\partial \mathcal{L}}{\partial \rho} = 1 - \sum_{m=1}^{M} \lambda_m = 0, \tag{4.15}$$

$$\frac{\partial \mathcal{L}}{\partial \gamma_m} = \lambda_m P_m - \mu = 0, \quad \forall m, \tag{4.16}$$

$$\lambda_m (\rho - P_m \gamma_m) = 0, \quad \forall m, \tag{4.17}$$

$$\mu \left(\sum_{m=1}^{M} \gamma_m - \overline{\gamma} \right) = 0. \tag{4.18}$$

The first two equations are sufficient to demonstrate that the multipliers are strictly positive:

$$\frac{\mu}{P_m} = \lambda_m \Rightarrow \mu \sum_{m=1}^{M} \frac{1}{P_m} = \sum_{m=1}^{M} \lambda_m \Rightarrow \mu = \left(\sum_{m=1}^{M} \frac{1}{P_m} \right)^{-1},$$

where the third equality is due to (4.15). Therefore, the last two conditions leads to

$$\overline{\gamma} = \sum_{m=1}^{M} \gamma_m, \tag{4.19}$$

$$\rho - P_m \gamma_m = 0 \Rightarrow \rho \sum_{m=1}^{M} \frac{1}{P_m} = \sum_{m=1}^{M} \gamma_m = \overline{\gamma} \Rightarrow$$

$$\rho = \overline{\gamma} \left(\sum_{m=1}^{M} \frac{1}{P_m} \right)^{-1} \Rightarrow \gamma_m = \frac{\rho}{P_m}. \tag{4.20}$$

∎

Corollary 1. *The entanglement distribution plan becomes uniform, denoted by $\gamma_m = 2\overline{\gamma} / (N(N-1)) \ \forall m$, when the probabilities $P_m \to P \in [0,1] \ \forall m$, leading to the maximum number of qubits per link $\rho = \overline{\gamma} P$. This phenomenon takes place when the impact of the distances among the nodes is negligible. It occurs in two cases: (i) the inter-node distances are similar, which is topologically challenging with a significant number of quantum nodes, and (ii) the area in which the nodes are deployed is small enough, i.e., in the order of a few kilometers.*

Corollary 2. *As a result of the above theorem, ρ can now be defined as the average number of qubits successfully received by each couple of nodes m.*

The computational complexity of the procedure to calculate the optimal solution is $\mathcal{O}(2M+1) = \mathcal{O}(M)$, since the single complexities to compute ρ and γ are both

72

Chapter 4. A Probability-Based Optimization Approach for Entanglement Distribution and Source Position in Quantum Networks

linear with respect to the number of node pairs.

4.5.2 Sub-problem 2: Quantum source position

The second sub-problem aims to derive the optimal source location $\mathbf{q}$, given a fixed scheduling plan $\boldsymbol{\gamma}$ and the definition of ρ obtained in (4.20). Hence, (4.9) can be written as:

$$\max_{\mathbf{q}} \rho \quad \textbf{s.t.} \quad (4.10). \tag{4.21}$$

However, problem (4.21) is non-convex due to the presence of $\mathbf{q}$ in the exponent of P_m. To tackle this issue, let equivalently rearrange (4.8) as

$$P_m = \alpha_m 10^{-\frac{\eta}{10}(d_n^{\mathrm{S}}+d_{n'}^{\mathrm{S}})-\beta|d_n^{\mathrm{S}}-d_{n'}^{\mathrm{S}}|}, \tag{4.22}$$

with

$$\alpha_m = a10^{-\frac{\eta}{10}d_m^{\mathrm{N}}} e^{-(15\tau+t_m^{\mathrm{C}})R^{\mathrm{DH}}-6\tau R^{\mathrm{DL}}} \tag{4.23}$$

and $\beta = \frac{R^{\mathrm{DH}}}{\ln(10)c}$. Then, recalling the definition of ρ and $\boldsymbol{\gamma}$ derived from Theorem 1, substituting (4.14) in (4.21) leads to

$$\max_{\mathbf{q}} \left(\sum_{m=1}^{M} \frac{1}{P_m}\right)^{-1} = \min_{\mathbf{q}} \sum_{m=1}^{M} \alpha_m^{-1} 10^{\frac{\eta}{10}(d_n^{\mathrm{S}}+d_{n'}^{\mathrm{S}})+\beta|d_n^{\mathrm{S}}-d_{n'}^{\mathrm{S}}|}, \tag{4.24}$$

which is still intractable due to the presence of the module term that depends on $\mathbf{q}$ through the difference of the nodes' distances. To cope with the non-convexity of the above, a vector composed by M slack variables $\mathbf{r} = [r_1, \ldots, r_M]^{\mathsf{T}}$ is introduced as well as the following constraints

$$\big| \|\mathbf{q} - \mathbf{u}_n\| - \|\mathbf{q} - \mathbf{u}_{n'}\| \big| \leq r_m, \quad \forall m = 1, \ldots, M, \tag{4.25}$$

which can be squared on both sides and manipulated as

$$\begin{aligned}
&\|\mathbf{q} - \mathbf{u}_n\|^2 + \|\mathbf{q} - \mathbf{u}_{n'}\|^2 - 2\|\mathbf{q} - \mathbf{u}_n\| \|\mathbf{q} - \mathbf{u}_{n'}\| \\
&= 2\left(\|\mathbf{q} - \mathbf{u}_n\|^2 + \|\mathbf{q} - \mathbf{u}_{n'}\|^2\right) \\
&\quad - (\|\mathbf{q} - \mathbf{u}_n\| + \|\mathbf{q} - \mathbf{u}_{n'}\|)^2 \leq r_m^2.
\end{aligned} \tag{4.26}$$

Then, the SCA technique [129] is applied. Indeed, reminding that the first-order Taylor expansion is a global underestimator for convex functions, (4.26) can be approximated as

$$
\begin{aligned}
2\big(\|\mathbf{q} - \mathbf{u}_n\|^2 &+ \|\mathbf{q} - \mathbf{u}_{n'}\|^2\big) - \big(\|\overline{\mathbf{q}} - \mathbf{u}_n\| + \|\overline{\mathbf{q}} - \mathbf{u}_{n'}\|\big)^2 \\
&- 2\left(\frac{\overline{\mathbf{q}} - \mathbf{u}_n}{\|\overline{\mathbf{q}} - \mathbf{u}_n\|} + \frac{\overline{\mathbf{q}} - \mathbf{u}_{n'}}{\|\overline{\mathbf{q}} - \mathbf{u}_{n'}\|} \right)^{\!\top} \big(\|\overline{\mathbf{q}} - \mathbf{u}_n\| + \|\overline{\mathbf{q}} - \mathbf{u}_{n'}\|\big) \\
&\times (\mathbf{q} - \overline{\mathbf{q}}) \le \overline{r}_m^2 + 2\overline{r}_m(r_m - \overline{r}_m)
\end{aligned}
\tag{4.27}
$$

where $\overline{\mathbf{q}}$ and $\overline{\mathbf{r}} = [\overline{r}_1, \ldots, \overline{r}_M]^{\top}$ are the local point of the expansion. Finally, given the above convex set of constraints, problem (4.24) can be reformulated as

$$
\min_{\mathbf{q},\mathbf{r}} \xi \triangleq \sum_{m=1}^{M} \alpha_m^{-1} 10^{\frac{\eta}{10}(d_n^{\mathrm{S}} + d_{n'}^{\mathrm{S}}) + \beta r_m} \quad \textbf{s.t.} \quad (4.27),
\tag{4.28}
$$

which can be iteratively solved until convergence to a prescribed tolerance ϵ is achieved [129], since its convexity is proved in the following Theorem.

Theorem 2. *Problem* (4.28) *is convex and can be solved with a generic optimization tool, such as CVX.*

Proof. The convexity of the objective function is guaranteed as (i) the euclidean norm is convex, (ii) the sum of convex functions is convex, and (iii) the composition $g(f(x))$ of a convex non-decreasing function $g(y)$ and a convex function $f(x)$ is convex as well. Moreover, constraints (4.27) are quadratic in the source position and linear in the slack variables, and hence convex by definition. ∎

Remark 1. *It is worth noting that, even if the source position has a non-linear effect over the objective function in* (4.28)*, the optimal solution is intuitively the centroid computed over the quantum nodes' positions, when these are uniformly deployed over the area. Indeed, it minimizes all d_n^S at the same time.*

The computational complexity of the optimization procedure, due to the summation of the inverse probabilities in (4.28), is $\mathcal{O}\left(K(M + (M+2)^{3.5}\right) = \mathcal{O}\left(KM^{3.5}\right)$ with K being the number of iterations of the SCA procedure.

4.5.3 Overall algorithm and complexity

The overall optimization procedure, summarized in Algorithm 2, derives the optimal location of the quantum source by leveraging the optimal closed-form expression of the maximum number of qubits per node. The total computational complexity, obtained as the sum of the single complexities, is $\mathcal{O}\left(KM^{3.5}\right) + \mathcal{O}\left(M\right) = \mathcal{O}\left(KM^{3.5}\right)$.

Algorithm 2 Proposed algorithm

1: Initialize the quantum node positions $\mathbf{u}_n$;
2: Compute the probabilities P_m derived in (4.8);
3: Randomly initialize local points $\overline{\mathbf{q}}$ and $\overline{\mathbf{r}}$;
4: **repeat**
5:    Solve (4.28) to obtain the optimal $\mathbf{q}$ and $\mathbf{r}$;
6:    $\overline{\mathbf{q}} \leftarrow \mathbf{q}$;
7:    $\overline{\mathbf{r}} \leftarrow \mathbf{r}$;
8: **until** convergence is achieved
9: According to Theorem 1, compute the photon distribution plan $\boldsymbol{\gamma}$ and the maximum number of qubits per quantum node ρ;

4.6 Performance Evaluation and Results

A simulation campaign is carried out to analyze and validate the findings of this work.

The first part investigates the impact of different parameter settings, such as (i) dephasing rate R^{DH}, (ii) initial probability of losing a photon once it enters a channel P^{G}, (iii) the attenuation factor η, and (iv) inter-node distance d_m^{N}, on the overall probability derived in (4.8).

In the second part, the results obtained from the proposed optimization algorithm are discussed and compared with a baseline approach. The latter exploits the optimal solution derived in sub-problem 1 for what concerns the scheduling plan, while for the position of the quantum source it adopts the centroid computed over the quantum nodes' locations. The analysis focuses on the impact that system conditions, which are made varying, have on the network performance.

According to [120] and [122], the considered configuration parameters in all simulations, unless otherwise specified, are $P^{\mathrm{G}} = 0.1$, $\eta = 0.1$ dB/km, $R^{\mathrm{DH}} = 0.1$ MHz, $R^{\mathrm{DL}} = 10$ kHz, $\epsilon = 10^{-6}$, $\tau = 10$ ns, $\overline{\gamma} = 1.2 \cdot 10^9$, and $c = 2 \cdot 10^5$ km/s. The quantum nodes are deployed in square-shaped areas with all sides having a length of ℓ. In all the simulation two different methodologies are employed to generate the nodes' coordinates: the first consists in sampling the positions of all nodes from circumference, i.e., $U_1 \sim \mathcal{C}(0, \ell)$; the second one generates the locations according to a uniform distribution $U_2 \sim \mathcal{U}(0, \ell)$; the third samples from a beta distribution $U_3 \sim \mathrm{Beta}(0.5, 0.5)$; the fourth generates the positions following a triangular distribution $U_4 \sim \mathcal{T}(0, 0.5, 1)$; the fifth U_5 distributes half of the nodes from U_2 and the second one from a scaled version of it, i.e., $\mathcal{U}(0, \ell/3)$.
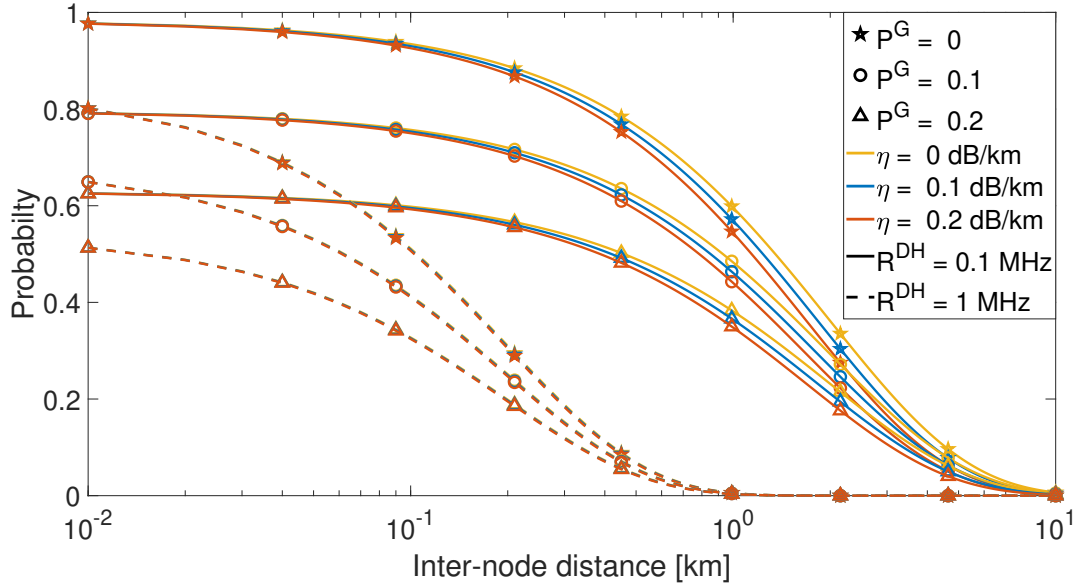
FIGURE 4.2: Overall probability of correctly receiving a qubit.

4.6.1 Analysis on the overall teleportation probability

In the first scenario, a quantum network composed of $N = 2$ quantum nodes, i.e, $M = 1$, is considered. Specifically, the nodes are aligned along an axes and the quantum source is placed exactly in the middle. Thus, the inter-node distance d_1^N is varied from 0 km to 2 km. This initial analysis highlights the significant challenges in transmitting quantum information over long distances due to the loss and noise in the transmission channel.

The results, as shown in Fig. 4.2, confirm that the probability of correctly receiving a qubit exponentially decreases as the inter-node distance grow. This effect is highly influenced by the dephasing rate, which affects the decoherence probability of qubits, especially at the receiver node. Notably, when the dephasing rate is set to 1 MHz, the probability drops close to zero once the inter-node distance reaches 1 km. For $R^{DH} = 0.1$ MHz, instead, it almost zeros out around 10 km. Another parameter that significantly affects the overall probability is P^G, which, regardless of other parameters, causes the curves in Fig. 4.2 to start at a higher value and decline more gradually to zero. Therefore, the dephasing rate and the generation probability, which are associated with the technology on which the system is based on, represent fundamental aspects to potentially expand the network area and hence to assess the feasibility of quantum teleportation.
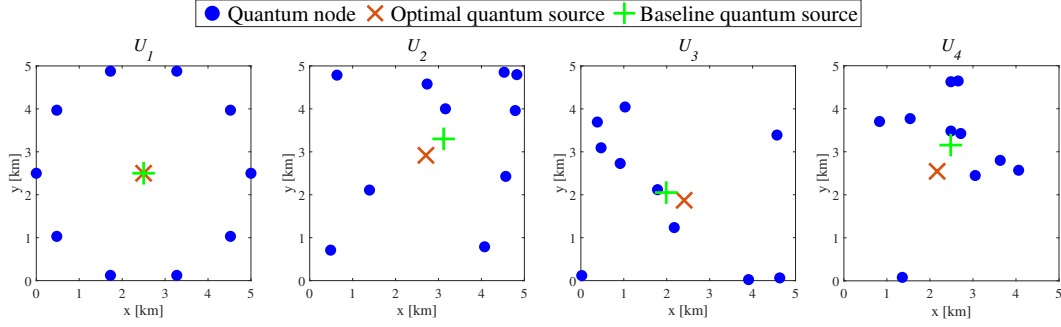
FIGURE 4.3: Optimal and Baseline quantum source position with $N = 10$ nodes in different topologies.
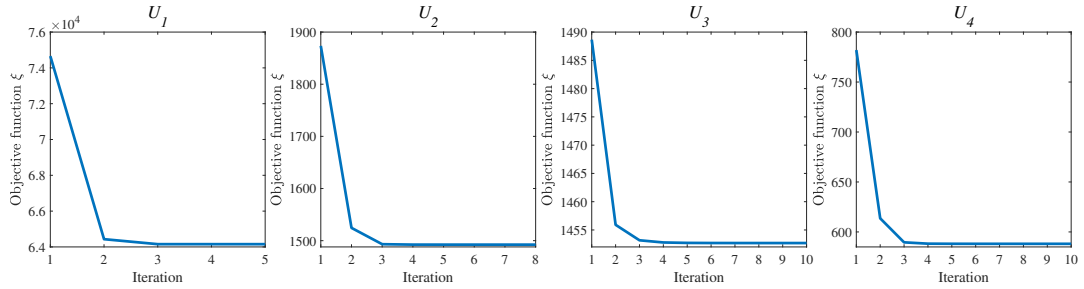

FIGURE 4.4: Convergence curves of the proposed algorithm.

4.6.2   Impact of the topology

In this simulation, a quantum network consisting of $N = 10$ nodes, distributed in an area characterized by $\ell = 5$ km, is considered. Four different topologies, generated according to U_1, U_2, U_3, and U_4, are examined.

Fig. 4.3 illustrates the comparison between the baseline and the proposed approach for the optimal positioning of the quantum source. In the first considered topology, all nodes are equidistant from the same point, i.e, the center of the circumference, which is the optimal position to deploy the quantum source, thus proving Remark 1. Indeed, both algorithms achieve the same solution in terms of source location (as can be seen in the left graph of the figure) and minimum number of successfully received qubits $\rho = 3.8 \cdot 10^5$. However, in the case of random distribution, the optimal position of the source is not the centroid (as depicted in the right graph of Fig. 4.3). As a matter of fact, the optimal source location cannot be simply derived by averaging the nodes positions, which would lead to worse performance. Indeed, considering the last three topologies, the baseline approach achieves a minimum number of transmitted qubit ρ of $2.6 \cdot 10^6, 1.6 \cdot 10^6$, and $2.7 \cdot 10^6$, respectively, whereas the proposed approach reaches a remarkable $3.3 \cdot 10^6, 2 \cdot 10^6$, and $3.7 \cdot 10^6$, which corresponds to a minimum increase of 25%. Finally, Fig. 4.4 shows the convergence of the proposed algorithm in all topologies in terms of the objective function ξ defined
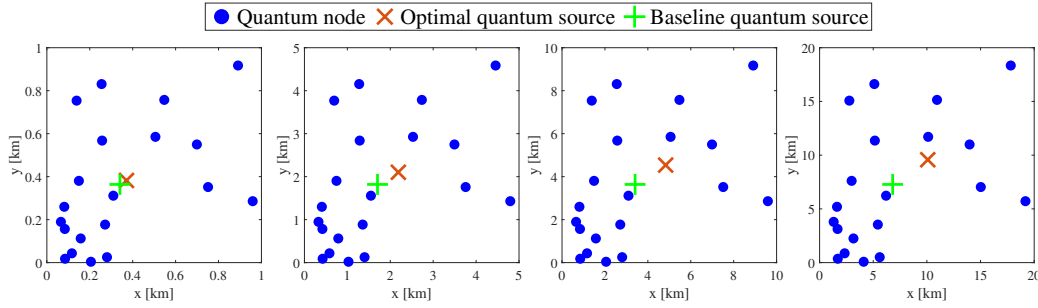
FIGURE 4.5: Comparison between optimal and baseline approaches with fixed topology of $N = 20$ nodes deployed within areas of different scale.
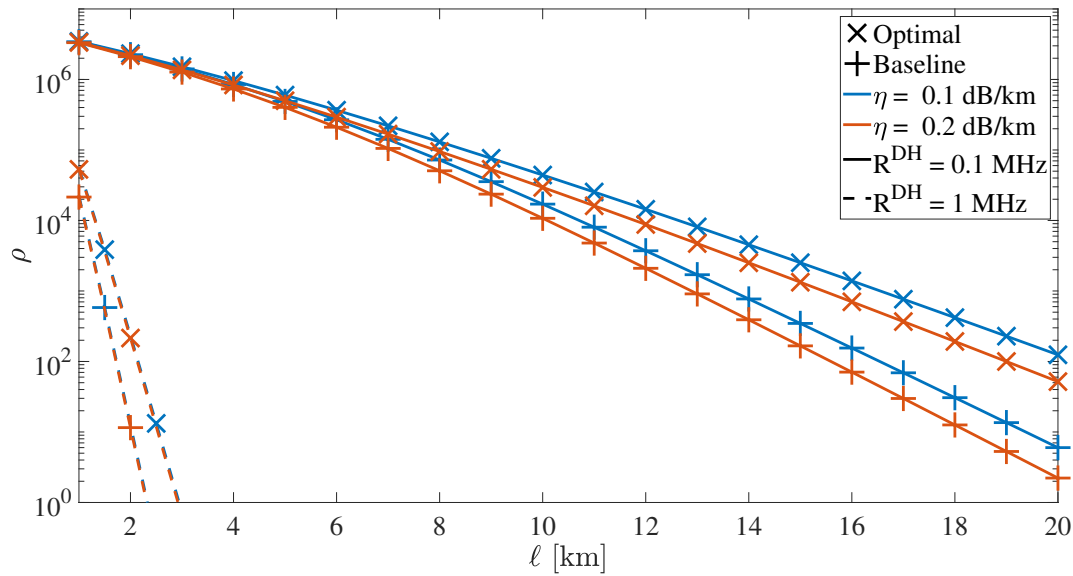

FIGURE 4.6: Number of correctly received qubits ρ as a function of ℓ for different system parameters.

in Eq. (4.28), which represents a local approximation of ρ in the iterative optimization process. Clearly, the number of iterations required to converge in the first case is smaller, with respect to the other configurations, due to the regular shape of the network graph.

4.6.3 Impact of the system parameters

To assess the impact of the inter-node distance on the entanglement distribution, $N = 20$ quantum nodes are sampled from U_5 and deployed within various areas characterized by $\ell \in [0, 20]$ km.

In particular, Fig. 4.5 shows the quantum source location for both the considered algorithm, when $\ell = \{1, 5, 10, 20\}$. As can be seen, the source position provided by the baseline approach remains the same, i.e., the centroid, except for the scale. On the contrary, the proposed solution changes with ℓ, thus demonstrating to be able
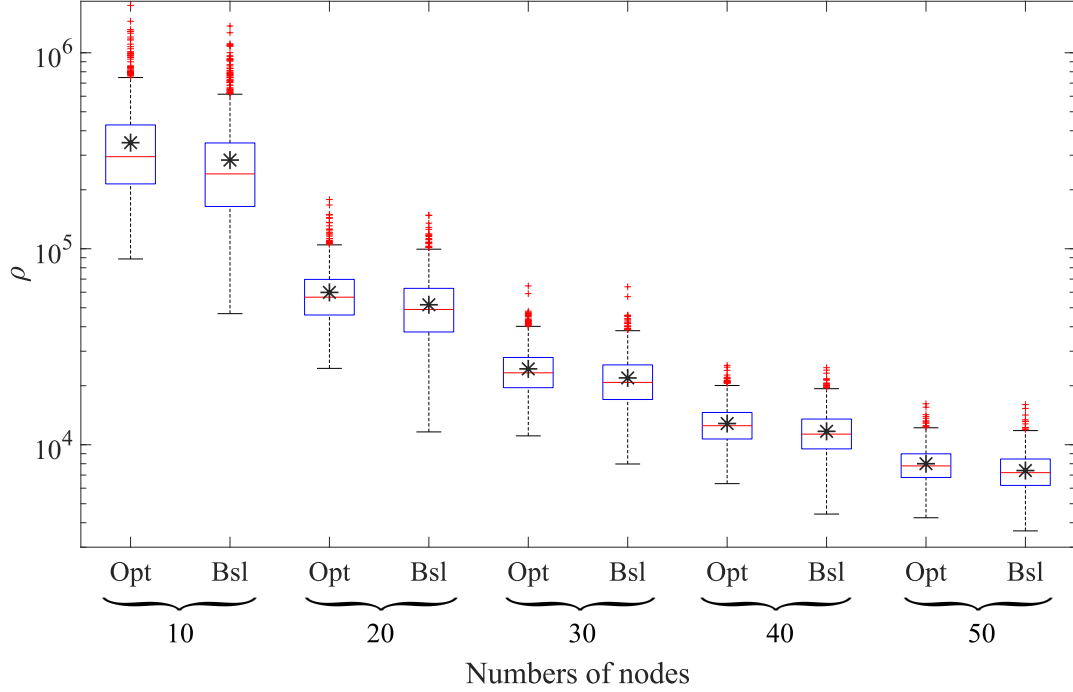
78

Chapter 4. A Probability-Based Optimization Approach for Entanglement Distribution and Source Position in Quantum Networks

FIGURE 4.7: Comparison between proposed (Opt) and baseline (Bsl) approaches with respect to ρ as a function of quantum nodes N with U_2. The black stars represent the mean value.

to capture the non-linearity of the probability expression derived in Section 4.3. It is worth noting that, in case of $\ell = 1$ km, the area is small enough to adopt the baseline as quasi-optimal solution. Indeed, the impact of the inter-node distances is negligible in small areas, as predicted by Corollary 1. To further corroborate the above findings and to give more insights about the performance gain provided by the optimal algorithm, Fig. 4.6 depicts the trend of ρ as a function of $\ell \in [0, 20]$. As a matter of fact, for a limited area the solutions are comparable but as ℓ increases, a major gap in terms of successfully received qubits arises. This demonstrates the crucial importance of the proposed optimal design in case of quantum networks deployed, especially, in wide areas. Specifically for $R^{\mathrm{DH}} = 0.1$ MHz and $\ell = 20$ km, the optimal algorithm allows the transmission of 124 qubits for $\eta = 0.1$ and 52 qubits for $\eta = 0.2$, while the baseline approach just 6 and 2 qubits. As a consequence, the proposed algorithm provides, in terms of received qubits, $\sim$20 and $\sim$25 times better solutions, respectively. In case of higher dephasing rate $R^{\mathrm{DH}} = 1$ MHz, the resulting loss constrains the maximum possible area, thus producing no difference between the two algorithms, which again confirms Corollary 1.

4.6.4 Analysis on network scalability

In this last analysis, the impact of the number of nodes in a quantum network having $\ell = 10$ km is investigated. In this regard, a Monte Carlo simulation is carried out
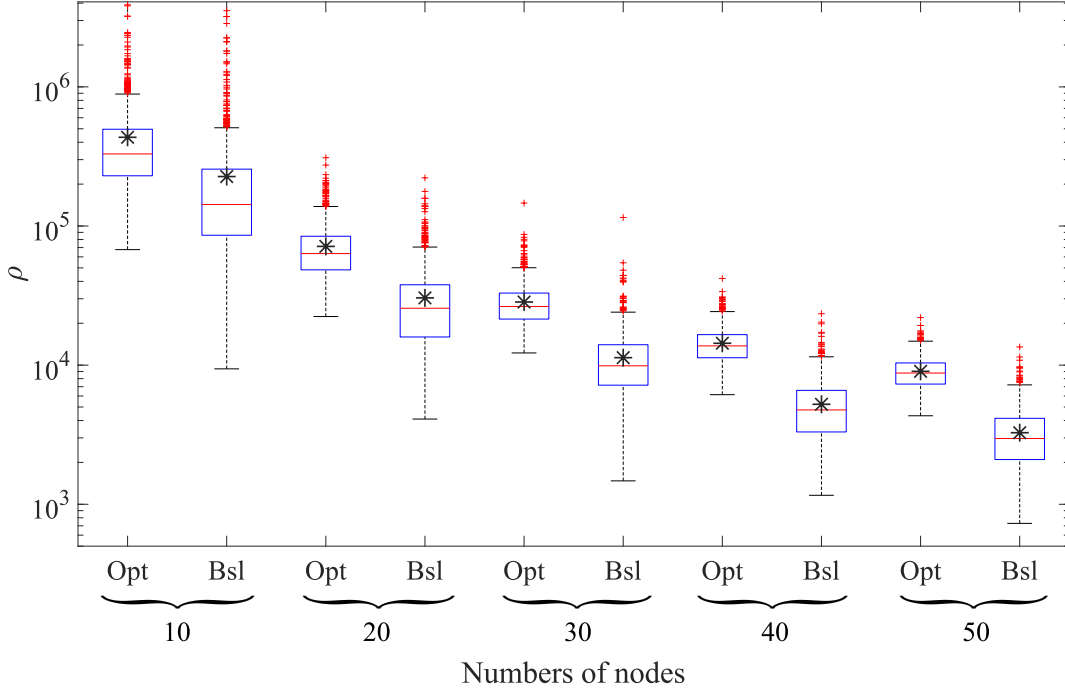
FIGURE 4.8: Comparison between proposed (Opt) and baseline (Bsl) approaches with respect to ρ as a function of quantum nodes N with U_5. The black stars represent the mean value.

by generating the nodes' positions according to both U_2 and U_5, for a total of 10^3 samples. This procedure is iterated by making the number of nodes vary, i.e., $N = \{10, 20, 30, 40, 50\}$.

Figure 4.7 and Figure 4.8 illustrate the relationship between ρ and the number of nodes for U_2 and U_5, respectively. As expected, in both cases, the proposed and the baseline approaches exhibit a decreasing trend as the number of nodes increases. This is due to the reduction in the number of entangled pairs available for each pair of nodes as the network size grows. Notably, the proposed algorithm performs better than the baseline approach, in terms of number of transmitted qubits with a much smaller variance, in both cases. Nonetheless, this difference becomes more evident when the nodes are generated according to U_5. Vice versa, as already stated in Remark 1 and proved in Section 4.6.2, when U_2 is chosen, i.e., the uniform distribution, the optimal source position becomes the centroid of the network. Therefore, the proposed and baseline approaches perform similarly, even if the former still provides better results. Specifically, when considering U_2 with $N = 50$, the proposed algorithm and the baseline approach achieve a mean value of $\rho = 8 \cdot 10^3$ and $\rho = 7 \cdot 10^3$, whereas for U_5, they attain a $\rho = 9 \cdot 10^3$ and $\rho = 3 \cdot 10^3$, respectively.

Conclusions and Future Works

QC and quantum communication are opening up a fascinating new frontier of research, driven by the principles of quantum mechanics. This groundbreaking field promises to have a direct impact on the telecommunications industry, offering novel strategies to tackle classical complex problems, such as network optimization, data analysis and resource management. This thesis has been dedicated to exploring different strategies to integrate this disruptive paradigms into future wireless communication systems.

In particular, as discussed in Chapters 2, existing architectures currently lack the computational capabilities necessary to handle the expected growing in data volumes within the realms of 6G and B6G use cases, and WMNs. Consequently, design principles for centralized and distributed architecture were presented for enhancing network intelligence through QML, alongside the description of logical nodes, interactions, and offered functionalities.

Given the limited availability of quantum computers and qubits, due to physical and economic factors, the centralized approach presents the most practical solution. It offers ease of management and control, as the few quantum computers in the cloud can be efficiently overseen. However, since any issue affecting the central nodes in the cloud inevitably causes impairment throughout the network, this approach is vulnerable. Additionally, when QML operations are required, transmitting substantial amounts of data from the Data Aggregators to the remote cloud leads to high bandwidth and energy consumption, along with potential congestion episodes. Furthermore, the centralized approach introduces significant communication latency, impairing the benefits provided by the introduction of quantum computers.

The limitations associated with the centralized architecture can be effectively addressed through the proposed distributed architecture. In fact, the deployment of multiple quantum computers closer to the end user mitigates possible network congestion episodes, improves scalability, and reduces communication latency. Nevertheless, since quantum Internet is in its fancy, the entanglement distribution and heterogeneity of qubits may represent a first hindrance for the physical implementation of the distributed architecture. As per the long-term vision of the scientific community, this proposed architecture will become viable when considering the hardware diversity of various quantum computers and distributing entangled particles between distant

quantum nodes. Another concern lies in the simplicity of the quantum computers involved, particularly in terms of the number qubits. In this case, complex QML tasks will demand larger clusters, leading to increased quantum state transfers, delays, and error rates due to the quantum teleportation process.

To prove the advantages brought by QC, in Chapter 3 is formulated a scheduling optimization problem to fairly allocate channel resources of a UAVs-enabled IoT network. A combinatorial problem stem from the proposed formulation, which is first encoded into QUBO form and then solved by (i) hybrid quantum-classical approach, (ii) SA, and (iii) TS. The results highlight the need for additional research and advancements in quantum annealers hardware, as no substantial improvements in solution quality has been found. Regarding the execution time, classical algorithms take less or comparable time with respect to the hybrid solver, with the only exception of SA in case of large number of sensors.

Lastly, Chapter 4 addresses the entanglement distribution problem, which can hinder the quantum communication efficiency whithin a network composed of quantum nodes, especially in the proposed distributed architecture. In particular, this work focusing on the achievable performance of a quantum network through mathematical modeling of the probability of a qubit successfully reaching the receiver node. Unlike other contributions, the derived expression considers multiple sources of impairment affecting the teleportation protocol. Building upon this model, a MINLP problem was formulated with the objective of maximizing the number of qubits received by nodes in a fair manner. Therefore, the optimal entanglement distribution and quantum source positions are compared with a baseline approach. The results underscore a significant performance gap between the two algorithms in terms of the number of qubits exchanged per node pair. In conclusion, this comprehensive study highlights the considerable challenges associated with transmitting quantum information over long distances due to losses and noise in the transmission channel. Simultaneously, the theoretical insights generated are invaluable for the design and optimization of quantum communication networks, which hold immense potential to reshape the landscape of communication and computation in the future.

Although a remarkable number of challenges brought by the QC and quantum communication remain disregarded, the achieved results prompt the scientific community to conduct more studies in this field. In the future, research will focus on the following aspects.

- With the involvement of numerous quantum computers, a critical task lies in the efficient distribution of quantum algorithms. This involves the simultaneous minimization of cluster size and user-quantum computer distance, necessitating investigation.

- Another critical research challenge involves developing effective strategies for the allocation of quantum computational resources, especially in situations where there is a significant need for computational power.

- The limitations encountered when applying quantum computing to optimization problems need for further investigation. Future research will also delve into the holistic optimization of transmission scheduling plans, multiple drones' trajectories, and their corresponding energy consumption, seeking innovative solutions.

- Fidelity, a key resource in quantum communication that assesses the closeness of two quantum states, can affect the quantum communication efficiency. Beyond optimizing entanglement distribution plans and source positions, future research will aim at meeting specific fidelity requirements.

Bibliography

[1] E. Gibney, "The quantum gold rush," *Nature*, vol. 574, no. 7776, pp. 22–24, 2019.

[2] E. Cartlidge, "Europe's €1 billion quantum flagship announces grants," *Science*, vol. 362, no. 6414, pp. 512–512, 2018. DOI: 10.1126/science.362.6414.512.

[3] V. Martin, J. P. Brito, C. Escribano, *et al.*, "Quantum technologies in the telecommunications industry," *EPJ Quantum Technology*, vol. 8, no. 1, p. 19, 2021.

[4] F. Phillipson, "Quantum computing in telecommunication — a survey," *Mathematics*, vol. 11, no. 15, p. 3423, 2023.

[5] M. R. Mahmood, M. A. Matin, P. Sarigiannidis, and S. K. Goudos, "A comprehensive review on artificial intelligence/machine learning algorithms for empowering the future iot toward 6g era," *IEEE Access*, vol. 10, pp. 87 535–87 562, 2022.

[6] B. Narottama, Z. Mohamed, and S. Aïssa, "Quantum machine learning for next-g wireless communications: Fundamentals and the path ahead," *IEEE Open Journal of the Communications Society*, 2023.

[7] P. Rebentrost, M. Mohseni, and S. Lloyd, "Quantum support vector machine for big data classification," *Physical review letters*, vol. 113, no. 13, p. 130 503, 2014.

[8] M. Benedetti, J. Realpe-Gómez, and A. Perdomo-Ortiz, "Quantum-assisted helmholtz machines: A quantum–classical deep learning framework for industrial datasets in near-term devices," *Quantum Science and Technology*, vol. 3, no. 3, p. 034 007, 2018.

[9] K. Beer, D. Bondarenko, T. Farrelly, *et al.*, "Training deep quantum neural networks," *Nature communications*, vol. 11, no. 1, p. 808, 2020.

[10] J. Amin, M. Sharif, N. Gul, S. Kadry, and C. Chakraborty, "Quantum machine learning architecture for covid-19 classification based on synthetic data generation using conditional adversarial neural network," *Cognitive Computation*, vol. 14, no. 5, pp. 1677–1688, 2022.

[11] A. Kole, D. De, and A. J. Pal, "Solving graph coloring problem using ant colony optimization, simulated annealing and quantum annealing—a comparative study," in *Intelligence Enabled Research: DoSIER 2021*, Springer, 2022, pp. 1–15.

[12] E. Osaba, E. Villar-Rodriguez, and I. Oregi, "A systematic literature review of quantum computing for routing problems," *IEEE Access*, vol. 10, pp. 55 805–55 817, 2022.

[13] W. da Silva Coelho, L. Henriet, and L.-P. Henry, "Quantum pricing-based column-generation framework for hard combinatorial problems," *Physical Review A*, vol. 107, no. 3, p. 032 426, 2023.

[14] G. Brassard, A. Broadbent, J. Fitzsimons, S. Gambs, and A. Tapp, "Anonymous quantum communication," in *Advances in Cryptology–ASIACRYPT 2007: 13th International Conference on the Theory and Application of Cryptology and Information Security, Kuching, Malaysia, December 2-6, 2007. Proceedings 13*, Springer, 2007, pp. 460–473.

[15] D. Cuomo, M. Caleffi, K. Krsulich, *et al.*, "Optimized compiler for distributed quantum computing," *ACM Transactions on Quantum Computing*, vol. 4, no. 2, pp. 1–29, 2023.

[16] D. Cuomo, M. Caleffi, and A. S. Cacciapuoti, "Towards a distributed quantum computing ecosystem," *IET Quantum Communication*, vol. 1, no. 1, pp. 3–8, 2020.

[17] S. Imre and F. Balazs, *Quantum Computing and Communications: an engineering approach*. John Wiley & Sons, 2005.

[18] M. A. Nielsen and I. L. Chuang, *Quantum Computation and Quantum Information: 10th Anniversary Edition*. Cambridge University Press, 2010. DOI: 10.1017/CBO9780511976667.

[19] P. A. M. Dirac, "On the theory of quantum mechanics," *Proceedings of the Royal Society of London. Series A, Containing Papers of a Mathematical and Physical Character*, vol. 112, no. 762, pp. 661–677, 1926.

[20] D. P. DiVincenzo, "Quantum gates and circuits," *Proceedings of the Royal Society of London. Series A: Mathematical, Physical and Engineering Sciences*, vol. 454, no. 1969, pp. 261–276, 1998.

[21] G. L. Light, "Pauli matrices immersion," *Materials Science and Engineering: B*, vol. 264, p. 114 910, 2021, ISSN: 0921-5107. DOI: https://doi.org/10.1016/j.mseb.2020.114910. [Online]. Available: https://www.sciencedirect.com/science/article/pii/S0921510720304177.

[22] A. Barenco, C. H. Bennett, R. Cleve, *et al.*, "Elementary gates for quantum computation," *Physical review A*, vol. 52, no. 5, p. 3457, 1995.

[23] A. Zeilinger, "Quantum entanglement: A fundamental concept finding its applications," *Physica Scripta*, vol. 1998, no. T76, p. 203, 1998.

[24] R. Horodecki, P. Horodecki, M. Horodecki, and K. Horodecki, "Quantum entanglement," *Reviews of modern physics*, vol. 81, no. 2, p. 865, 2009.

[25] A. Einstein, B. Podolsky, and N. Rosen, "Can quantum-mechanical description of physical reality be considered complete?" *Physical review*, vol. 47, no. 10, p. 777, 1935.

[26] A. S. Cacciapuoti, M. Caleffi, R. Van Meter, and L. Hanzo, "When entanglement meets classical communications: Quantum teleportation for the quantum internet," *IEEE Transactions on Communications*, vol. 68, no. 6, pp. 3808–3833, 2020. DOI: 10.1109/TCOMM.2020.2978071.

[27] G. K. Kitaeva and A. N. Penin, "Spontaneous parametric down-conversion," *Journal of Experimental and Theoretical Physics Letters*, vol. 82, pp. 350–355, 2005.

[28] D. Matsukevich, T. Chaneliere, S. Jenkins, S.-Y. Lan, T. Kennedy, and A. Kuzmich, "Entanglement of remote atomic qubits," *Physical review letters*, vol. 96, no. 3, p. 030405, 2006.

[29] S. Ritter, C. Nölleke, C. Hahn, *et al.*, "An elementary quantum network of single atoms in optical cavities," *Nature*, vol. 484, no. 7393, pp. 195–200, 2012.

[30] S. Welte, B. Hacker, S. Daiss, S. Ritter, and G. Rempe, "Photon-mediated quantum gate between two neutral atoms in an optical cavity," *Physical Review X*, vol. 8, no. 1, p. 011018, 2018.

[31] A. Zeilinger, "Quantum teleportation," *Scientific American*, vol. 282, no. 4, pp. 50–59, 2000, ISSN: 00368733, 19467087. [Online]. Available: http://www.jstor.org/stable/26058672 (visited on 08/27/2023).

[32] C. H. Bennett, G. Brassard, C. Crépeau, R. Jozsa, A. Peres, and W. K. Wootters, "Teleporting an unknown quantum state via dual classical and einstein-podolsky-rosen channels," *Phys. Rev. Lett.*, vol. 70, pp. 1895–1899, 13 1993.

[33] D. Boschi, S. Branca, F. De Martini, L. Hardy, and S. Popescu, "Experimental realization of teleporting an unknown pure quantum state via dual classical and einstein-podolsky-rosen channels," *Physical Review Letters*, vol. 80, no. 6, p. 1121, 1998.

[34] D. Bouwmeester, J.-W. Pan, K. Mattle, M. Eibl, H. Weinfurter, and A. Zeilinger, "Experimental quantum teleportation," *Nature*, vol. 390, no. 6660, pp. 575–579, 1997.

[35] J.-G. Ren, P. Xu, H.-L. Yong, *et al.*, "Ground-to-satellite quantum teleportation," *Nature*, vol. 549, no. 7670, pp. 70–73, 2017.

[36] J. Illiano, A. S. Cacciapuoti, A. Manzalini, and M. Caleffi, "The impact of the quantum data plane overhead on the throughput," in *Proceedings of the Eight Annual ACM International Conference on Nanoscale Computing and Communication*, ser. NANOCOM '21, New York, NY, USA: Association for Computing Machinery, 2021. DOI: 10.1145/3477206.3477448.

[37] S. Imre, "Quantum communications: Explained for communication engineers," *IEEE Communications Magazine*, vol. 51, no. 8, pp. 28–35, 2013.

[38] S. Yarkoni, E. Raponi, T. Bäck, and S. Schmitt, "Quantum annealing for industry applications: Introduction and review," *Reports on Progress in Physics*, 2022.

[39] D. E. Deutsch, A. Barenco, and A. Ekert, "Universality in quantum computation," *Proceedings of the Royal Society of London. Series A: Mathematical and Physical Sciences*, vol. 449, no. 1937, pp. 669–677, 1995.

[40] S. Morita and H. Nishimori, "Mathematical foundation of quantum annealing," *Journal of Mathematical Physics*, vol. 49, no. 12, p. 125 210, 2008.

[41] A. Das and B. K. Chakrabarti, "Colloquium: Quantum annealing and analog quantum computation," *Reviews of Modern Physics*, vol. 80, no. 3, p. 1061, 2008.

[42] P. Hauke, H. G. Katzgraber, W. Lechner, H. Nishimori, and W. D. Oliver, "Perspectives of quantum annealing: Methods and implementations," *Reports on Progress in Physics*, vol. 83, no. 5, p. 054 401, 2020.

[43] M. W. Johnson, M. H. Amin, S. Gildert, *et al.*, "Quantum annealing with manufactured spins," *Nature*, vol. 473, no. 7346, pp. 194–198, 2011.

[44] F. Neukart, G. Compostella, C. Seidel, D. Von Dollen, S. Yarkoni, and B. Parney, "Traffic flow optimization using a quantum annealer," *Frontiers in ICT*, vol. 4, p. 29, 2017.

[45] D. Venturelli, D. J. Marchand, and G. Rojo, "Quantum annealing implementation of job-shop scheduling," *arXiv preprint arXiv:1506.08479*, 2015.

[46] H. Neven, V. S. Denchev, G. Rose, and W. G. Macready, "Training a large scale classifier with the quantum adiabatic algorithm," *arXiv preprint arXiv: 0912.0779*, 2009.

[47] I. F. Akyildiz, A. Kak, and S. Nie, "6G and Beyond: The Future of Wireless Communications Systems," *IEEE Access*, vol. 8, pp. 133 995–134 030, 2020.

[48] E. Hossain and K. K. Leung, *Wireless mesh networks: architectures and protocols*. Springer, 2007.

[49] I. F. Akyildiz, X. Wang, and W. Wang, "Wireless mesh networks: A survey," *Computer networks*, vol. 47, no. 4, pp. 445–487, 2005.

[50] Z. Zhang, Y. Xiao, Z. Ma, *et al.*, "6G Wireless Networks: Vision, Requirements, Architecture, and Key Technologies," *IEEE Vehicular Technology Magazine*, vol. 14, no. 3, pp. 28–41, 2019.

[51] K. B. Letaief, W. Chen, Y. Shi, J. Zhang, and Y.-J. A. Zhang, "The Roadmap to 6G: AI Empowered Wireless Networks," *IEEE Communications Magazine*, vol. 57, no. 8, pp. 84–90, 2019.

[52] S. J. Nawaz, S. K. Sharma, S. Wyne, M. N. Patwary, and M. Asaduzzaman, "Quantum Machine Learning for 6G Communication Networks: State-of-the-Art and Vision for the Future," *IEEE Access*, vol. 7, pp. 46 317–46 350, 2019.

[53] T. M. Khan and A. Robles-Kelly, "Machine learning: Quantum vs classical," *IEEE Access*, vol. 8, pp. 219 275–219 294, 2020.

[54] G. Sergioli, "Quantum and Quantum-Like Machine Learning: A Note on Differences and Similarities," *Soft Computing*, vol. 24, no. 14, pp. 10 247–10 255, 2020.

[55] Y. Li, M. Tian, G. Liu, C. Peng, and L. Jiao, "Quantum Optimization and Quantum Learning: A Survey," *IEEE Access*, vol. 8, pp. 23 568–23 593, 2020.

[56] D. Sierra-Sosa, M. Telahun, and A. Elmaghraby, "TensorFlow Quantum: Impacts of Quantum State Preparation on Quantum Machine Learning Performance," *IEEE Access*, vol. 8, pp. 215 246–215 255, 2020.

[57] J. R. Bhat and S. A. AlQahtani, "6G Ecosystem: Current Status and Future Perspective," *IEEE Access*, vol. 9, pp. 43 134–43 167, 2021. DOI: 10.1109/ACCESS.2021.3054833.

[58] J. F. Monserrat, D. Martin-Sacristan, F. Bouchmal, O. Carrasco, J. Flores de Valgas, and N. Cardona, "Key Technologies for the Advent of the 6G," in *2020 IEEE Wireless Communications and Networking Conference Workshops (WCNCW)*, 2020, pp. 1–6.

[59] W. O'Quinn and S. Mao, "Quantum Machine Learning: Recent Advances and Outlook," *IEEE Wireless Commununications*, vol. 27, no. 3, pp. 126–131, 2020.

[60] M. Caleffi, D. Chandra, D. Cuomo, S. Hassanpour, and A. S. Cacciapuoti, "The Rise of the Quantum Internet," *Computer*, vol. 53, no. 6, pp. 67–72, 2020. DOI: 10.1109/MC.2020.2984871.

[61] W. Saad, M. Bennis, and M. Chen, "A Vision of 6G Wireless Systems: Applications, Trends, Technologies, and Open Research Problems," *IEEE Netw.*, vol. 34, no. 3, pp. 134–142, 2020.

[62] M. Giordani, M. Polese, M. Mezzavilla, S. Rangan, and M. Zorzi, "Toward 6G Networks: Use Cases and Technologies," *IEEE Commun. Mag.*, vol. 58, no. 3, pp. 55–61, 2020.

[63] C.-X. Wang, X. You, X. Gao, *et al.*, "On the road to 6g: Visions, requirements, key technologies and testbeds," *IEEE Communications Surveys & Tutorials*, 2023.

[64] D. C. Nguyen, M. Ding, P. N. Pathirana, *et al.*, "6g internet of things: A comprehensive survey," *IEEE Internet of Things Journal*, vol. 9, no. 1, pp. 359–383, 2021.

[65] I. F. Akyildiz and X. Wang, "A survey on wireless mesh networks," *IEEE Communications magazine*, vol. 43, no. 9, S23–S30, 2005.

[66] M. Bano, A. Qayyum, R. N. B. Rais, and S. S. A. Gilani, "Soft-mesh: A robust routing architecture for hybrid sdn and wireless mesh networks," *IEEE Access*, vol. 9, pp. 87 715–87 730, 2021. DOI: 10.1109/ACCESS.2021.3089020.

[67] H. Kusumoto, H. Okada, K. Kobayashi, and M. Katayama, "Performance comparison between single-user mimo and multi-user mimo in wireless mesh networks," in *The 15th International Symposium on Wireless Personal Multimedia Communications*, IEEE, 2012, pp. 202–206.

[68] W. Jaafar, W. Ajib, and S. Tabbane, "The capacity of mimo-based wireless mesh networks," in *2007 15th IEEE International Conference on Networks*, IEEE, 2007, pp. 259–264.

[69] R. Kumar, U. Venkanna, and V. Tiwari, "A time granular analysis of software defined wireless mesh based iot (sdwm-iot) network traffic using supervised learning," *Wireless Personal Communications*, vol. 116, no. 3, pp. 2083–2109, 2021.

[70] H. Elzain and W. Yang, "Qos-aware topology discovery in decentralized software defined wireless mesh network (d-sdwmn) architecture," in *Proceedings of the 2018 2nd international conference on computer science and artificial intelligence*, 2018, pp. 158–162.

[71] M. Al-Jarrah, E. Alsusa, A. Al-Dweik, and M.-S. Alouini, "Performance analysis of wireless mesh backhauling using intelligent reflecting surfaces," *IEEE Transactions on Wireless Communications*, vol. 20, no. 6, pp. 3597–3610, 2021. DOI: 10.1109/TWC.2021.3052370.

[72] S. Karunaratne and H. Gacanin, "An overview of machine learning approaches in wireless mesh networks," *IEEE Communications Magazine*, vol. 57, no. 4, pp. 102–108, 2019.

[73] R. Choudhary and H. K. Gianey, "Comprehensive review on supervised machine learning algorithms," in *2017 International Conference on Machine Learning and Data Science (MLDS)*, 2017, pp. 37–43. DOI: 10.1109/MLDS.2017.11.

[74] M. Usama, J. Qadir, A. Raza, *et al.*, "Unsupervised machine learning for networking: Techniques, applications and research challenges," *IEEE access*, vol. 7, pp. 65 579–65 615, 2019.

[75] Y. LeCun, Y. Bengio, and G. Hinton, "Deep learning," *nature*, vol. 521, no. 7553, pp. 436–444, 2015.

[76] V. Mnih, K. Kavukcuoglu, D. Silver, *et al.*, "Human-level control through deep reinforcement learning," *nature*, vol. 518, no. 7540, pp. 529–533, 2015.

[77] C. Zhang, P. Patras, and H. Haddadi, "Deep Learning in Mobile and Wireless Networking: A Survey," *IEEE Communications Surveys & Tutorials*, vol. 21, no. 3, pp. 2224–2287, 2019.

[78] X. Wang, J. S. Wong, F. Stanley, and S. Basu, "Cross-layer based anomaly detection in wireless mesh networks," in *2009 ninth annual international symposium on applications and the internet*, IEEE, 2009, pp. 9–15.

[79] E. A. Shams and A. Rizaner, "A novel support vector machine based intrusion detection system for mobile ad hoc networks," *Wireless Networks*, vol. 24, no. 5, pp. 1821–1829, 2018.

[80] B. Das, A. K. Roy, A. K. Khan, and S. Roy, "A new approach for gateway-level load balancing of wmns through k-means clustering," in *2014 International Conference on Computational Intelligence and Communication Networks*, IEEE, 2014, pp. 515–519.

[81]   Z. R. Zaidi, S. Hakami, B. Landfeldt, and T. Moors, "Real-time detection of traffic anomalies in wireless mesh networks," *Wireless Networks*, vol. 16, no. 6, pp. 1675–1689, 2010.

[82]   M. Boushaba, A. Hafid, A. Belbekkouche, and M. Gendreau, "Reinforcement learning based routing in wireless mesh networks," *Wireless Networks*, vol. 19, no. 8, pp. 2079–2091, 2013.

[83]   M. Yin, J. Chen, X. Duan, B. Jiao, and Y. Lei, "Qebr: Q-learning based routing protocol for energy balance in wireless mesh networks," in *2018 IEEE 4th International Conference on Computer and Communications (ICCC)*, IEEE, 2018, pp. 280–284.

[84]   F. Tang, B. Mao, Z. M. Fadlullah, *et al.*, "On removing routing protocol from future wireless networks: A real-time deep learning approach for intelligent traffic control," *IEEE Wireless Communications*, vol. 25, no. 1, pp. 154–160, 2017.

[85]   L. Nie, D. Jiang, S. Yu, and H. Song, "Network traffic prediction based on deep belief network in wireless mesh backbone networks," in *2017 IEEE Wireless Communications and Networking Conference (WCNC)*, IEEE, 2017, pp. 1–5.

[86]   Q. Liu, L. Cheng, A. L. Jia, and C. Liu, "Deep Reinforcement Learning for Communication Flow Control in Wireless Mesh Networks," *IEEE Network*, vol. 35, no. 2, pp. 112–119, 2021.

[87]   C. Yin, R. Yang, X. Zou, and W. Zhu, "Research on topology planning for wireless mesh networks based on deep reinforcement learning," in *2020 2nd International Conference on Computer Communication and the Internet (IC-CCI)*, IEEE, 2020, pp. 6–11.

[88]   Y. Xu, J. Yu, W. C. Headley, and R. M. Buehrer, "Deep reinforcement learning for dynamic spectrum access in wireless networks," in *MILCOM 2018-2018 IEEE Military Communications Conference (MILCOM)*, IEEE, 2018, pp. 207–212.

[89]   M. Schuld and F. Petruccione, *Supervised learning with quantum computers*. Springer, 2018, vol. 17.

[90]   F. Phillipson, "Quantum machine learning: Benefits and practical examples.," in *QANSWER*, 2020, pp. 51–56.

[91] D. Fastovets, Y. I. Bogdanov, B. Bantysh, and V. Lukichev, "Machine learning methods in quantum computing theory," in *International Conference on Micro-and Nano-Electronics 2018*, International Society for Optics and Photonics, vol. 11022, 2019, 110222S.

[92] L. Gyongyosi and S. Imre, "A survey on quantum computing technology," *Computer Science Review*, vol. 31, pp. 51–71, 2019, ISSN: 1574-0137. DOI: https://doi.org/10.1016/j.cosrev.2018.11.002.

[93] S. DiAdamo, M. Ghibaudi, and J. Cruise, "Distributed Quantum Computing and Network Control for Accelerated VQE," *IEEE Trans. on Quantum Eng.*, vol. 2, pp. 1–21, 2021.

[94] J. Illiano, M. Caleffi, A. Manzalini, and A. S. Cacciapuoti, "Quantum internet protocol stack: A comprehensive survey," *Computer Networks*, p. 109 092, 2022.

[95] J. Yin, Y. Cao, Y.-H. Li, *et al.*, "Satellite-based entanglement distribution over 1200 kilometers," *Science*, vol. 356, no. 6343, pp. 1140–1144, 2017.

[96] H.-Y. Liu, X.-H. Tian, C. Gu, *et al.*, "Drone-based entanglement distribution towards mobile quantum networks," *National Science Review*, vol. 7, no. 5, pp. 921–928, 2020.

[97] M. Caleffi, A. S. Cacciapuoti, and G. Bianchi, "Quantum internet: From communication to distributed computing!" In *Proceedings of the 5th ACM International Conference on Nanoscale Computing and Communication*, ser. NANOCOM '18, New York, NY, USA: Association for Computing Machinery, 2018. DOI: 10.1145/3233188.3233224.

[98] M. Kim, D. Venturelli, and K. Jamieson, "Leveraging quantum annealing for large mimo processing in centralized radio access networks," in *Proceedings of the ACM Special Interest Group on Data Communication*, Association for Computing Machinery, 2019, pp. 241–255.

[99] F. Ishizaki, "Computational Method Using Quantum Annealing for TDMA Scheduling Problem in Wireless Sensor Networks," in *2019 13th International Conference on Signal Processing and Communication Systems (ICSPCS)*, 2019, pp. 1–9.

[100] C. Wang, H. Chen, and E. Jonckheere, "Quantum versus simulated annealing in wireless interference network optimization," *Scientific Reports*, vol. 6, no. 1, pp. 1–9, 2016.

[101] C. Wang and E. Jonckheere, "Simulated versus reduced noise quantum annealing in maximum independent set solution to wireless network scheduling," *Quantum Information Processing*, vol. 18, no. 1, pp. 1–25, 2019.

[102] J. Cai, W. G. Macready, and A. Roy, "A practical heuristic for finding graph minors," *arXiv preprint arXiv:1406.2741*, 2014.

[103] Y. Zeng and R. Zhang, "Energy-efficient UAV communication with trajectory optimization," *IEEE Transaction on Wireless Communications*, vol. 16, no. 6, pp. 3747–3760, 2017.

[104] F. Glover, G. Kochenberger, and Y. Du, "Quantum Bridge Analytics I: a tutorial on formulating and using QUBO models," *4OR*, vol. 17, no. 4, pp. 335–371, 2019.

[105] F. Vista, G. Iacovelli, and L. A. Grieco, "Quantum Scheduling Optimization for UAV-Enabled IoT Networks," in *Proceedings of the CoNEXT Student Workshop*, ser. CoNEXT-SW '21, 2021, pp. 19–20.

[106] G. Iacovelli and L. A. Grieco, "Drone Swarm as Mobile Relaying System: A Hybrid Optimization Approach," *IEEE Transactions on Vehicular Technology*, vol. 70, no. 11, pp. 12 272–12 277, 2021.

[107] S. Feld, C. Roch, T. Gabor, *et al.*, "A Hybrid Solution Method for the Capacitated Vehicle Routing Problem Using a Quantum Annealer," *Frontiers in ICT*, vol. 6, p. 13, 2019.

[108] H. Hussain, M. B. Javaid, F. S. Khan, A. Dalal, and A. Khalique, "Optimal control of traffic signals using quantum annealing," *Quantum Information Processing*, vol. 19, no. 9, pp. 1–18, 2020.

[109] R. C. Kizilirmak, "Quantum Annealing Approach to NOMA Signal Detection," in *2020 12th International Symposium on Communication Systems, Networks and Digital Signal Processing (CSNDSP)*, 2020, pp. 1–5.

[110] H. J. Kimble, "The quantum internet," *Nature*, vol. 453, no. 7198, pp. 1023–1030, 2008.

[111] S. Wehner, D. Elkouss, and R. Hanson, "Quantum internet: A vision for the road ahead," *Science*, vol. 362, 2018. DOI: 10.1126/science.aam9288.

[112] F. Vista, V. Musa, G. Piro, L. A. Grieco, and G. Boggia, "Network intelligence with quantum computing in 6g and b6g: Design principles and future directions," in *2021 IEEE Globecom Workshops (GC Wkshps)*, IEEE, 2021, pp. 1–6.

[113] W. Kozlowski, A. Dahlberg, and S. Wehner, "Designing a quantum network protocol," in *Proceedings of the 16th International Conference on Emerging Networking EXperiments and Technologies*, ser. CoNEXT '20, Barcelona, Spain: Association for Computing Machinery, 2020, pp. 1–16. DOI: 10.1145/3386367.3431293.

[114] K. Chakraborty, D. Elkouss, B. Rijsman, and S. Wehner, "Entanglement distribution in a quantum network: A multicommodity flow-based approach," *IEEE Transactions on Quantum Engineering*, vol. 1, pp. 1–21, 2020. DOI: 10.1109/TQE.2020.3028172.

[115] C. Li, T. Li, Y.-X. Liu, and P. Cappellaro, "Effective routing design for remote entanglement generation on quantum networks," *npj Quantum Information*, vol. 7, no. 1, p. 10, 2021.

[116] J. Li, M. Wang, K. Xue, *et al.*, "Fidelity-guaranteed entanglement routing in quantum networks," *IEEE Transactions on Communications*, vol. 70, no. 10, pp. 6748–6763, 2022.

[117] Y. Zhao, G. Zhao, and C. Qiao, "E2e fidelity aware routing and purification for throughput maximization in quantum networks," in *IEEE INFOCOM 2022 - IEEE Conference on Computer Communications*, 2022, pp. 480–489. DOI: 10.1109/INFOCOM48880.2022.9796814.

[118] W. Dai, T. Peng, and M. Z. Win, "Quantum queuing delay," *IEEE Journal on Selected Areas in Communications*, vol. 38, no. 3, pp. 605–618, 2020. DOI: 10.1109/JSAC.2020.2969000.

[119] W. Dai, T. Peng, and M. Z. Win, "Optimal remote entanglement distribution," *IEEE Journal on Selected Areas in Communications*, vol. 38, no. 3, pp. 540–556, 2020. DOI: 10.1109/JSAC.2020.2969005.

[120] C. Cicconetti, M. Conti, and A. Passarella, "Request scheduling in quantum networks," *IEEE Transactions on Quantum Engineering*, vol. 2, pp. 2–17, 2021. DOI: 10.1109/TQE.2021.3090532.

[121] L. Chen, K. Xue, J. Li, *et al.*, "A heuristic remote entanglement distribution algorithm on memory-limited quantum paths," *IEEE Transactions on Communications*, vol. 70, no. 11, pp. 7491–7504, 2022. DOI: 10.1109/TCOMM.2022.3205683.

[122] M. Chehimi and W. Saad, "Entanglement rate optimization in heterogeneous quantum communication networks," in *2021 17th International Symposium on Wireless Communication Systems (ISWCS)*, IEEE, 2021, pp. 1–6.

[123]   C. Qiao, Y. Zhao, G. Zhao, and H. Xu, "Quantum data networking for dis-
        tributed quantum computing: Opportunities and challenges," in *IEEE INFO-
        COM 2022 - IEEE Conference on Computer Communications Workshops
        (INFOCOM WKSHPS)*, 2022, pp. 1–6. DOI: 10.1109/INFOCOMWKSHPS54753.
        2022.9798138.

[124]   J.-W. Pan, C. Simon, Č. Brukner, and A. Zeilinger, "Entanglement purifica-
        tion for quantum communication," *Nature*, vol. 410, no. 6832, pp. 1067–1070,
        2001.

[125]   L. Gyongyosi, S. Imre, and H. V. Nguyen, "A survey on quantum channel ca-
        pacities," *IEEE Communications Surveys & Tutorials*, vol. 20, no. 2, pp. 1149–
        1205, 2018. DOI: 10.1109/COMST.2017.2786748.

[126]   G. Vardoyan, S. Guha, P. Nain, and D. Towsley, "On the stochastic analysis of
        a quantum entanglement distribution switch," *IEEE Transactions on Quan-
        tum Engineering*, vol. 2, pp. 1–16, 2021. DOI: 10.1109/TQE.2021.3058058.

[127]   I. Adler, M. G. Resende, G. Veiga, and N. Karmarkar, "An implementation of
        karmarkar's algorithm for linear programming," *Mathematical programming*,
        vol. 44, pp. 297–335, 1989.

[128]   S. P. Boyd and L. Vandenberghe, *Convex optimization*. Cambridge university
        press, 2004.

[129]   G. Scutari and Y. Sun, "Parallel and Distributed Successive Convex Approx-
        imation Methods for Big-Data Optimization," in *Multi-agent Optimization:
        Cetraro, Italy 2014*. Springer International Publishing, 2018, ISBN: 978-3-
        319-97142-1. DOI: 10.1007/978-3-319-97142-1_3.